1. Report No.	2. Government Accession No.	3. Recipient's Catalog No.
NASA TM X-3075		

4. Title and Subtitle	5. Report Date
DIGITAL INTEGRATED CONTROL OF A MACH 2.5 MIXED-COMPRESSION SUPERSONIC INLET AND AN AUGMENTED MIXED-FLOW TURBOFAN ENGINE	OCTOBER 1974
	6. Performing Organization Code
7. Author(s)	8. Performing Organization Report No.
Peter G. Batterton, Dale J. Arpasi, and Robert J. Baumbick	E-7965
	10. Work Unit No.
9. Performing Organization Name and Address	501-24
Lewis Research Center National Aeronautics and Space Administration Cleveland, Ohio 44135	11. Contract or Grant No.
	13. Type of Report and Period Covered
12. Sponsoring Agency Name and Address	Technical Memorandum
National Aeronautics and Space Administration Washington, D.C. 20546	14. Sponsoring Agency Code

15. Supplementary Notes

16. Abstract

A digitally implemented integrated inlet-engine control system was designed and tested on a mixed-compression, axisymmetric, Mach 2.5, supersonic inlet with 45 percent internal supersonic area contraction and a TF30-P-3 augmented turbofan engine. The control matched engine airflow to available inlet airflow. By monitoring inlet terminal shock position and overboard bypass door command, the control adjusted engine speed so that in steady state, the shock would be at the desired location and the overboard bypass doors would be closed. During engine-induced transients, such as augmentor light-off and cutoff, the inlet operating point was momentarily changed to a more supercritical point to minimize unstarts. The digital control also provided automatic inlet restart. A variable inlet throat bleed control, based on throat Mach number, provided additional inlet stability margin.

17. Key Words (Suggested by Author(s))

Digital control
Integrated control
Inlet control
Engine control
Propulsion control

18. Distribution Statement

Unclassified - unlimited
Category 10

19. Security Classif. (of this report)	20. Security Classif. (of this page)	21. No. of Pages	22. Price*
Unclassified	Unclassified	90	$4.00

* For sale by the National Technical Information Service, Springfield, Virginia 22151

DIGITAL INTEGRATED CONTROL OF A MACH 2.5 MIXED-COMPRESSION SUPERSONIC INLET AND AN AUGMENTED MIXED-FLOW TURBOFAN ENGINE

by Peter G. Batterton, Dale J. Arpasi, and Robert J. Baumbick

Lewis Research Center

SUMMARY

There is considerable interest in the use of augmented turbofan engines coupled to ıixed-compression inlets as propulsion systems for future transport-type supersonic ırcraft. There, however, has been little actual experience with this combination of a ırbofan engine and mixed-compression supersonic inlet. This is the first experimental ːst in the United States to study the interactions of such a system and to determine its ɔntrollability.

A digitally implemented integrated inlet-engine control system was designed and ːsted on a mixed-compression, axisymmetric, Mach 2.5, supersonic inlet with 45 per-ent internal supersonic area contraction (55-45 inlet) and a TF30-P-3 augmented turbo-ın engine in the Lewis Research Center 10- by 10-Foot Supersonic Wind Tunnel. The ːst demonstrated an on-line digital control that provided integration of both engine and ıixed-compression supersonic inlet control systems. By monitoring inlet terminal hock position and overboard bypass door command, the control adjusted engine speed so ıat in steady state, the shock would be at the desired location and the overboard bypass ɔors would be closed. The control thus obtained a match in inlet and engine mass flow, s well as in maximum pressure recovery, that was consistent with inlet stability.

During engine-induced transients, such as augmentor light-off and cutoff, the inlet perating point was momentarily changed to a more supercritical point. This minimized nstarts during the augmentor transients. The digital control also provided automatic estart of the inlet should an inlet unstart occur and provided automatic augmentor op-ration. The use of variable bleed flow from the inlet throat slot was also investigated. his control, based on inlet throat Mach number, provided additional inlet stability mar-in, which reduced the requirement of momentarily moving the inlet shock supercritical ɔr augmentor light-off.

A description of the final version of the digital integrated control is also included.

INTRODUCTION

Considerable interest exists in the use of augmented turbofan engines coupled to mixed-compression supersonic inlets as propulsion systems for future transport-type supersonic aircraft. Control of these supersonic propulsion systems has been a topic of much interest (refs. 1 to 4) for supersonic transports. There has been little actual experience with this combination of a turbofan engine and mixed-compression supersonic inlet. This is the first experimental test in the United States to study the interactions of such a system and to determine its controllability. Several difficulties can arise from the use of such combinations in the area of overall reliability and efficiency and in providing sufficient stable operating range for the inlet while minimizing the probability of engine stall.

There are several interrelated control problems for this engine and inlet. Any changes in augmentor operation will result in temporary changes in fan airflow. These airflow changes can cause inlet unstarts if they are of sufficient magnitude and if the rat of change is outside the control bandwidth of the inlet terminal shock control system. This relation results from the fact that, at the high Mach numbers, the fan operating point is generally at a low corrected speed on the fan operating map. Relatively large airflow changes can therefore result from small changes in fan pressure ratio. The inl terminal shock could be positioned further downstream in the inlet throat, which would provide sufficient margin against this problem. But this results in poor inlet pressure recovery (poor efficiency) and greater distortion at the engine. If an inlet unstart shoul occur, an engine stall is likely. Also during inlet restart and/or engine stall recovery, there is the possibility of further engine stalls due to high inlet distortion. This unstart stall-restart problem is discussed further in reference 5.

This project was undertaken to determine the nature of a control system that would avoid or at least minimize these problems while at the same time minimizing overboard spillage of inlet capture air. The approach taken was to tie together the inlet, engine, and augmentor control systems in an appropriate manner so as, first, to monitor, in steady state, inlet shock position and overboard bypass door command and to adjust engine airflow to match available inlet airflow; second, to provide information on augmentor-induced transients to the inlet and engine control systems which can be used to prevent inlet unstart and/or engine stall; and third, to provide automatic restart should the inlet unstart. Since there is considerable logic involved in this type of contr system and since much experience has already been gained in the use of digital compute control of supersonic inlets (ref. 6) and of an augmented engine (ref. 7), it was decided that this control would be implemented on a digital computer. This is the first attempt at simultaneously controlling both a supersonic inlet and an engine with the same digital computer. It was also felt that this choice would provide support material for the Air

Force - NASA cooperative digital integrated control flight program (ref. 8) now under contract.

The digital integrated control was tested at Mach 2.5 and at zero angle of attack in the Lewis Research Center 10- by 10-Foot Supersonic Wind Tunnel. No angle-of-attack data were obtained. At angle of attack, the inlet control would require more shock position instrumentation than was provided in this inlet. The inlet was of the axisymmetric type with 45 percent internal area contraction (55-45 inlet), and the augmented turbofan was a TF30-P-3. In addition, only the first two of the five augmentor zones were available for test purposes.

A complete description of the inlet and the engine is provided in this report. The inlet, but terminated with a long pipe and choked orifice, is also described in reference 9. Also provided in this report is a complete description of the final configuration of the integrated control system, including a detailed flow chart and a summary of how the control was developed by using an all-digital transient engine-inlet simulation and a real-time hybrid engine simulation. During the test, two bandwidth capabilities for the inlet overboard bypass doors were investigated, as well as the use of a controlled centerbody throat bleed system for further overall system improvement. The results of the test include steady-state changes in inlet airflow; step and sinusoidal changes in inlet airflow; augmentor light-off, cutoff, and level changes; and inlet unstart and automatic restart.

Data were taken in the U.S. customary system of units. Conversion to the International System of Units (SI) was done for reporting purposes only.

APPARATUS, INSTRUMENTATION, AND PROCEDURE

The digital integrated control was tested in the Lewis 10- by 10-Foot Supersonic Wind Tunnel. The propulsion system was composed of a mixed-compression inlet coupled to a dual-rotor turbofan engine. Figure 1 shows the system installed in the 10- by 10-Foot Supersonic Wind Tunnel. Figure 2 is a cross section of the inlet and engine in the tunnel test section. All tests were conducted at the following average free-stream conditions: Mach number, 2.5; total temperature, 297 K (note that standard-day temperature for Mach 2.5 at an altitude of 20 000 m would be 488 K); total pressure, 9.3 N/cm^2; Reynold's number index, RNI, 0.86; and specific-heat ratio, 1.4. The propulsion system was operated at zero angle of attack during all control tests.

Inlet

The Lewis-designed inlet (fig. 3) is an axisymmetric, mixed-compression inlet with a translating centerbody and 45 percent internal supersonic area contraction. The inlet is designed for Mach 2.5 operation with a TF30-P-3 engine. The inlet has a capture area of 0.707 square meter and measures 180 centimeters from the cowl lip to the fan

face. Provisions are made for boundary-layer bleed on the centerbody and cowl. The inlet was tested with the cowl bleed sealed. The centerbody bleed is a slot-type bleed. The centerbody bleed flow is ducted to four equally spaced struts located in the diffuser section. Centerbody bleed flow is controlled by a butterfly valve in each strut. The butterfly valves are positioned by electrohydraulic servocontrols that use vane-type hydraulic motor actuators.

The inlet is equipped with eight slotted-plate overboard bypass doors used to match inlet-engine airflow. Figure 4 shows a cross section of the diffuser, indicating the circumferential location of the bypass doors and the centerbody bleed flow struts. The even-numbered doors were used for disturbance; the odd-numbered doors by the control system. The disturbance doors had 87.5 percent of their area blocked. The total area of the four control doors is 0.161 square meter, and the total area of the four disturbance doors is 200 square centimeters.

Inlet Instrumentation

Linear motion of the bypass doors was measured by linear variable differential transformers (LVDT's). The LVDT's have negligible dynamics in the frequency range covered during these tests (0.1 to 100 Hz).

Figure 5 shows the inlet pressure instrumentation locations and indicates the appropriate inlet station numbers. Steady-state pressure instrumentation was used to measure the terminal shock position. These 16 steady-state transducers are located from a point 23 centimeters from the cowl lip to a point 66 centimeters from the cowl lip. The 14 transducers further upstream are spaced 2.54 centimeters apart. The last two are spaced 5.08 centimeters apart.

The dynamic pressures were measured with strain-gage-type transducers connected to the cowl with short tubes. The frequency response of the pressure-measuring system had negligible dynamics in the range covered in these tests (0.1 to 100 Hz). As shown in figure 5, there is a plane containing dynamic instrumentation located 66 centimeters from the cowl lip, station 1.1. There are four transducers in this plane, spaced 90° apart, which are electrically averaged. The average pressure is identified as $p_{1.1}$. In addition to these transducers, dynamic transducers were included to measure total and static pressure at the geometric throat (P_1 and p_1, respectively), and static pressure on the cowl near the lip ($p_{0.5}$). (All symbols are defined in appendix A.)

Engine

The engine used in this investigation is a Pratt & Whitney TF30-P-3. The TF30-P-3 is an axial, mixed-flow, augmented, twin-spool, low-bypass-ratio turbofan engine with a variable-area convergent primary nozzle. The engine is shown schematically in figure 6 with the engine station designations indicated. The engine includes a three-stage, axial-flow fan mounted on the same shaft with a six-stage, axial-flow, low-pressure compressor. This unit is driven by a three-stage, low-pressure turbine. A seven-stage, axial-flow compressor driven by a single-stage, air-cooled, turbine makes up the high-pressure spool. The compressor is equipped with 7th-stage (low-pressure compressor) and 12th-stage (high-pressure compressor) bleeds. The 7th-stage bleed is operated by the aircraft systems, and the 12th-stage bleed is normally operated automatically by the engine control system.

The augmentor consists of a diffuser section, five concentric-ring fuel manifolds (zones), three V-gutter ring flame holders, a combustion chamber liner, and a fully modulating flap-type convergent primary nozzle. Variable thrust augmentation is accomplished by adjusting fuel through the fuel manifolds. The augmentor is ignited by means of two "slugs" of fuel injected into the engine gas stream, one upstream of each turbine. This "hot streak" continues aft and ignites the augmentor fuel. The augmentor zones are ignited sequentially, each zone reaching a predetermined level before the next zone is ignited.

Engine Control System Modifications

The standard TF30-P-3 fuel control systems consist of a hydromechanical main fuel control (MFC) and a hydromechanical combined augmentor and exhaust nozzle control (A/B-ENC). A single power lever commands the MFC and A/B-ENC. However, to provide access to the augmentor at the nonstandard wind tunnel conditions, the A/B-ENC was completely removed from the engine and replaced with servocontrolled throttles for fuel flow control, a position servocontrol for the exhaust nozzle, and solenoid valves for generation of the logic signals used by the augmentor ignitor.

Integral with the MFC is a so-called "weapons derichment port," to which for some engine installations an electrically operated valve is connected to allow derichment of fuel during the firing of aircraft weapons. A servocontrolled throttling valve was attached to this port to allow the bypassing of fuel. This scheme is shown schematically in figure 7. By setting the power lever angle (PLA) to a high enough value, the MFC computer would provide acceleration fuel flow. The excess fuel could then be bypassed and engine speed regulation obtained externally of the MFC. The hydromechanical control could then be used for startup as well as for emergency procedures during wind tunnel operation.

The 12th-stage compressor bleed is normally operated automatically on the TF30. However, for the tunnel test it was also operated manually. The 7th-stage bleed was set open and the 12th-stage bleed was set closed.

The first augmentor zone has both primary and secondary flow paths. The secondary flow path is used only when the engine combustor pressure exceeds 124 N/cm^2 and thus was not connected for these tests since combustor pressure was not expected to exceed 70 N/cm^2. Zone 1 primary and zone 2 were the only zones to which fuel throttles were connected. This would allow as much as 55 percent thrust augmentation, which was felt to be sufficient for these tests as well as for other portions of the TF30 wind tunnel program.

The hydraulically actuated exhaust nozzle modulates between established limits, which for this test were from 0.289 square meter to 0.596 square meter, where 0.348 square meter is defined as "military." The normal minimum area is 0.384 square meter. The nonstandard area was obtained by attaching "mice" to some of the nozzle leaves (fig. 8). For the control tests, 0.348 square meter was used as the nominal area and was achieved by biasing the command to the exhaust nozzle position servocontrol. The capability of submilitary area was not used for this test.

Engine Instrumentation

Also shown in figure 6 is the pressure and temperature instrumentation used by the digital integrated control system and the Lewis data acquisition system. The engine station numbers are indicated in the figure also. All pressures used engine-supplied probes (i.e., the p_3 signal comes from the pressure signal tube going to the MFC). All pressure signals were sensed by strain-gage-type pressure transducers. The fan inlet temperature T_2 was sensed by a thermocouple, but the high-pressure-turbine inlet temperature T_4 is the Pratt & Whitney supplied signal and is based on the temperature rise across the compressors and the low-pressure-turbine discharge temperature. The low-pressure-rotor speed was sensed by a magnetic pickup and gear located in the "bullet nose." The high-pressure-rotor speed was sensed by a magnetic pickup and gear located on the gearbox. All fuel flow rates were measured by turbine flowmeters. The two speeds and the fuel flow rates were converted to high-level analog signals for use by the digital integrated control and recording equipment. The nozzle exit area and the compressor bleed positions were obtained from potentiometers.

Digital Computer

The digital integrated control was implemented on a digital computer located at the analog computer facility in a building approximately 500 meters from the test facility. It was connected to the test facility by means of land lines with ground isolation amplifiers at the receiving end of each line. A small (desk-top size), 10-volt, general-purpose analog computer was also used for signal conditioning and biasing of both sensed model parameters and returned control commands. The analog computer was located at the test facility.

Figure 9 shows the digital computer setup. It is a general-purpose control system designed for implementation of both inlet and engine controls. This is the first test in which both were accomplished at the same time. Figure 10 shows part of the test facility control room, including the analog computer and the termination for the digital computer. The digital system, shown in block diagram form in figure 11, consists of four major units:

(1) A digital computer with 16 384 words of memory, a read-restore memory cycle of 750 nanoseconds, and a word length of 16 bits

(2) A digital interface capable of converting both analog and frequency signals to computer-compatible digital words and of converting computer-generated words to analog and logical outputs

(3) A signal processing unit which provides signal conditioning and monitoring capability between the digital interface and the propulsion system to be controlled

(4) Programming peripherals consisting of a high-speed paper-tape reader and punch and a teletype

The capabilities of the system are given in table I, and a comprehensive description is available in reference 10.

All inlet and engine pressure measurements were passed through signal conditioners and isolation amplifiers to provide high-level (-10 to +10 V) inputs to the digital interface unit. This unit consists of a random-access multiplexer, a sample-and-hold amplifier, and a 13-bit digitizer. The complete digitizing process from channel sample to entry of the digitized measurement into computer memory requires approximately 50 microseconds. This process was automated through the use of a block transfer unit which ties up the computer program execution for only one memory cycle per word transferred. Completion of the sampling process is transmitted to the computer by a priority interrupt from the block data transfer unit.

Digital commands are issued directly from the digital computer to the 13-bit digital-to-analog converters. These outputs are passed through isolation amplifiers in the control room to provide ground isolation of the digital system and then to the servoamplifiers driving the manipulated variables.

Procedure

The inlet, engine, and control system were tested at Mach 2.5 and zero angle of attack. The mass flow delivered to the engine was varied by adjusting the amount of airflow bypassed by the disturbance doors of the inlet. This allowed observance of the behavior of the system to steady-state, step, and sinusoidal disturbances in airflow. The inlet was unstarted by momentarily reducing the inlet throat bleed until the throat Mach number dropped low enough for the inlet to unstart. The throat bleed was reduced by momentarily closing the strut butterfly valves. Behavior of the control to unstarts could then be determined. For testing of the augmentor control, the primary method of disturbing the control was the PLA. Step changes in the PLA were used. In order to attain the required conditions for these tests, the engine was started with the hydromechanical MFC and the inlet on an electronic analog control.

Steady-state data were recorded on the Lewis data acquisition systems. Transient data were recorded on two eight-channel strip-chart recorders and on magnetic tape.

CONTROL DESIGN

In this portion of the report, the basic inlet and engine control functions are described, followed by a description of the basic integration scheme and how it modifies the basic control functions. A complete description of the digital integrated control is provided. And finally, a brief description is given of how simulations were used to test preliminary control designs.

Basic Control Functions

There are three basic control functions for this mixed-compression-inlet and augmented-turbofan propulsion system. These are (1) inlet terminal shock and restart control, (2) engine rotor speed regulation and fuel flow limiting control, and (3) augmentor and exhaust nozzle control. These control functions are shown in figure 12. A brief explanation of each of these control functions follows.

Basic inlet control functions. - The basic control function of a mixed-compression supersonic inlet is that of maintaining the terminal shock in the throat to maximize inlet pressure recovery but not allowing the inlet to unstart (i.e., not allowing the terminal shock to be expelled from the inlet). The usual method of control is to manipulate overboard bypass doors to bypass inlet airflow, which in turn positions the terminal shock. By increasing bypass airflow, the shock is pulled downstream in the inlet throat; the

reverse occurs if bypass airflow is decreased. Thus, a control which senses shock position is used to drive the overboard bypass doors.

The second function of the inlet control is that of starting the inlet. Starting is defined as causing the externally located normal shock to enter the throat region of the inlet. (The inlet is unstarted when a normal shock is located forward of the cowl lip.) Starting is accomplished by increasing the ratio of throat area to capture area until the throat goes supersonic. Extending the spike increases the ratio of throat area to capture area for this inlet. Once the inlet is started, the spike returns to its design position. The started (or unstarted) condition is detected by the presence of supersonic (or subsonic) airflow at the cowl lip.

Basic engine control functions. - For the TF30-P-3, speed regulation is obtained normally by using the PLA to schedule a high-pressure-rotor speed reference in the MFC. The speed reference and actual speed are used in a droop governor to provide a ratio of fuel flow to combustor pressure which, when multiplied by combustor pressure, determines fuel flow to the engine. Speed regulation is obtained in that manner. The MFC also limits maximum fuel flow during acceleration to avoid turbine inlet overtemperature and/or compressor stall, and it limits minimum fuel flow during deceleration to avoid combustor blowout and/or compressor stall. The MFC also provides operating-point information (high-pressure-rotor corrected speed, $XNH/\sqrt{\theta_2}$) to the augmentor - exhaust-nozzle control. A signal from the augmentor control indicating that an augmentor blowout has occurred causes the MFC to reduce fuel flow to avoid overspeeding the low-pressure rotor.

Basic augmentor - exhaust-nozzle control functions. - The augmentor control uses the PLA to command a level of augmentor fuel flow and to determine which zones should be ignited. The zone fuel flow schedules are also ratio-of-fuel-flow-to-combustor-pressure schedules because combustor pressure is used as a measure of engine core airflow. Thus, changes in engine bypass ratio are taken into account to bias those augmentor zones which are in the fan duct airstream. The exhaust nozzle is positioned to drive the error in the MFC-determined fan operating point to zero. The fan operating-point schedule is the ratio of combustor pressure to turbine discharge total pressure P_3/P_5 as a function of $XNH/\sqrt{\theta_2}$. The rate of change in P_5 is used to indicate that the first zone of the augmentor is ignited or whether an augmentor blowout occurred.

Integrated Control Goals

By matching engine airflow to available inlet airflow, inlet pressure recovery is maximized and spillage airflow is minimized, and both these effects usually maximize inlet performance. This is the primary goal of the digital integrated control. The TF30-P-3 is a turbofan engine; and the bypass ratio of the fan varies, depending on

conditions, from about 1 to 2. Augmentor transients, such as zone light-off and cutoff, disturb the fan airflow directly; and these disturbances propagate into the inlet relativel unimpeded when compared to turbojets. Therefore, the second goal of the control is to provide a more stable operating point while attempting augmentor transients. The engin will stall immediately following an inlet unstart. Also the inlet tends to produce high dis tortion during inlet restart. Therefore, the third goal for the control is to provide auto- matic inlet restart and an adequate engine recovery feature.

Basic Integration Functions

The inlet and engine are defined as being matched when the shock is at the desired location and the bypass doors are closed. Therefore, a signal can be generated which could tell the engine to increase speed (and thus airflow) if more airflow is available, an conversely if less airflow is available. It is this type of scheme which was designed to achieve the primary goal of the integrated control. The overall integration loops are shown in figure 13. The airflow match signal is defined as the bypass door command sig nal or, if the bypass door command is zero, the shock position error signal. This signa is used as an input to a proportional-plus-integral control which provides a delta speed reference signal to the engine speed governor. This scheme will operate successfully except during propulsion system transients such as augmentor transients (including blow outs) and inlet unstarts. Therefore, an augmentor transient signal causes the delta spee reference control to hold its present value until the transient is over. The unstart signa causes the delta speed control to be reset to zero. The augmentor blowout signal causes the MFC to switch from the speed governor to a special fuel flow schedule. Thus, durin this time, the delta speed control is also placed in the hold mode. (The PLA normally generates the base speed reference schedule.)

During augmentation, the exhaust nozzle is also available to adjust engine airflow. Therefore, during augmented operation, the airflow match error signal biases the fan operating-point schedule. This is done in a manner to cause the exhaust nozzle to open more than normal if the bypass doors are open or to close more than normal if the shock is supercritical. This action was made proportional to allow the delta speed reference control to reset it to zero. This allows the nozzle to return to its normal schedule, which is desirable since significant changes in the fan operating point can lead to engine stall.

The augmentor transient signal is generated by the augmentor - exhaust-nozzle con- trol to tell the engine and inlet controls that engine-induced airflow transients can be ex- pected. The signal is simply a logic signal that indicates whether or not the augmenta- tion level has reached that commanded by the PLA. Besides locking the delta speed ref- erence control, this signal is used by the inlet control to command the shock to a more

supercritical location. And because the delta speed reference control is locked, the bypass doors open. Both these effects are desirable when large airflow transients are expected from the engine. The response of the inlet bypass door control may not be capable of handling the augmentor-induced airflow transient. Thus, the supercritical shock position reduces, if not avoids, the possibility of an inlet unstart.

The unstart-restart signal for the engine is the unstart-restart signal used by the inlet control except that, as far as the engine is concerned, the restart is not complete until the spike has returned to its design point. The augmentor - exhaust-nozzle control uses the unstart portion of this signal to cause an automatic shutdown of the augmentor. This is based on the assumption that the engine will stall when the inlet unstarts, and it is felt that the augmentor should be turned off following an engine stall.

These then are the basic design ideas used in the digital integrated control.

Integrated Control

Block diagrams of the digital integrated control are provided in figures 14 to 16. Figure 14 diagrams the inlet terminal shock position and restart control. And figures 15 and 16 diagram the main fuel control and augmentor - exhaust-nozzle control, respectively. These block diagrams are meant to represent the control logic of the digital control system and are not meant to be analog computer diagrams. For example, the block labeled "Delay 1 DT" indicates that the output of the previous block is not used until the next calculation of the control. These block diagrams are discussed in detail in appendix B. Flow charts and schedules for the digital integrated control which were used for the actual coding of the control logic in the computer are provided in appendix C.

Digital Computer Programming

The integrated control was programmed to allow independent selection of control update intervals for the inlet and engine segments. Separate interval timers were used in each control, but both controls shared a common data acquisition unit (multiplexer-digitizer). This was accomplished by using the structure of external priority interrupts given in table II and diagrammed in figure 17.

The highest priority level was assigned to the interval timer, which specified the update interval for the inlet control. The program assigned to this level reinitiated the timer. Then, depending on whether the data acquisition unit was busy or not, the program either set a data request latch to be interrogated by the level 5 program upon completion of the present data acquisition if busy, or initiated the inlet data acquisition immediately if not busy.

The second priority level was assigned to the unstart comparator. In going to the high state (indicating the occurrence of an unstart) the comparator would trigger a one-shot multivibrator, and this priority level would be initiated. The program assigned to this level would set the unstart latch which would be interrogated on the next control computation.

The third level, also assigned to the unstart comparator, would reset the unstart latch when the inlet restarted.

The fourth level was assigned to the engine control interval timer and functioned similarly to the inlet timer program.

The fifth level was assigned to the data acquisition unit and would become active as each block of data was digitized and transferred into memory. The inlet data consisted of one block and contained the sampled measurements of $p_{1.1}$, spike position, and by-pass door bias. The acquisition time for this block was 150 microseconds. The engine data consisted of five data blocks. The sampled data content of each block was as follows:

(1) Block 1: engine fan inlet total temperature and pressure, T_2 and P_2

(2) Block 2: power level angle, PLA; and engine total exhaust nozzle exit area, A_T

(3) Block 3: high rotor speed, XNH; and engine high-pressure-compressor inlet static pressure, $p_{2.2}$

(4) Block 4: engine low-pressure-turbine exit total pressure, P_5; and engine high-pressure-compressor static pressure, p_3

(5) Block 5: inlet throat exit static pressure $p_{1.1}$ command

This block structure enabled the engine data acquisition to be interrupted by a request fo inlet data after a maximum of two engine parameter samples (100 μsec), thus minimizin inlet control calculation delay.

At this priority level, then, it was necessary to provide a data transfer "busy" ind cation to the interval timers, to interrogate data request latches, and to sequence the en gine data block sampling. When it was determined, at this priority level, that all inlet data were in memory, priority level 6 would be initiated. Similarly, when all engine da were in memory, priority level 7 would be initiated. This was done in both cases by commanding a digital-to-analog converter (DAC) to 10 volts. This would trigger a one-shot multivibrator assigned to the desired level, and the appropriate control routine would be executed. A flow-diagram of this priority structure is given in figure 17.

Because of the interleaving of controls, the actual computation time of each control (as measured from interval timer interrupt to control output) was variable. The min-imum computation time for the inlet control was 490 microseconds and the maximum wa 790 microseconds. For the engine control, the minimum computation time was 2.1 mil liseconds and the maximum was 2.61 milliseconds.

Simulations

The preliminary control designs were tested by using a digital computer simulation of the TF30-P-3 and a one-dimensional flow analysis of the 55-45 inlet. The digital simulation is based on a technique developed by the Air Force called SMOTE (ref. 11). This technique was modified by Pratt & Whitney to include heat storage as well as speed, pressure, and temperature derivatives so that program output could be generated as a function of time. (The program does not use normal integration schemes.) The basic time step for the simulation is 0.1 second. The program was modified by the Lewis Research Center to include the inlet simulation. The inlet simulation operated with a basic time step of 0.01 second and assumed that engine airflow varied as a ramp over the 10 inlet time steps per engine time step. In this manner, it was possible to investigate most of the control functions. The principal function not investigated was the unstart-restart phenomenon. However, the results of this simulation predicted reasonably well the performance of the inlet and engine with the integrated control.

A second simulation was used to investigate the digital controller itself. Once the basic control loops had been defined and gains determined using the digital computer simulation, the control laws were programmed on the digital controller. The Lewis Research Center has developed a hybrid real-time simulation of the TF30-P-3 (ref. 12). The digital controller was connected to this simulation to allow a complete check of the digital engine and augmentor - exhaust-nozzle control programming. It was also to determine if any instabilities would appear that might have been lost in the digital engine-inlet simulations, as well as any control program scaling problems that might have been overlooked.

The principal result of the hybrid investigation was that the engine and augmentor - exhaust-nozzle controls could be run with sampling intervals as long as 250 milliseconds. It was determined that control stability was relatively unaffected by sampling intervals of 50 milliseconds or less. Therefore, it was decided that a sampling interval of 50 milliseconds would be used during the wind tunnel test program.

RESULTS AND DISCUSSION

The results of the 55-45 inlet/TF30 test can be put into three categories: (1) digital control of the inlet alone, (2) digital integrated control of the inlet and engine with 80-hertz-bandwidth inlet bypass doors, and (3) digital integrated control of the inlet and engine with 10-hertz-bandwidth inlet bypass doors. Figures 18 and 19 define in terms of frequency response what is meant by 80- and 10-hertz-bandwidth bypass doors.

Digital Inlet Control

The final values of the inlet control gains were determined after the test program was started. Once gains were determined, the inlet shock position control loop was tested. The shock position could be measured directly only in steady state for the inlet instrumentation provided with this inlet. Therefore, to provide the dynamic measurement, a wall static pressure tap just downstream of the inlet throat was used to represent the shock position while the shock was in its normal operating region. Figure 20 shows the relation of this pressure $p_{1.1}$ to shock position. The results of the inlet shock position control loop tests are shown in figures 21 and 22. Figure 21 compares the uncontrolled (open loop) and the digitally controlled (closed loop) response of $p_{1.1}$ pressure error to bypass door disturbance. For these tests, the disturbance doors were moved sinusoidally. The amplitude of $p_{1.1}$ was measured and plotted on the ordinate, after normalization to its 0.1-hertz open-loop value. Under closed-loop control, it is desired that the $p_{1.1}$ amplitude be held to a minimum. Generally, this is possible at low frequencies, where the control has time to react, but becomes impossible at higher frequencies. This type of result is observed in the closed-loop response in figure 20. Above 6 hertz the control provides an increase in the error response which is typical of the simple proportional-plus-integral control on the inlet terminal shock. The closed-loop control in figure 21 updated the inlet bypass door command every 5 milliseconds. The open-loop $p_{1.1}$ error response indicates that adequate digital control might be obtained for sampling intervals as long as 10 to 15 milliseconds. Therefore, in figure 22, $p_{1.1}$ error response is shown for three sampling intervals - 1, 5, and 10 milliseconds. The 10-millisecond results indicate that a slight degradation begins to occur above 20 hertz. The conclusion was to use the 5-millisecond sampling interval even though the 10-millisecond results were adequate.

The preceding responses are for the 80-hertz-bandwidth inlet bypass doors. Figure 23 shows the $p_{1.1}$ error response for the control driving the 10-hertz-bandwidth doors. The control uses a lower gain, and therefore does not provide as good a low-frequency error response. However, the 10-hertz-bandwidth bypass door capability was felt to be adequate for inlet shock position control on this inlet.

Also determined during this portion of the test were the unstarted- and started-inlet $p_{1.1}$ pressure command schedules as functions of spike position. These schedules are used to provide the $p_{1.1}$ command during the restart sequence of the inlet control. These schedules, shown in figure 24, were chosen in an attempt to minimize distortion, which in turn minimizes the chance of an engine stall during the restart sequence. This is the primary reason for the rapid dropoff at the extended spike positions. (The gradual slope on the started schedule will provide a smoother transition to the set point value of $p_{1.1}$ command.)

Digital Integrated Control With 80-Hertz-Bandwidth Bypass Doors

The control was first tested with the inlet control using the 80-hertz-bandwidth inlet bypass doors. The operating point from which all the digital integrated control tests were made is specified in table III. The results of the transient tests are presented on strip charts, and in almost all cases two recorders were used to obtain the data. As a result, the grid lines at any given time for the two recorders were not at the same position. Therefore, there is some misalinement of grid lines in the following figures. Figure 25 shows activation of the controller, which causes the bypass doors to slew closed as the engine speed increases and then settles out with the bypass doors closed and with $p_{1.1}$ near the desired value. In the startup case, the $p_{1.1}$ pressure command was set to a value that positioned the shock at a somewhat supercritical location, which would provide extra stability margin during the startup transient. However, at this shock location the $p_{1.1}$ pressure was unstable as a result of an aerodynamic effect in the inlet (i.e., the $p_{1.1}$ pressure was unstable with no control).

Figure 26 shows the performance of the control during a square-wave-type input disturbance of inlet airflow. In this figure, the shock is positioned less supercritically and the unstable motion of the shock position observed in figure 25 is gone. The disturbance doors were used to generate the airflow disturbance. Figure 26(a) shows data obtained on line, and figure 26(b) shows data played back from tape. Included in figure 26(b) is a blowup of the engine speed traces, showing the action of the integrated control, and is provided for that purpose only. During recording of these data, the tape speed was not constant; this is indicated by the drift in the playback signal level. These errors are particularly apparent in the blownup speed traces. (The blownup speed traces are inverted such that increasing speed is downward.) The initial values of the speeds, pressures, and so forth, are the same in both parts of figure 26. The magnitude of the disturbance was 0.9 percent peak-to-peak of the engine total corrected airflow of 68.7 kg/sec. The traces in figure 26 show that the desired result of no bypass airflow is achieved in steady state. In addition, the shock is positioned by the control at the desired location in the inlet throat ($p_{1.1}$ at the commanded value). During the transient, the following events occur: For step closing of the disturbance doors, the control doors step open to correct for the error in shock position ($p_{1.1}$). The engine speed then increases to allow the control doors to close. This process is somewhat underdamped; and speed overshoots, pulling the shock to a slightly supercritical position momentarily. For a step opening, this process is reversed. When the disturbance doors step open, the shock moves to a supercritical location. Engine speed then is reduced, allowing the shock to return to the desired position. Again the system is slightly underdamped.

Augmentor transients were investigated next. Figures 27(a), (b), and (c) show augmentor light-off to minimum zone 1 fuel flow, zone 2 light-off from maximum zone 1 fuel flow, and a complete light-off transient ending at maximum zone 2 fuel flow,

respectively. In figure 27(a), the traces have been marked with numbers to aid the following description: The T_4 shown in these figures and those that follow is the Pratt & Whitney indicated turbine inlet temperature and not an actual measurement of T_4. At 1 in figure 28(a), the control reduces the $p_{1.1}$ pressure slightly in anticipation of the augmentor light-off. (The control no longer lets the engine speed reset the bypass doors.) At 2, the augmentor fuel flow is turned on. At 3, P_5 increases rapidly, indicating that the augmentor has lit-off. At 4, the bypass doors move to prevent the inlet from unstarting. At 5, A_{T7} reacts to correct the error in fan suppression, p_3/P_5, but is rate limited. At 6, minor oscillations in fuel flow reflect the variation in p_3, since all fuel flows are proportional to p_3. And at 7, the system returns to the desired steady-state condition for the shock and bypass doors. As noted previously, the control is slightly underdamped. In figure 27(b), the $p_{1.1}$ command is again reduced in anticipation of the augmentor transient. Fuel flow then increases, indicating that zone 2 fuel flow has started. The system continues to be slightly oscillatory during augmentor transient time periods, which indicates that the nozzle-airflow matching loop gain may be too high. Figure 27(c) shows primarily the results of figures 27(a) and (b) combined. The delay for the zone 2 light-off, which is the third step in the fuel flow trace, is due to a manifold fill-delay calculation. In figures 27(a) and (c), one can observe the definite P_5 pressure transient that is used by the control to indicate a successful augmentor light-off. However, the control prevents the inlet from unstarting, and this action of the inlet bypass doors is also shown in the figure. After each transient, the control returns the $p_{1.1}$ to the desired value and closes the inlet bypass doors.

Figure 28 shows an augmentor cutoff transient. During augmentor cutoff, the augmentor fuel flow is essentially reduced, in the reverse of the light-off sequence. The only exception is that there are no fill delays. As a result of the rapid cutoff of fuel flow from the minimum of each zone, the engine total airflow momentarily increases, causing the inlet to go supercritical. The nozzle soon catches up and the shock is positioned less supercritically. After zone 1 is cut off and the nozzle returns to the "military" area, the inlet and engine are returned to the desired operating point for the shock and bypass doors.

Figure 29 is also an augmentor cutoff transient, but for some reason a blowout occurred - or at least the control blowout logic was activated. The P_5 excursion tripped the blowout logic which cuts off the augmentor fuel flow and slews the nozzle closed. The blowout is indicated in the figure by the drop in P_5 and $p_{1.1}$. The system recovered from the transient successfully.

Reaction of the control to an inlet unstart is shown in figure 30. In order to obtain the inlet unstart, the inlet throat bleed was momentarily reduced, thereby reducing the throat Mach number until the inlet unstarted. The throat bleed was reduced by momentarily closing the strut butterfly valves. At 1, the expelling of the shock causes the pressures in the inlet to drop rapidly. At 2, an engine high-pressure-compressor stall

is indicated by the small spike on the $p_{2.2}$ pressure signal just after the pressure starts to decrease. The P_2 transducer was located at the fan tip and could not be used to indicate a low-pressure-compressor stall. At 3, the inlet pressure recovers partially to the preunstart value, presumably because steady flow conditions have been achieved in the inlet. At 4, the bypass doors are controlled in an effort to achieve the scheduled values for $p_{1.1}$ shown in figure 24. The second drop in the $p_{1.1}$ signal is caused by these schedules. At 5, toward the end of the transient, the engine speeds are increasing and the shock is pulled supercritical momentarily. The figure shows that the inlet is successfully restarted and the inlet and engine returned to the preunstart condition, with the exception that the $p_{1.1}$ command was not returned to its starting value. Again the $p_{1.1}$ signal appears to be unstable. At the time this particular test was run, there was a small problem in the control logic, which did not return the $p_{1.1}$ command to its initial value. This problem was corrected and does not appear in the unstart-restart results presented later for the 10-hertz door control. The engine experiences a stall immediately after the inlet unstart, but the stall clears quickly and the engine recovers without much overshoot in T_4.

Digital Integrated Control With 10-Hertz-Bandwidth Bypass Doors

Essentially the same results were obtained in testing the control implemented with the slower inlet bypass doors. Figure 31 shows the response of the control system to a square-wave disturbance. These results are essentially the same as those with the 80-hertz-bandwidth bypass door control (fig. 26), except that there was slightly less damping. This can be observed in figure 31(b) in the XNL trace. The tape data traces again suffer from the same problems mentioned for the 80-hertz-bandwidth door results, and therefore the absolute magnitude scales are not provided. However, the initial values of the speeds, pressures, and so forth, are the same in both parts of the figure. The magnitude of the disturbance was 0.85 percent (peak to peak) of the engine total corrected airflow of 68.7 kg/sec. This figure indicates that the desired results of no bypass airflow in steady state are achieved.

A light-off transient to maximum zone 2 fuel flow is shown in figure 32, and a cutoff from maximum zone 2 fuel flow in figure 33. These figures can be compared to figures 27(c) and 28, respectively. (The time scale for figs. 32 and 33 is different than that for figs. 27(c) and 28.) In figures 32 and 33, the control reduces the $p_{1.1}$ pressure significantly while waiting for the transient to end. This action reduces the possibility of an inlet unstart occurring by pulling the shock back to a more supercritical location. For the 10-hertz-bandwidth door control, it was necessary to reduce the $p_{1.1}$ command pressure to 4.97 N/cm^2 to avoid unstarts during augmentor light-off. This reduction was not required for the 80-hertz-bandwidth bypass door control.

Figure 34 shows the performance of the control during an inlet unstart. These results are essentially the same as those shown in figure 30. Figure 35 also shows an unstart, but with the augmentor in operation and at the maximum zone 2 condition. A second stall occurs during this transient, and a second inlet unstart immediately follows the inlet restart. It is not clear what caused the second engine stall. It is possible that the stall was caused by the exhaust nozzle having considerably more open area than normal with the inlet producing high distortion immediately after restart. During the test program we were not able to determine what control action, if any, should be taken to prevent this effect. However, it seems desirable to shut off the augmentor as quickly as possible in case the engine should remain in stall.

As shown in figure 32, prior to an augmentor light-off, the value of $p_{1.1}$ is reduced, pulling the shock back to a more supercritical position in the inlet. Because of the location of the throat bleed slot, it was decided to attempt to use the bleed as a "shock trap." This scheme was based on the idea that the throat bleed volume would be able to absorb part of the augmentor airflow disturbance. A simple "bang-bang" type control was designed for the throat bleed butterfly valves that would cause them to open to their maximum whenever the inlet throat Mach number dropped below 1.14. This simple control is shown in figure 36. The bandwidth capability of these valves is shown in figure 37.

Figure 38 shows what happens without the throat bleed control and when the shock is not pulled back sufficiently during an augmentor light-off. The inlet unstart at augmentor light-off is one of the most severe transients experienced by the system. The T_4 signal shows an increase, and this could possibly overtemperature the engine under normal operating temperatures, where T_4 might be 1100° C. With the control described in the preceding paragraph, the augmentor light-off transient produced the results shown in figure 39. The throat bleed control greatly reduced the requirement of pulling the shock back in the inlet throat for augmentor light-off. Without the throat bleed control, $p_{1.1}$ command had to be reduced to at least 4.97 N/cm^2 in order to avoid an inlet unstart. However, with the throat bleed control, $p_{1.1}$ command needed to be reduced only to 5.35 N/cm^2. Figure 40 shows an augmentor cutoff, also with the throat bleed control active.

The throat bleed control was programmed on an analog computer. However, it could have been programmed on the digital computer by the use of two additional priority interrupts: one to detect when the throat Mach number dropped too low, and one to indicate that the throat Mach number was no longer below the minimum.

SUMMARY OF RESULTS

The general problems associated with a mixed-compression inlet and augmented turbofan engine should be similar to those experienced with this particular combination. The results of this test program indicate that the problems of control of an augmented turbofan engine and mixed-compression inlet can be minimized by integrating the engine and inlet control systems. This integration required no instrumentation other than that normally required for this combination of engine and inlet.

The digital integrated control demonstrated an on-line digital control that provided integration of both augmented turbofan engine and mixed-compression supersonic inlet control systems. The control matched engine mass flow to available inlet mass flow. By monitoring inlet terminal shock position and overboard bypass door command, the control adjusted engine speed so that in steady state, the shock would be at the desired location and the overboard bypass doors would be closed. The control thus obtained maximum mass flow recovery as well as maximum pressure recovery consistent with inlet stability. During engine-induced transients, such as augmentor light-off and cutoff, the inlet operating point was changed to a more supercritical point, and thus unstarts were minimized. The digital control also provided automatic restart of the inlet should an unstart occur, as well as automatic augmentor operation. Also investigated was the use of variable bleed flow from the throat slot located on the centerbody. This control, based on throat Mach number, provided an additional inlet stability margin, which reduced the requirement to move the inlet shock supercritical for augmentor light-off.

For the system studied herein, an improvement in response and damping could be expected with further effort and could possibly lead to other sensed parameters. Both digital and hybrid simulations were used in the development of this control system. They reasonably predicted both the transient and steady-state behavior of the complete inlet and engine system.

Not investigated for this control system were the effects a turbine inlet temperature limit or of a mechanical speed limit on either rotor of the engine. Three sampling times were used to evaluate the inlet terminal shock control, but only one sampling interval (50 msec) was investigated for the engine. It is felt that further work on the digital integrated control approach should include these areas.

The control tested in this work matched inlet and engine mass flow while maximizing inlet recovery. Other approaches to the integration might be to maximize thrust specific fuel consumption or overall thrust subject to the appropriate restrictions. It is possible

that these approaches would result in a different match between the engine and inlet than the control described herein.

Lewis Research Center,
National Aeronautics and Space Administration,
Cleveland, Ohio, June 20, 1974,
501-24.

APPENDIX A

SYMBOLS

A	area, m^2
DT	digital controller sampling interval, sec
K_I	engine speed reset integral gain
K_{IS}	started-inlet terminal shock control integral gain
K_{IU}	unstarted-inlet terminal shock control integral gain
K_P	engine speed reset proportional gain
K_{PS}	started-inlet terminal shock control proportional gain
K_{PU}	unstarted-inlet terminal shock control proportional gain
M	Mach number
MFC	main fuel control
NRL	negative rate limit of augmentor control, linear units per second
P	total pressure, N/cm^2
PLA	power lever angle, deg
PRL	positive rate limit of augmentor control, linear units per second
PSPE	percent error in fan suppression
p	static pressure, N/cm^2
RNI	Reynolds number index, $\delta_2(T_2 + 384)/399\ \theta_2^2$, ratio of Reynolds number to Reynolds number at sea level
T	total temperature, ^oC
TL1, TL2, and TL6	control logic signals
W_f	fuel flow, kg/hr
X	position, m
XNH	high-pressure-rotor speed, rpm
XNL	low-pressure-rotor speed, rpm
X_{dif}	augmentor power error
X_{oo}	augmentor power level

X_{req}	augmentor power request
Z2SW	augmentor zone 2 light-off signal
δ	pressure in $(N/cm^2)/10.135$
θ	temperature in kelvin/288.15
ΔXNH	bias on high engine rotor speed request
0	logical low
0.5	inlet cowl-lip station, 39 cm from cowl lip
1	inlet throat station, or logical high
1.1	inlet throat exit station, 66 cm from cowl lip
2	engine fan inlet station, 180 cm from cowl lip
2.1	engine low-pressure-compressor inlet station
2.2	engine high-pressure-compressor inlet station
3	engine high-pressure-compressor exit station
4	engine high-pressure-turbine inlet station
4.1	engine low-pressure-turbine inlet station
5	engine low-pressure-turbine exit station
6	engine core augmentor inlet station
7	engine core exhaust nozzle exit station
13	engine fan exit station
16	engine fan augmentor inlet station
17	engine fan exhaust nozzle exit station

Subscripts:

C1, C2, and C3	shock control command values
com	command
err	error
ref	reference
req	request
T7	engine total exhaust nozzle exit area
0	free-stream station

0.5	inlet cowl-lip station
1	inlet throat station, 39 cm from cowl lip
1.1	inlet throat exit station, 66 cm from cowl lip
2	engine fan inlet station, 180 cm from cowl lip
2.2	engine low-pressure-compressor exit station
3	engine high-pressure-compressor exit station
4	engine high-pressure-turbine inlet station
5	engine low-pressure-turbine discharge station

APPENDIX B

INTEGRATED CONTROL BLOCK DIAGRAMS

Block diagrams of the digital integrated control are provided in figures 14 to 16. Figure 14 diagrams the inlet terminal shock position and restart control. And figures 15 and 16 are block diagrams of the main fuel control and augmentor - exhaust-nozzle control, respectively. These block diagrams are meant to represent the control logic of the digital control system and are not meant to be analog computer diagrams. For example, the block labeled "Delay 1 DT" indicates that the output of the previous block is not used until the next calculation of the control. A detailed discussion of these block diagrams is provided in this appendix. Flow charts and schedules for the digital integrated control which were used for the actual coding of the control logic in the computer are provided in appendix C.

Inlet Control System

The inlet control system is shown in figure 14. The control system is made up of two parts: a terminal shock control system, and a restart control system. Figure 14(a) is the block diagram of the inlet terminal shock position control. Terminal shock position control is achieved by manipulating overboard bypass doors in response to variation in a variable which is indicative of terminal shock position. In this system the control signal used to control shock position is an average diffuser static pressure $p_{1.1}$. Terminal shock motion results in changes in the average pressure level. Figure 20 shows the variation of $p_{1.1}$ with shock position. This pressure variation results in an error which is modified by the controller, and the resulting controller output is used to manipulate overboard bypass doors to reposition the terminal shock at the operating point. A proportional-plus-integral-type controller was chosen because it provides zero steady-state error and desirable attenuation for low-frequency disturbances.

The airflow match signal is proportional to either bypass door command or shock position signal. By our definition, the inlet and engine are not matched if the bypass door command is zero and if the shock is supercritical of its desired location. Therefore, whenever the bypass door command was zero, the $p_{1.1}$ error was used, with appropriate scale factor, to provide an equivalent error signal (airflow match signal) to the engine.

The restart control system functions when inlet disturbances produce an unstart. The restart control logic is shown in figure 14(b). The unstart sensor is made up of the ratio of a cowl-lip static pressure $p_{0.5}$ and a throat total pressure P_1. This ratio

increases when the inlet unstarts because inlet recovery decreases and static pressure at the cowl lip increases as the terminal shock is expelled. When the inlet unstart is sensed, the restart control system causes the spike to extend to reduce the capture- to throat-area ratio to provide conditions for restarting the inlet. Additionally, the proportional K_{PS} and integral K_{IS} gains of the terminal shock controller are reduced to K_{PU} and K_{IU}, respectively, to avoid oscillations of the terminal shock during the restart cycle. After the inlet is restarted, the spike is commanded to return to the design point.

At the same time the spike starts to extend, an unstarted pressure command function is switched into the terminal shock controller. The logic for the selection of the $p_{1.1}$ command is shown in figure 14(c). This command pressure is a function of spike position. When the spike is back on design, the nominal command ($p_{1.1,C1}$, $p_{1.1,C2}$, or $p_{1.1,C3}$) is switched into the terminal shock controller, and the controller gains reset to their nominal values.

The nominal pressure command is varied depending on expected engine airflow transients. This logic is shown in figure 14(c). For example, when the augmentor is to be lit-off, the shock position is moved to a more supercritical location to provide addition margin against unstart. The signals used to switch in these various pressure commands are generated by the augmentor and exhaust nozzle control systems. Two levels of supercritical operation were possible with the setup shown in figure 14(c), where $p_{1.1,C3}$ is the value while waiting for zone ignition, $p_{1.1,C1}$ is used for augmentor level changes where zone switching is not going to occur, and $p_{1.1,C2}$ is the normal steady-state command value. Its value, set on a potentiometer external to the control, was sampled by the control so that it could be adjusted while the control was operational.

Main Fuel Control System

Figure 15 is a block diagram of the main fuel control. The basic features of the control are the same as those of the hydromechanical control. However, the implementation is slightly different due to the fact that the hydromechanical control was used as the "fuel pump" for the integrated control. As mentioned previously, the PLA for the hydromechanical control was set so that the hydromechanical control always outputted acceleration fuel flow. Therefore, the calculated fuel flow of the speed governor had to be biased in such a manner so as to command the appropriate bypass fuel flow. The control uses a proportional or "droop" type governor with approximately the same gain as the hydromechanical control. The inlet airflow error was inputted to a porportional-plus-integral control to bias the engine speed command. This achieved the main integration goal of matching engine to inlet airflow. The match error is generated by the inlet control system. For completeness, the PLA-to-speed-request function and the integration

lockout below military power setting are shown in figure 15. They were not actually implemented.

The blowout schedule is also the same as that provided by the hydromechanical control. However, instead of being activated by the augmentor blowout event only, it is also activated by the inlet unstart signal.

Augmentor - Exhaust-Nozzle Control

Figure 16 is a block diagram of the digital augmentor and exhaust nozzle control. This control provides an augmentor fuel flow as requested by the PLA and positions the exhaust nozzle to minimize the error in the fan operating point, or so-called fan suppression.

The exhaust nozzle control is shown in figure 16(a). For nonaugmented operation, the exhaust nozzle area is held fixed at its "military" value. During augmented operation, a percentage error in fan suppression (PSPE) is used by an integral-type control to command the nozzle area. Fan suppression is measured by the ratio of p_3/P_5. This ratio is scheduled as a function of $XNH/\sqrt{\theta_2}$. The commanded value of p_3/P_5 is biased by an airflow match signal and by a logic signal which indicates that the level of augmentation is being reduced. The purpose of the latter is to cause the exhaust nozzle to lead fuel flow slightly during reduction of augmentation. This does not allow the inlet to go as far supercritical during the transient as it might. The airflow match signal was only proportionally added to the fan suppression schedule which allows the main fuel control to reduce this signal to zero in steady state.

The light-off detector (fig. 16(b)) is used to release the exhaust nozzle as well as to allow fuel flow rate to increase above the minimum for zone 1. The detector monitors the fan suppression error signal for a positive change of 0.03. When this occurs, an augmentor light-off is assumed to have occurred. This sets the augmentor control light-off logic signal (ABON) high (1).

The blowout detector (also fig. 16(b)) works in a similar manner except that it monitors the suppression error for a -0.15 value. If the suppression error becomes more negative than -0.15, a blowout is assumed to have occurred. The blowout logic is also tripped by the inlet unstart signal since it was assumed that the unstart would stall the engine. The blowout logic can only be reset by reducing the PLA to below 70°. The nozzle feedback rotates a pully through an angle of 120°. The blowout signal is sent to the main fuel control only while the nozzle feedback is greater than 25°. This allows the main fuel control to recover the engine after the worst part of the blowout transient has died out.

The PLA schedules a level of augmentor fuel flow and is shown in figure 16(c). The output of this schedule is an equivalent throttle signal or power level request signal which

is used to schedule fuel for each zone as well as to determine which zones are to be lit. The X_{req} signal is modified to limit it to values which allow proper sequencing of the augmentor zones. For example, while waiting for an augmentor light-off, PLA may request a X_{req} equal to 0.25, which is calling for all of zone 1 fuel flow and part of zone 2. Thus, X_{req} is first modified to minimum zone 2, which is 0.22, since zone 2 has not lit-off, and then further reduced to 0.12 since zone 1 has not lit-off either. After zone 1 has lit-off, X_{req} will be allowed to increase to 0.22; and after zone 2 has lit-off, it will be allowed to increase to 0.25. The augmentor power request is allowed to move in a somewhat discontinuous manner. To smooth this effect so that fuel flow will increase smoothly and so that the exhaust nozzle will be able to keep the fan suppression error near the desired level, the rate of change of X_{req} is limited. The output of this rate limit system, designated X_{oo}, is then used to actually schedule the augmentor fuel flow. The rate of change of X_{oo} was made variable so that if the fan suppression error were large, the rate of change of X_{oo} would be small. This would allow the exhaust nozzle to "catch up." The equations that define the rate limits are

$$PRL = 0.25[1.0 - 10.0(PSPE + |PSPE|)] \tag{1}$$

$$NRL = -0.25[1.0 + 10.0(PSPE - |PSPE|)] \tag{2}$$

In both cases the rate limits were not allowed to pass through zero. If the fan suppression error exceeded 0.05, X_{oo} would not be allowed to increase, and if it became more negative than -0.05, X_{oo} would not be allowed to decrease.

The exceptions to these rate limit rules are that during a blowout the augmentor fuel valves and the exhaust nozzle are slewed closed at their maximum rates, and that during a light-off and cutoff X_{oo} is allowed to slew at rates independent of the fan suppression error. On light-off, X_{oo} is allowed to slew to 0.12 (minimum zone 1) independent of fan suppression error PSPE. And on cutoff, X_{oo} is allowed to slew from 0.765 to 0 independent of fan suppression error, forcing zone 1 fuel flow off.

Figure 16(d) shows the augmentor fuel flow logic and the zone 2 light-off detector. The zone 2 light-off detector is simply a time-delay calculation which is equal to the time it takes to fill the zone 2 fuel lines and manifold, based on the minimum zone 2 fuel flow. After the time has elapsed, zone 2 light-off signal Z2SW is set high.

Figure 16(e) shows the augmentor transient signal logic. This signal TL6 is high whenever the augmentor power level X_{oo} is not at steady state.

APPENDIX C

FLOW DIAGRAMS

This appendix contains the flow diagrams of the inlet and the engine and augmentor - exhaust-nozzle control programs. It also includes a listing of the various functions and symbols used in the flow diagrams.

Inlet Control Program

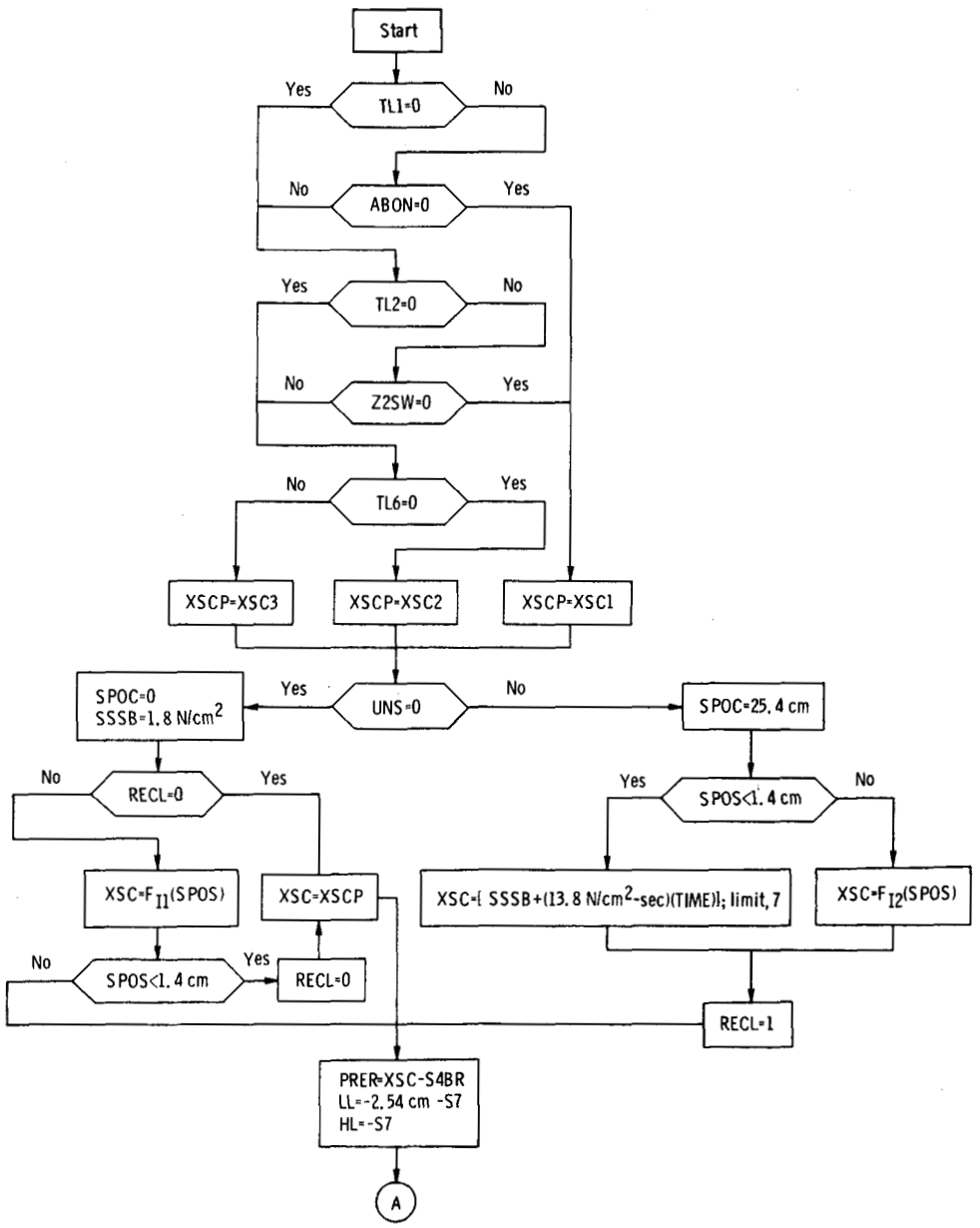

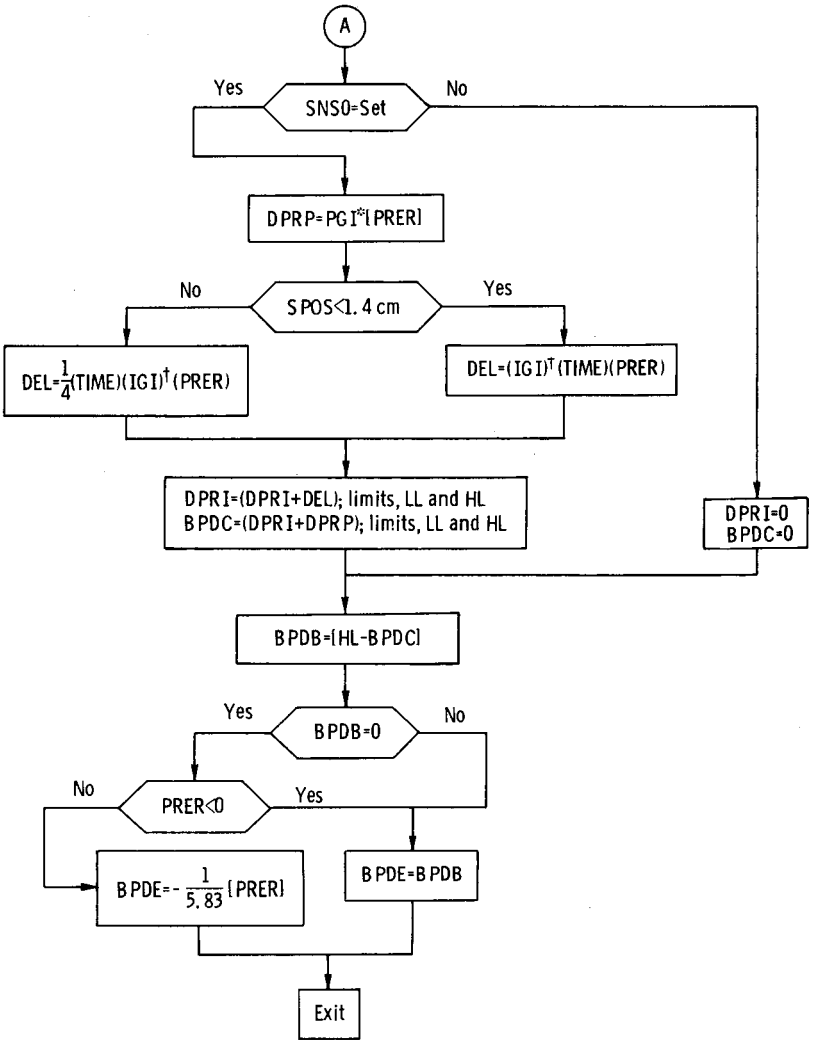

*PGI = 1.410 cm/(N/cm^2) for 80-hertz-bandwidth doors;
PGI = 2.065 cm/(N/cm^2) for 10-hertz-bandwidth doors.

†IGI = 14.74 cm/(N/cm^2-sec) for 80-hertz-bandwidth doors;
IGI = 3.68 cm/(N/cm^2-sec) for 10-hertz-bandwidth doors.

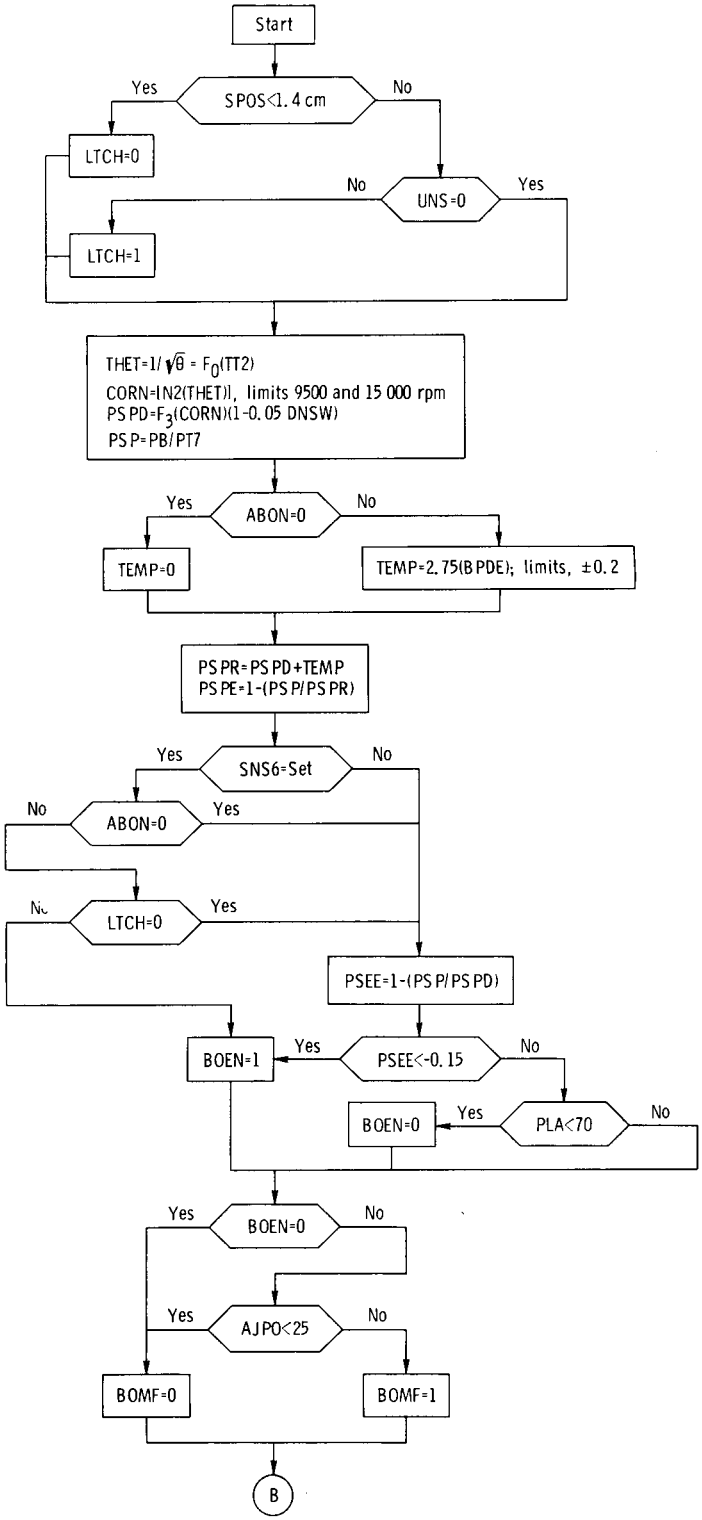
Start
SPOS<1.4 cm
Yes
No
LTCH=0
UNS=0
No
Yes
LTCH=1
THET=1/√θ = F0(TT2)
CORN=IN2(THET)], limits 9500 and 15 000 rpm
PSPD=F3(CORN)(1-0.05 DNSW)
PSP=PB/PT7
ABON=0
Yes
No
TEMP=0
TEMP=2.75(BPDE); limits, ±0.2
PSPR=PSPD+TEMP
PSPE=1-(PSP/PSPR)
SNS6=Set
Yes
No
ABON=0
No
Yes
LTCH=0
No
Yes
PSEE=1-(PSP/PSPD)
BOEN=1
Yes
PSEE<-0.15
No
BOEN=0
Yes
PLA<70
No
BOEN=0
Yes
No
AJPO<25
Yes
No
BOMF=0
BOMF=1
B

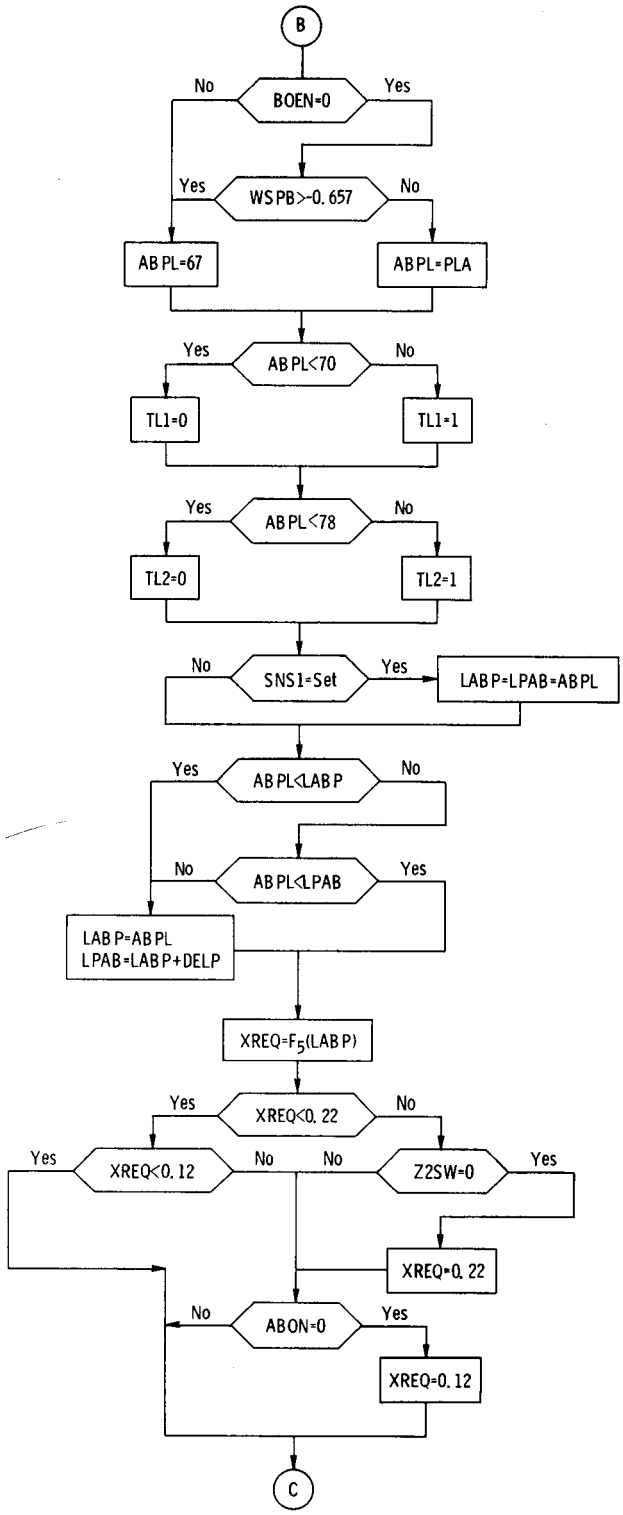
B
No
BOEN=0
Yes
Yes
WSPB>-0.657
No
ABPL=67
ABPL=PLA
Yes
ABPL<70
No
TL1=0
TL1=1
Yes
ABPL<78
No
TL2=0
TL2=1
No
SNS1=Set
Yes
LABP=LPAB=ABPL
Yes
ABPL<LABP
No
No
ABPL<LPAB
Yes
LABP=ABPL
LPAB=LABP+DELP
XREQ=F5(LABP)
Yes
XREQ<0.22
No
Yes
XREQ<0.12
No
No
Z2SW=0
Yes
XREQ=0.22
No
ABON=0
Yes
XREQ=0.12
C

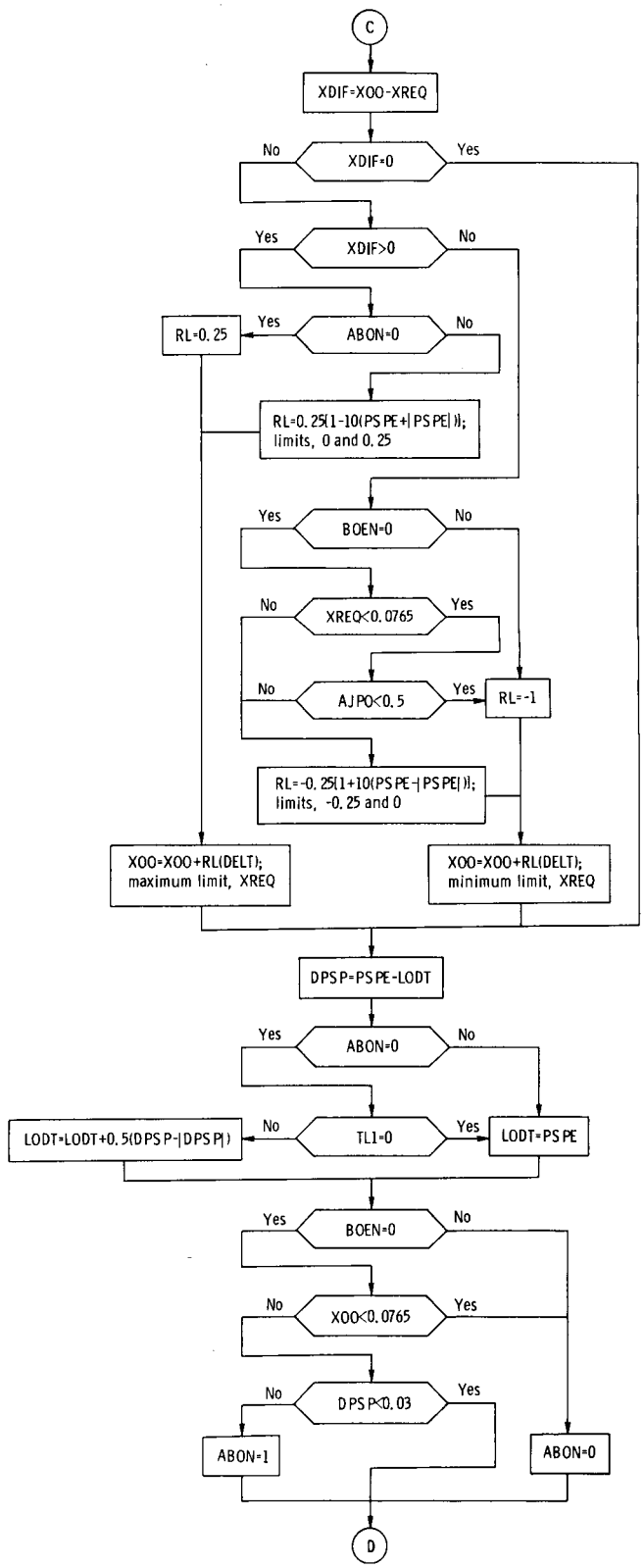
C
XDIF=XOO-XREQ
No
XDIF=0
Yes
Yes
XDIF>0
No
RL=0.25
Yes
ABON=0
No
RL=0.25(1-10(PSPE+|PSPE|));
limits, 0 and 0.25
Yes
BOEN=0
No
No
XREQ<0.0765
Yes
No
AJPO<0.5
Yes
RL=-1
RL=-0.25(1+10(PSPE-|PSPE|));
limits, -0.25 and 0
XOO=XOO+RL(DELT);
maximum limit, XREQ
XOO=XOO+RL(DELT);
minimum limit, XREQ
DPSP=PSPE-LODT
Yes
ABON=0
No
LODT=LODT+0.5(DPSP-|DPSP|)
No
TL1=0
Yes
LODT=PSPE
Yes
BOEN=0
No
No
XOO<0.0765
Yes
No
DPSP<0.03
Yes
ABON=1
ABON=0
D

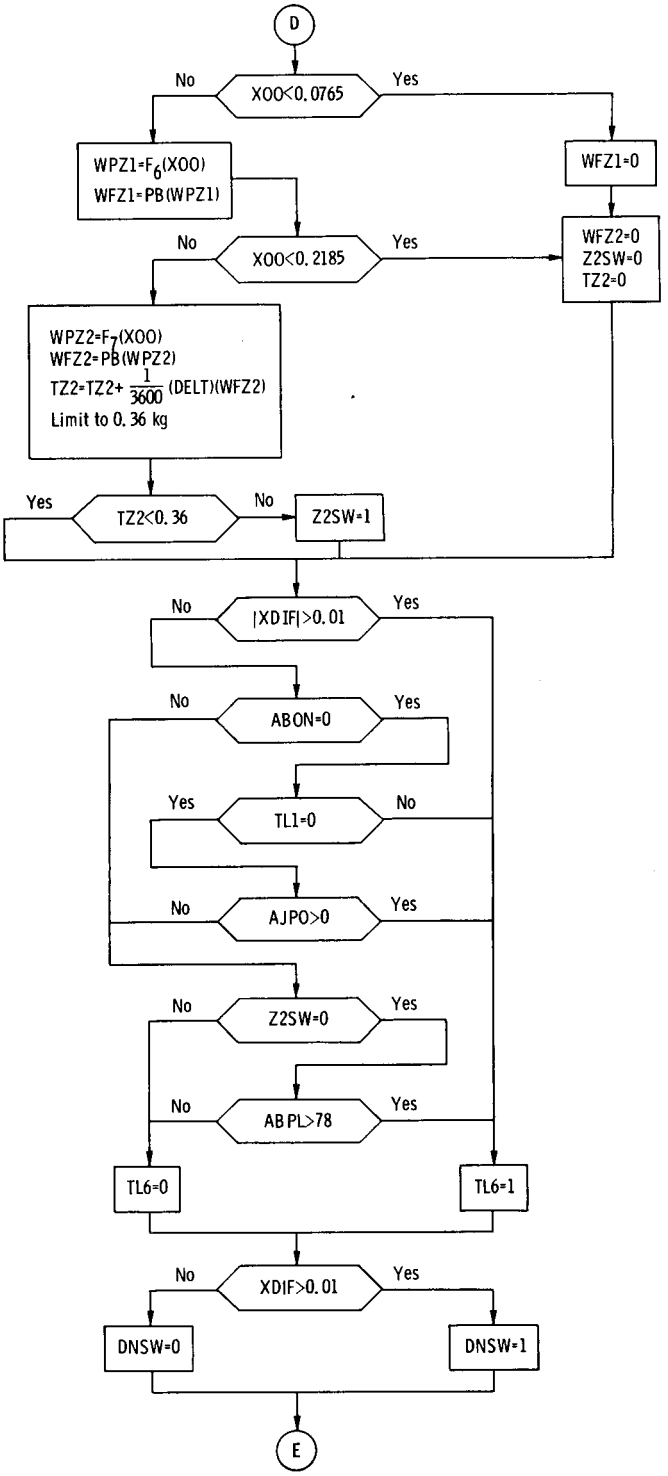
D
No
XOO<0.0765
Yes
WPZ1=F6(XOO)
WFZ1=PB(WPZ1)
WFZ1=0
No
XOO<0.2185
Yes
WFZ2=0
Z2SW=0
TZ2=0
WPZ2=F7(XOO)
WFZ2=PB(WPZ2)
TZ2=TZ2+ 1/3600 (DELT)(WFZ2)
Limit to 0.36 kg
Yes
TZ2<0.36
No
Z2SW=1
No
|XDIF|>0.01
Yes
No
ABON=0
Yes
Yes
TL1=0
No
No
AJPO>0
Yes
No
Z2SW=0
Yes
No
ABPL>78
Yes
TL6=0
TL6=1
No
XDIF>0.01
Yes
DNSW=0
DNSW=1
E

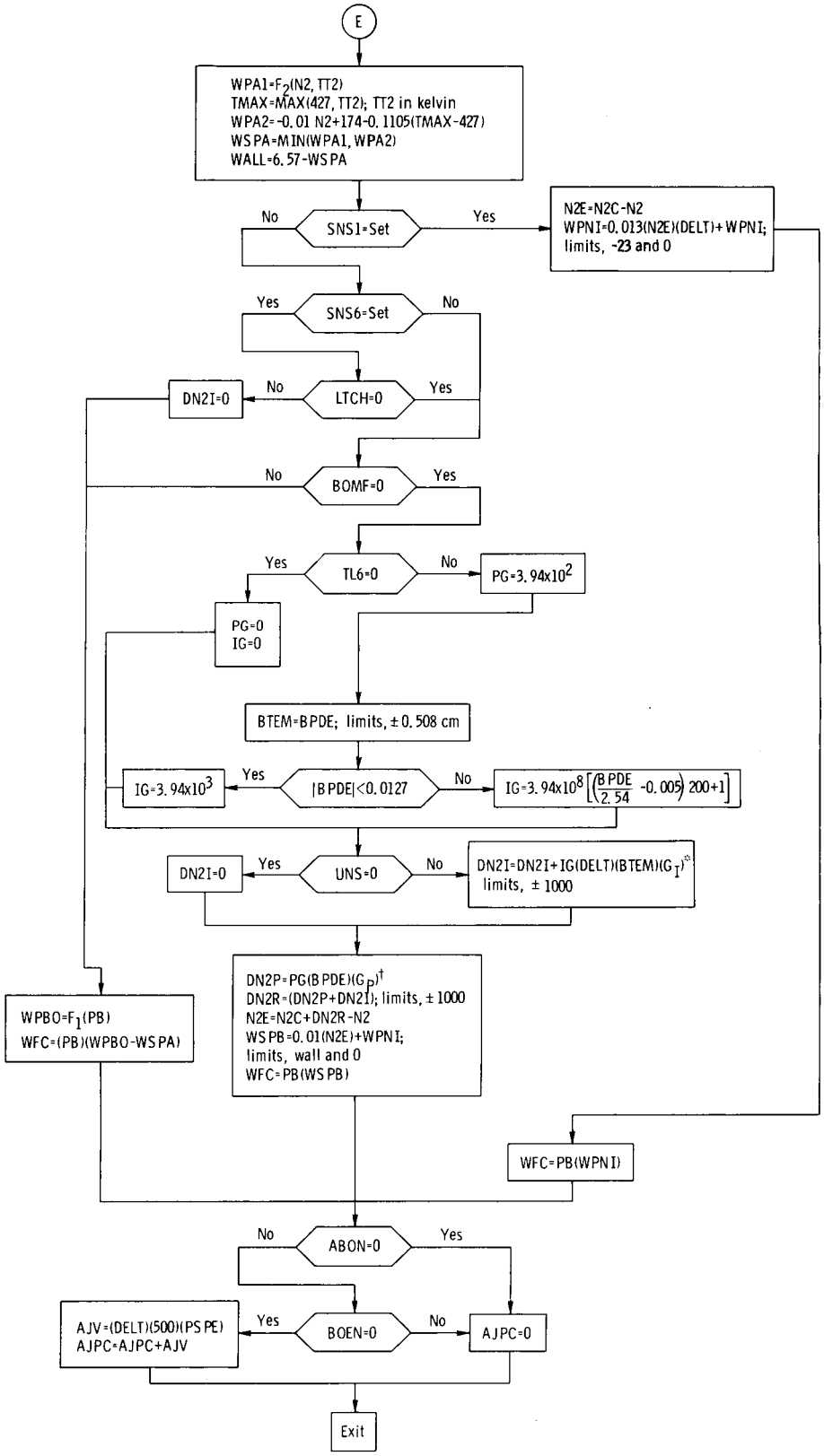

*G_I = 1/8 for 80-hertz-bandwidth doors; G_I = 1/4 for 10-hertz-bandwidth doors.

†G_P = 1/4 for 80-hertz-bandwidth doors; G_P = 1/2 for 10-hertz-bandwidth doors.

Inlet Control Schedules

(1) Function F_{I1}: Schedule of the $p_{1.1}$ command as a function of spike position with the inlet started, shown in figure 24(b)

(2) Function F_{I2}: Schedule of the $p_{1.1}$ command as a function of spike position with the inlet unstarted, shown in figure 24(a)

Engine and Augmentor - Exhaust-Nozzle Control Schedules

(1) Function F_0: Table lookup of function $1/\sqrt{\theta_2}$

(2) Function F_1: Table lookup of engine blowout derichment schedule, Bendix Corporation curve ECD-863-17329R

(3) Function F_2: Table lookup of the engine acceleration limit valve of the ratio of fuel flow to combustor pressure, Pratt & Whitney Aircraft curve 221721

(4) Function F_3: Table lookup of engine fan suppression schedule (experimentally determined curve), which is shown in figure 41

(5) Function F_5: Table lookup of augmentor power level schedule as a function of PLA, which is shown in figure 42

(6) Function F_6: Table lookup of zone 1 fuel flow schedule, which is shown in figure 43

(7) Function F_7: Table lookup of zone 2 fuel flow schedule, which is shown in figure 44

Digital Integrated Control Logic Symbols

ABON=1	zone 1 light-off
BOEN=1	blowout detected for exhaust nozzle control
BOMF=1	blowout detected for main fuel control
DNSW=1	reducing augmentor fuel flow demand
LTCH=1	spike extended beyond design
RECL=1	control in restart mode
SNS0=Set	inlet control operating
=Reset	inlet control reset to initial conditions
SNS1=Set	main fuel control on startup loop
=Reset	main fuel control operating

SNS6=Set	engine control derichment during inlet unstart (blowout logic tripped)
=Reset	blowout logic not activated by unstart
TL1=1	augmentor power level angle calling for zone 1 to be lit
TL2=1	augmentor power level angle calling for zone 2 to be lit
TL6=1	transient condition exists in augmentor
UNS=1	inlet unstarted
Z2SW=1	zone 2 light-off

Inlet Control Symbols

ABON	augmentor control light-off logic signal
BPDB	temporary storage
BPDC	bypass door output to servomechanism, cm
BPDE	bypass door error to engine control, cm
DEL	temporary storage
DPRI	integral control output, cm
DPRP	proportional control output, cm
F_{I1}, F_{I2}	inlet control schedules
HL	higher limit (S4BR control), cm
IGI	integral control gain, $cm/(N/cm^2\text{-sec})$
LL	lower limit (S4BR control), cm
PGI	proportional control gain, $cm/(N/cm^2)$
PRER	pressure error, N/cm^2
RECL	logic signal indicating restart complete
SPOC	spike position output to servomechanism, cm
SPOS	measured spike position, cm
SSSB	pressure command-time ramp initial condition, N/cm^2
S4BR	measured pressure, N/cm^2
S7	bypass door setpoint (sampled), cm
TIME	inlet sampling interval, sec

UNS	unstart signal
XSC	pressure command, N/cm^2
XSCP	pressure command, N/cm^2
XSC1	pressure command, N/cm^2
XSC2	pressure command (sampled), N/cm^2
XSC3	pressure command, N/cm^2

Engine and Augmentor - Exhaust-Nozzle Control Symbols

ABON	augmentor control light-off logic signal
ABPL	augmentor power lever angle, deg
AJPC	exhaust nozzle position output to servocontrol, deg
AJPO	measured exhaust nozzle area, deg
AJV	temporary storage
BOEN	augmentor control blowout logic signal
BOMF	augmentor blowout logic signal to main fuel control
BPDE	bypass door error, cm
BTEM	bypass door error (modified), cm
CORN	corrected speed, rpm
DELT	engine sampling interval, sec
DELP	specified hysteresis, deg
DNSW	logic level indicating reduction in augmentation request
DN2I	bypass reset integral control output, rpm
DN2P	bypass reset proportional control output, rpm
DN2R	bypass reset control output, rpm
DPSP	delayed suppression error difference
$F_0, F_1, F_2,$ F_3, F_5, F_6, F_7	engine control schedules
G_I	control integral gain modifier
G_P	control proportional gain modifier

IG	bypass reset integral gain, rpm/cm-sec
LABP	augmentor power level angle (hysteresis), deg
LODT	augmentor control light-off signal
LPAB	augmentor power level angle (hysteresis), deg
LTCH	intermediate logical result storage
N2	measured speed, rpm
N2C	speed command (sampled), rpm
N2E	speed error, rpm
PB	measured combustor pressure, N/cm^2
PG	bypass reset proportional gain, rpm/cm
PLA	measured power lever angle, deg
PSEE	suppression ratio error
PSP	measured suppression ratio
PSPD	suppression ratio command
PSPE	suppression ratio error (modified)
PSPR	suppression ratio command (modified)
PT7	measured duct pressure, N/cm^2
RL	rate of limit of augmentor power level
SNS	computer sense switch
SPOS	measured spike position, cm
TEMP	temporary storage
THET	temperature correction, $1/\sqrt{\theta}$
TL1	power lever zone 1 light-off command
TL2	power lever zone 2 light-off command
TMAX	maximum value of TT2 or 427 K
TT2	measured temperature, ^{o}C
TZ2	zone 2 fill, kg
UNS	unstart signal
WALL	main combustor ratio limit, $(kg/hr)/(N/cm^2)$
WFC	main fuel output to servocontrol, kg/hr

WFZ1 zone 1 fuel flow, kg/hr

WFZ2 zone 2 fuel flow, kg/hr

WPA1 main combustor acceleration (partial), $(kg/hr)/(N/cm^2)$

WPA2 main combustor acceleration (partial), $(kg/hr)/(N/cm^2)$

WPBO blowout ratio of fuel flow to pressure, $(kg/hr)/(N/cm^2)$

WPNI shuttle loop ratio of fuel to pressure, $(kg/hr)/(N/cm^2)$

WPZ1 ratio of fuel to pressure (zone 1), $(kg/hr)/(N/cm^2)$

WPZ2 ratio of fuel to pressure (zone 2), $(kg/hr)/(N/cm^2)$

WSPA main combustor acceleration schedule ratio, $(kg/hr)/(N/cm^2)$

WSPB ratio of fuel to pressure (main), $(kg/hr)/(N/cm^2)$

XDIF augmentor power level error

XREQ required augmentor power level

XOO actual augmentor power level

Z2SW augmentor zone 2 light-off signal

REFERENCES

1. Flanders, Theodore A.: The Inlet/Engine Control Vector. Paper 70-696, AIAA, June 1970.

2. Bayati, J. E.; and Tyson, R. M.: Propulsion Flow Transient Accommodation Control. Paper 70-694, AIAA, June 1970.

3. Cole, Gary L.; Neiner, George H.; and Wallhagen, Robert E.: Coupled Supersonic Inlet-Engine Control Using Overboard Bypass Doors and Engine Speed to Control Normal Shock Position. NASA TN D-6019, 1970.

4. Paulovich, Francis J.; Neiner, George H.; and Hagedorn, Ralph E.: A Supersonic Inlet-Engine Control Using Engine Speed as a Primary Variable for Controlling Normal Shock Position. NASA TN D-6021, 1971.

5. Marvin, I. E.; and Schilling, T. L.: Analysis for Special Engine Controls Requirements for Unstart-Restart of Mixed Compression Inlets. Proc. of Air Force Airframe Propulsion Compatibility Symp., AFAPL-TR-69-103, 1970, pp. 689-701. (Available to qualified requestors from DDC; others from Office of Director of Defense Research and Engineering, Attn: OADET, Washington, D.C. 20301.)

6. Neiner, George H.; Cole, Gary L.; and Arpasi, Dale J.: Digital-Computer Normal-Shock-Position and Restart Control of a Mach 2.5 Axisymmetric Mixed-Compression Inlet. NASA TN D-6880, 1972.

7. Arpasi, Dale J.; Cwynar, David S.; and Wallhagen, Robert E.: Sea-Level Evaluation of Digitally Implemented Turbojet Engine Control Functions. NASA TN D-6936, 1972.

8. Bentz, Charles E.; and Zeller, John R.: Integrated Propulsion Control System Program. Paper 730359, SAE, Apr. 1973.

9. Baumbick, Robert J.; Wallhagen, Robert E.; Neiner, George H.; and Batterton, Peter G.: Dynamic Response of Mach 2.5 Axisymmetric Inlet with 40 Percent Supersonic Internal Area Contraction. NASA TM X-2833, 1973.

10. Arpasi, Dale J.; Zeller, John R.; and Batterton, Peter G.: A General Purpose Digital System for On-Line Control of Airbreathing Propulsion Systems. NASA TM X-2168, 1971.

11. McKinney, John S.: Simulation of Turbofan Engine. Part I: Description of Method and Balancing Technique. AFAPL-TR-67-125-PT-1, Air Force Systems Command Aero Propulsion Laboratory (AD-825197), 1967.

12. Szuch, John R.; and Bruton, William M.: Real-Time Simulation of TF30-P-3 Turbofan Engine Using Hybrid Computer. NASA TM X-3106, 1974.

TABLE I. - DIGITAL SYSTEM CAPABILITIES

Digital computer	
Magnetic core memory size, words	16 384
Word length, bits plus parity	16
Memory cycle time, nsec	750
Add time, μsec	1.5
Multiply time, μsec	4.5
Divide time, μsec	8.25
Load time, μsec	1.5
Indirect addressing	Infinite
Indexing	Total memory
Priority interrupts	28 separate levels
Index registers	2
Interval timers	2
Analog acquisition unit	
Overall sample rate (maximum, kHz)	20
Resolution of digital data, bits	12 (plus sign)
Output code	Two's complement
Number of channels	64
Input range, V full scale	±10
Conversion time, μsec	38
Total error with calibration, percent	0.073
Analog output unit	
Total number of digital-to-analog conversion channels (DAC)	26
Resolution (13 bit DAC; 10 channels), bits	12 (plus sign)
Accuracy (13 bit DAC), percent of full scale	±0.05
Resolution (12 bit DAC; 16 channels), bits	11 (plus sign)
Accuracy (12 bit DAC), percent of full scale	±0.1
Output voltage range, V full scale	±10
Slew rate, V/μsec	1
Priority interrupt processor	
Number of channels	10
Input voltage range, V	±10
Computer switching	Trigger on rise or fall
Comparator hysteresis, mV	Adjustable from 35 to 650
Comparator output, V	7

TABLE II. - PRIORITY INTERRUPT STRUCTURE AND FUNCTIONS

Priority level	Interrupt initiated by-	Interrupt function
1	Inlet interval timer	(1) Reinitialize inlet timer (2) Start inlet data transfer if block data transfer not already in progress (3) Set inlet data request latch if block data transfer in progress
2	Unstart comparator	Set unstart latch for interrogation by control (inlet unstarts)
3	Unstart comparator	Reset unstart latch of interrogation by control (inlet restarts)
4	Engine interval timer	(1) Reinitialize engine timer (2) Start engine data transfer if block data transfer not already in progress (3) Set engine data request latch if block data transfer in progress
5	Block data transfer completion	(1) Check data request latches (2) Establish request priority and start appropriate data transfer (3) Sequence engine data transfer (4) Initiate inlet control interrupt when inlet data in memory (5) Initiate engine control interrupt when engine data in memory
6	Level 5 output to DAC	Compute inlet control
7	Level 5 output to DAC	Compute engine control

TABLE III. - STEADY-STATE NONAUGMENTED

OPERATING CONDITIONS

Bypass door position	Closed
Throat exit static pressure, $p_{1.1}$, N/cm^2	5.50
Engine total corrected airflow, kg/sec	70.8
Low-pressure-rotor speed, XNL, rpm	6570
High-pressure-rotor speed, XNH, rpm	11 719
Fan inlet pressure, P_2, N/cm^2	8.31
Low-pressure-compressor exit static pressure, $p_{2.2}$, N/cm^2	17.8
High-pressure-compressor exit static pressure, p_3, N/cm^2	49.4
Turbine discharge pressure, P_5, N/cm^2	8.75
Exhaust nozzle area, A_{T7}, m^2	0.349
Fuel flow, W_f, kg/hr	588

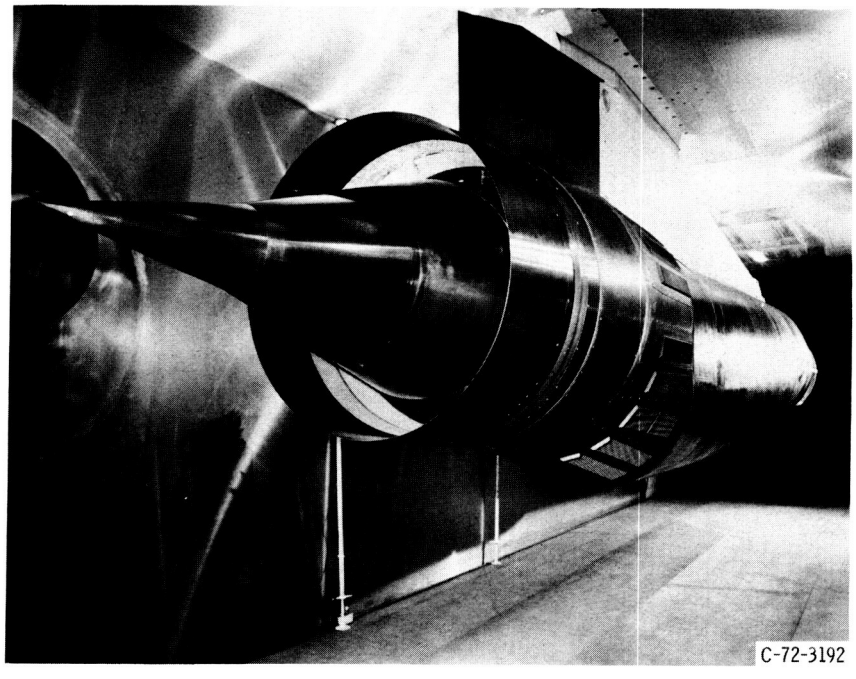

Figure 1. - Mixed-compression, Mach 2.5, axisymmetric, 45-percent-internal-supersonic-area-contraction inlet and TF30-P-3 augmented turbofan engine installed in 10- by 10-Foot Supersonic Wind Tunnel.

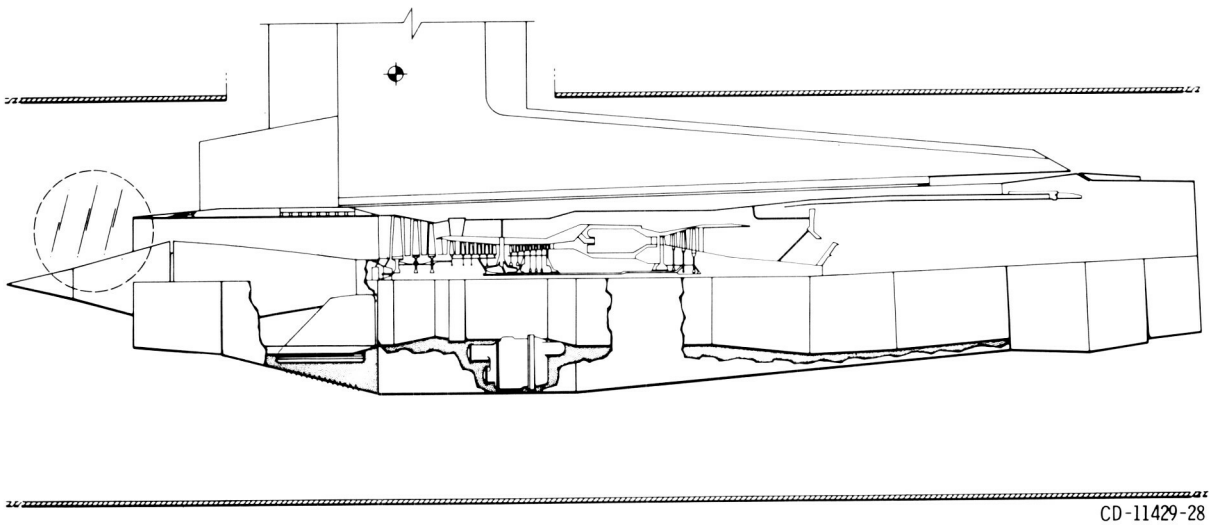

Figure 2. - Cross section of inlet and TF30-P-3 installed in 10- by 10-Foot Supersonic Wind Tunnel.

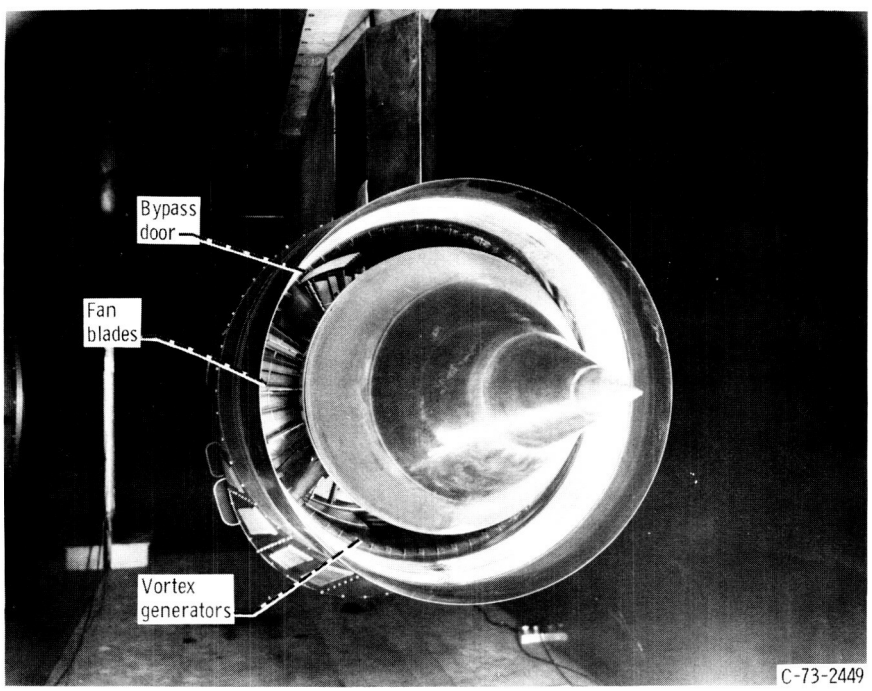

Figure 3. - View down throat of inlet showing TF30-P-3 fan.

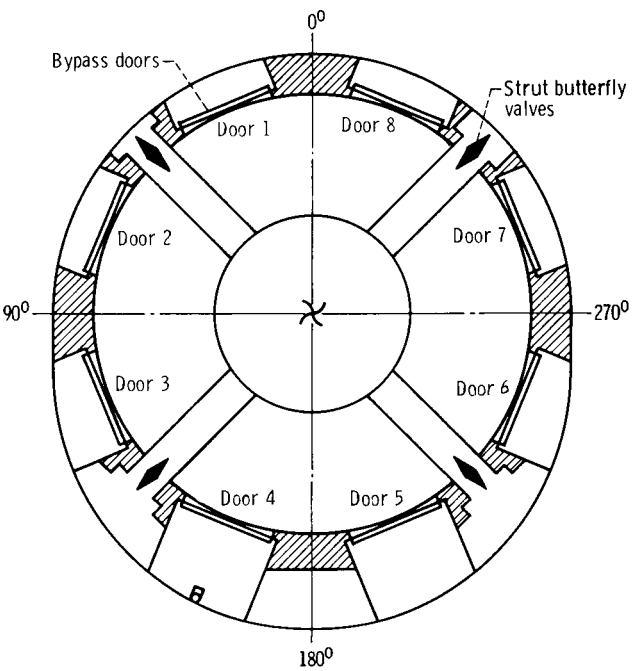

Figure 4. - View of inlet looking downstream showing bypass doors and centerbody bleed flow struts.

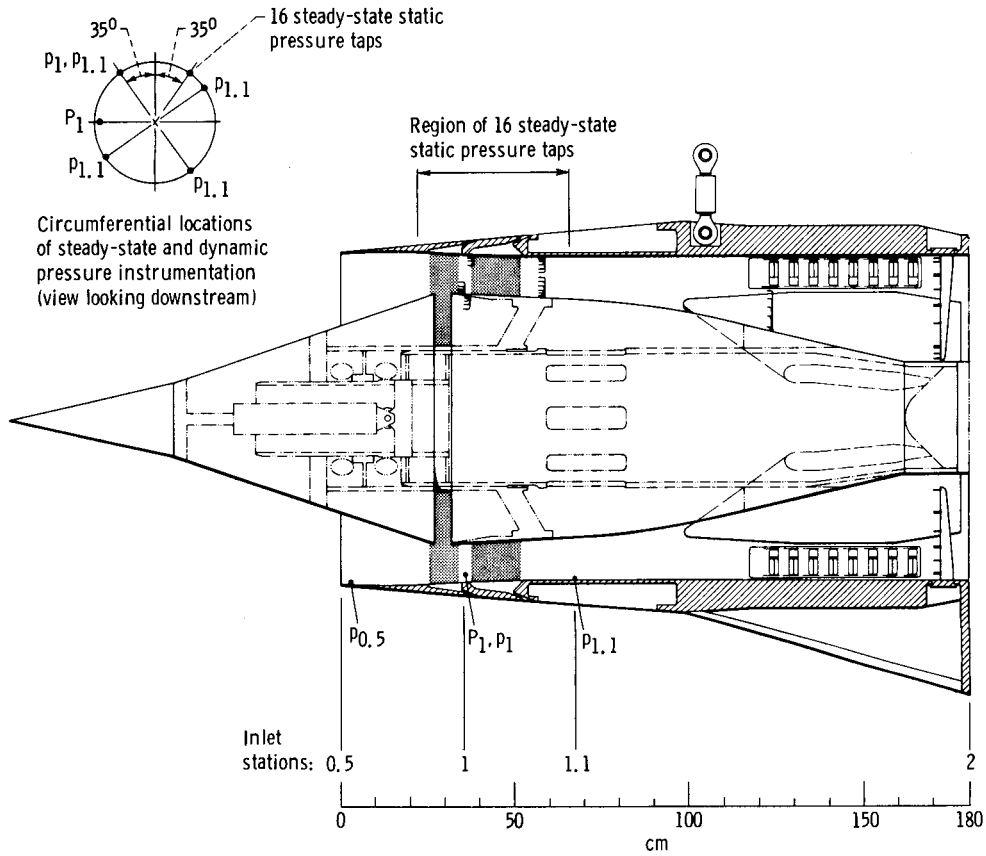

CD-11473-01

Figure 5. - Inlet stations and instrumentation locations.

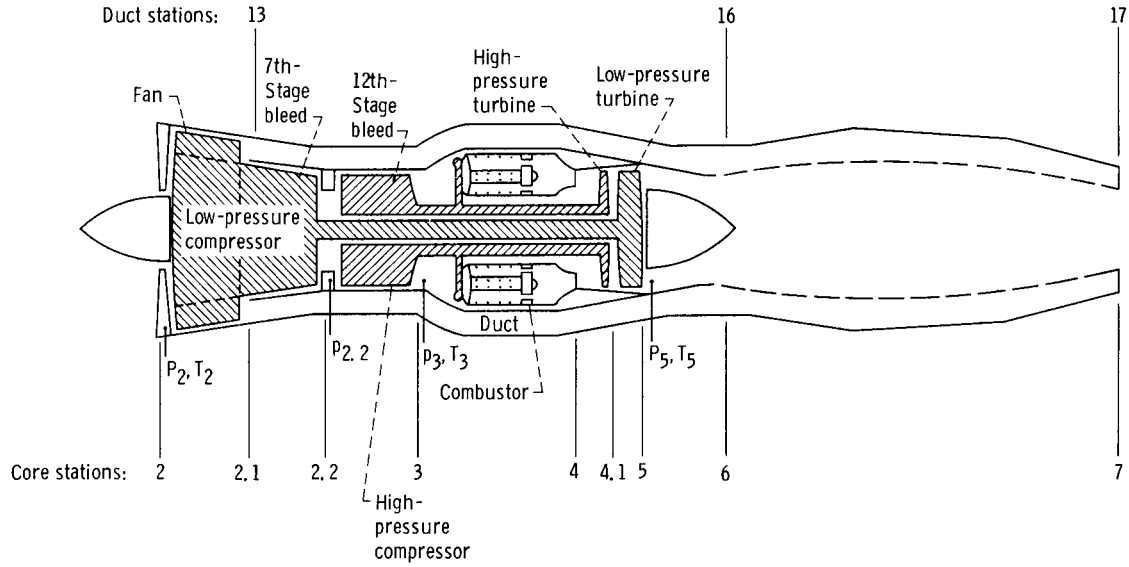

Figure 6. - Engine stations and instrumentation locations.

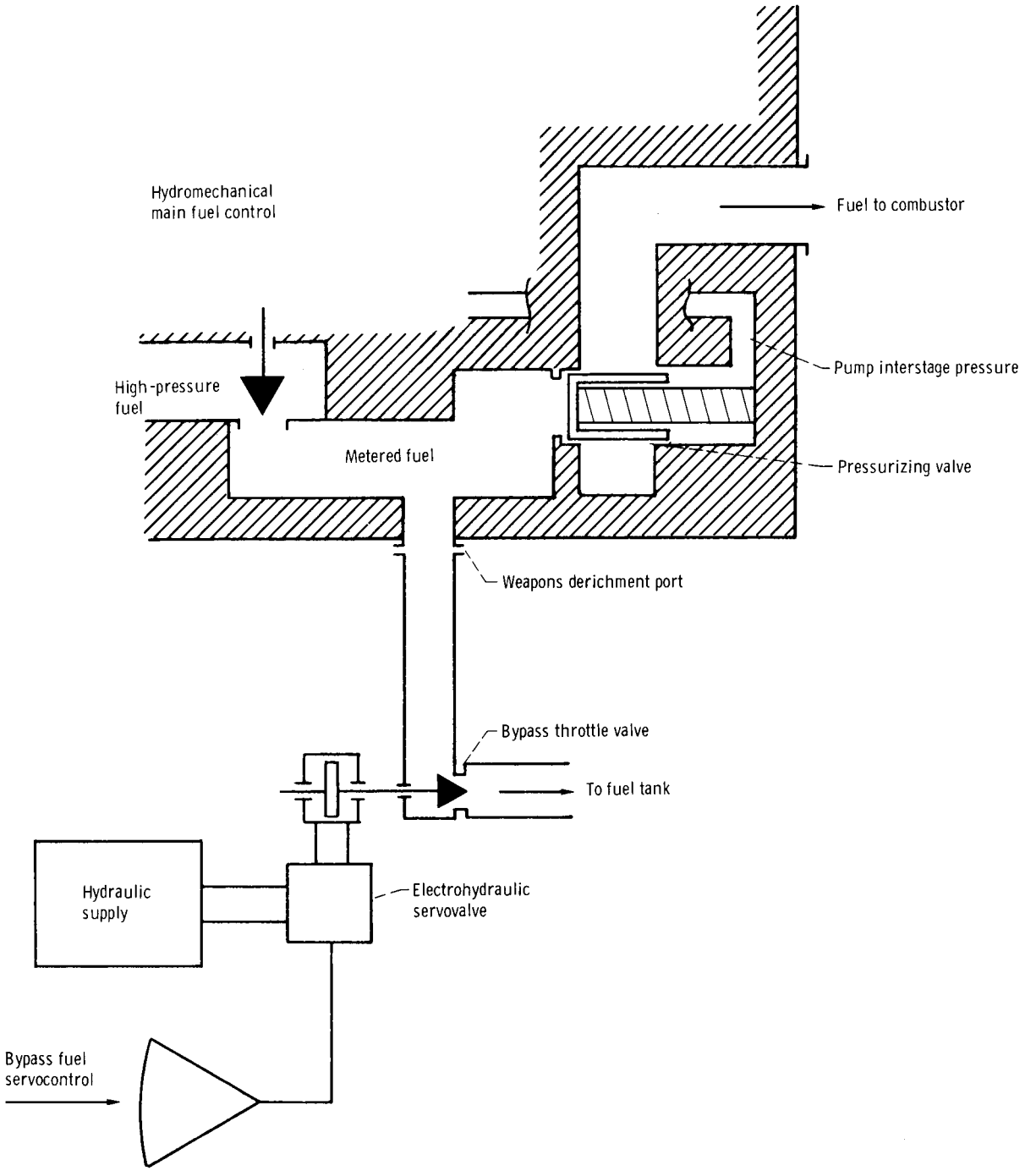

Figure 7. - Simplified schematic of main fuel control modification.

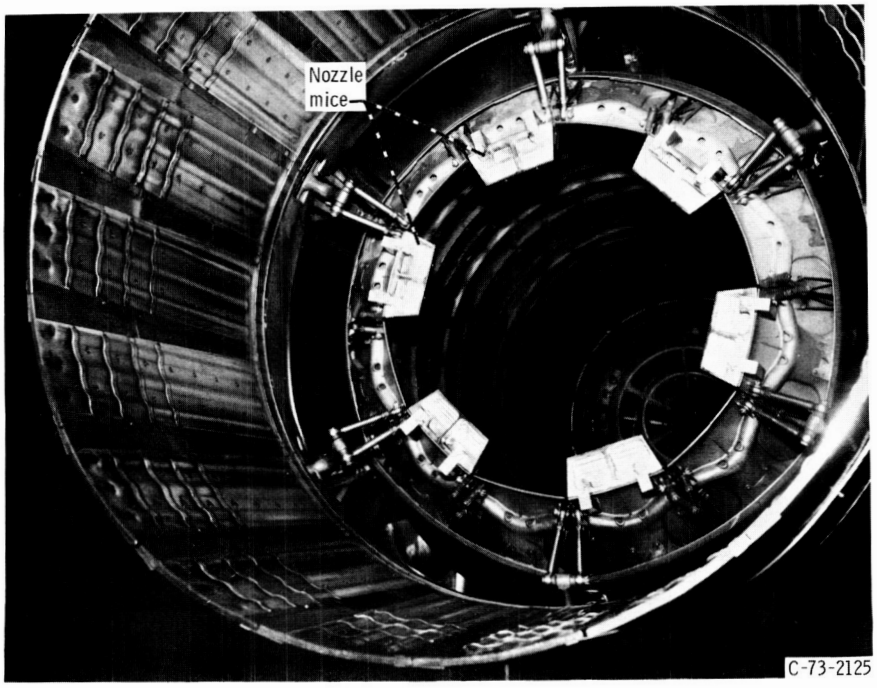

Figure 8. - TF30-P-3 exhaust nozzle showing location of "mice."

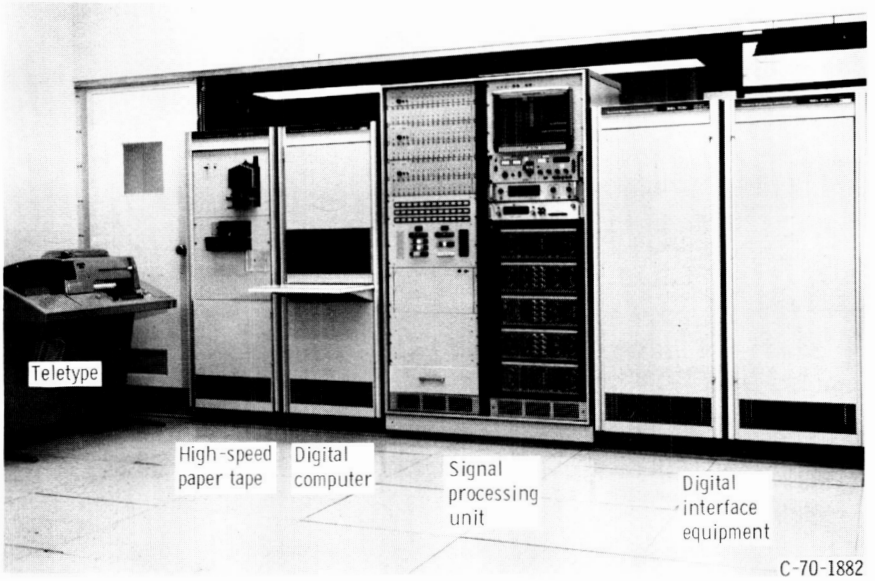

Figure 9. - Digital computer setup.

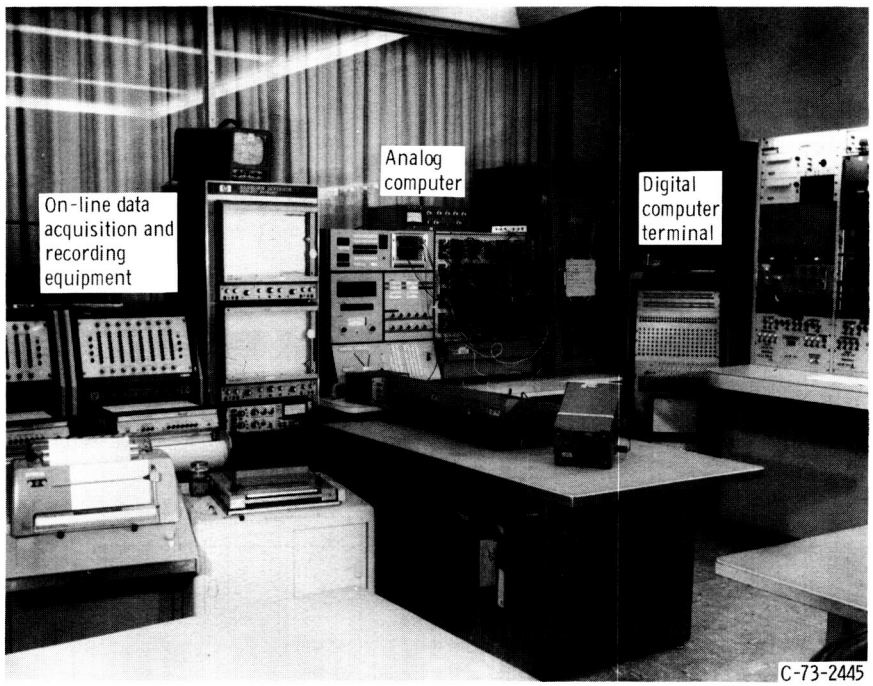

Figure 10. - View of 10- by 10-Foot Supersonic Wind Tunnel control room showing digital computer terminal and analog computer.

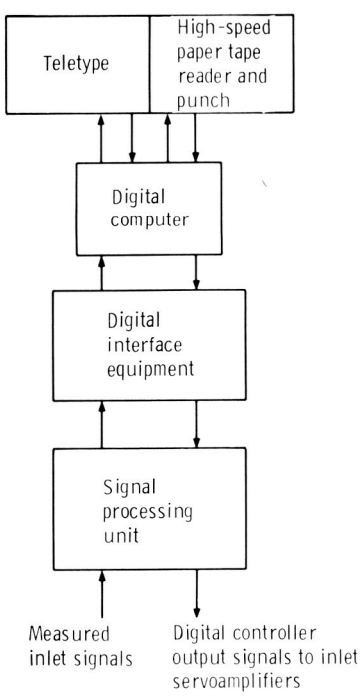

Figure 11. - Block diagram of digital computer setup.

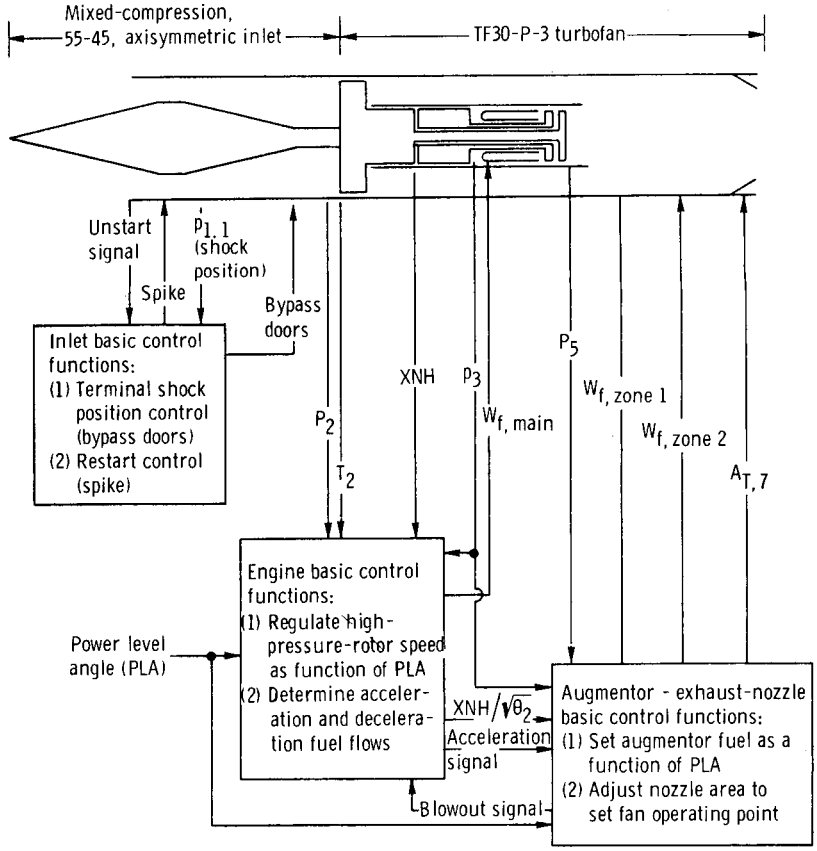

Figure 12. - Block diagram of basic control functions of nonintegrated supersonic propulsion system. (See appendix A for symbol definition.)

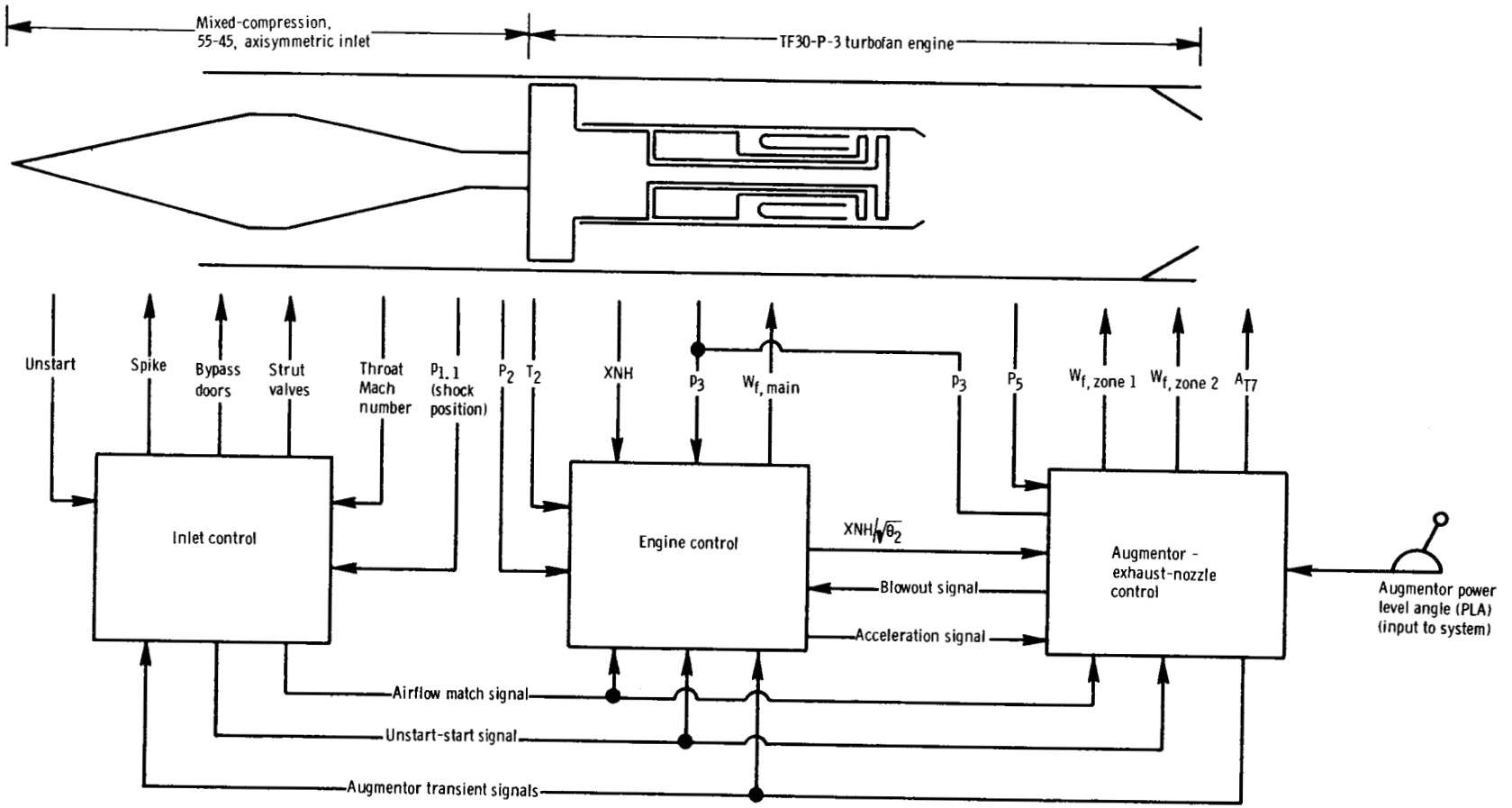

Figure 13. - Simplified block diagram of integrated supersonic propulsion control system. (See appendix A for symbol definition.)

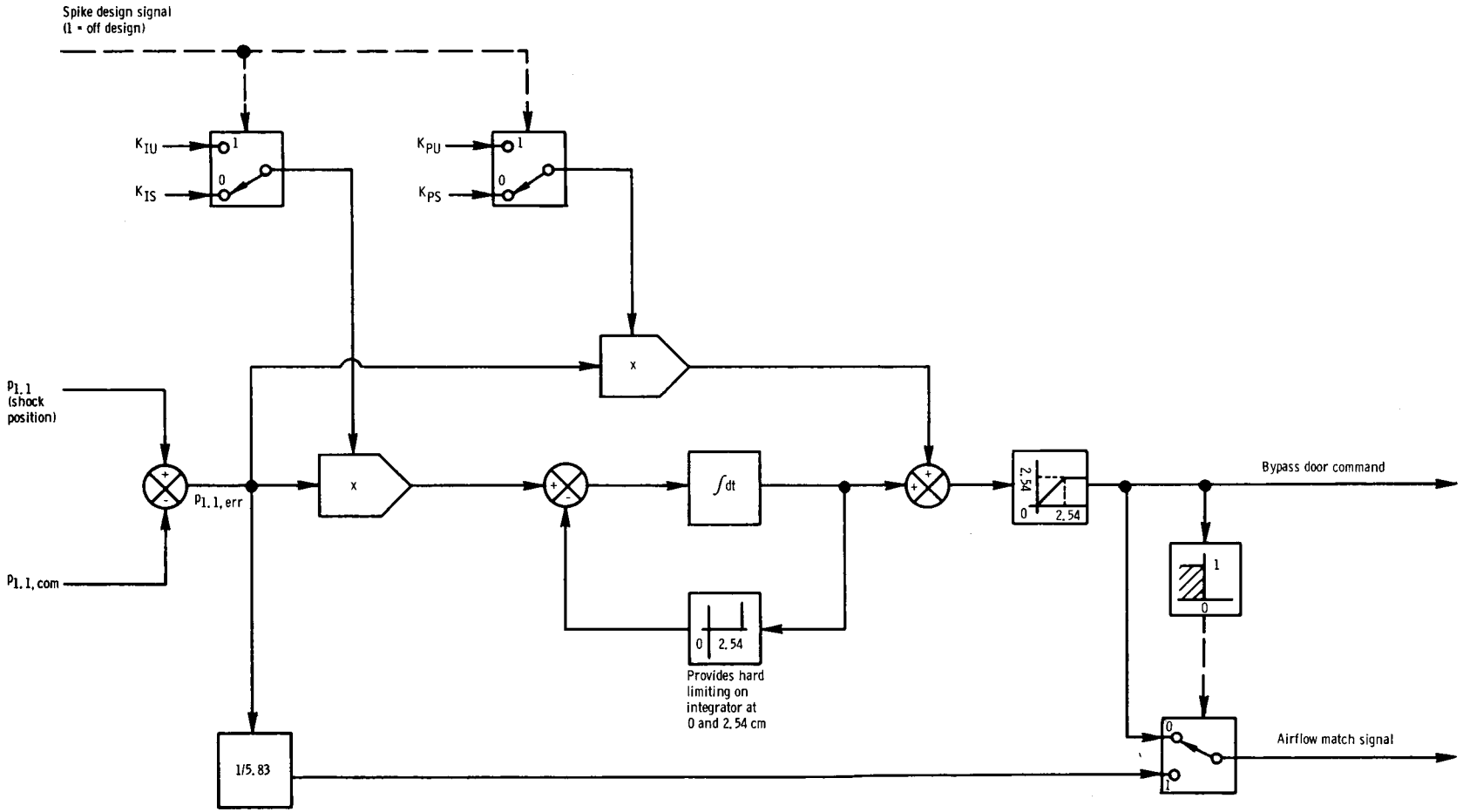

(a) Terminal shock control.

Figure 14. - Block diagram of digital integrated inlet terminal shock position and restart control. (See appendix A for symbol definition.)

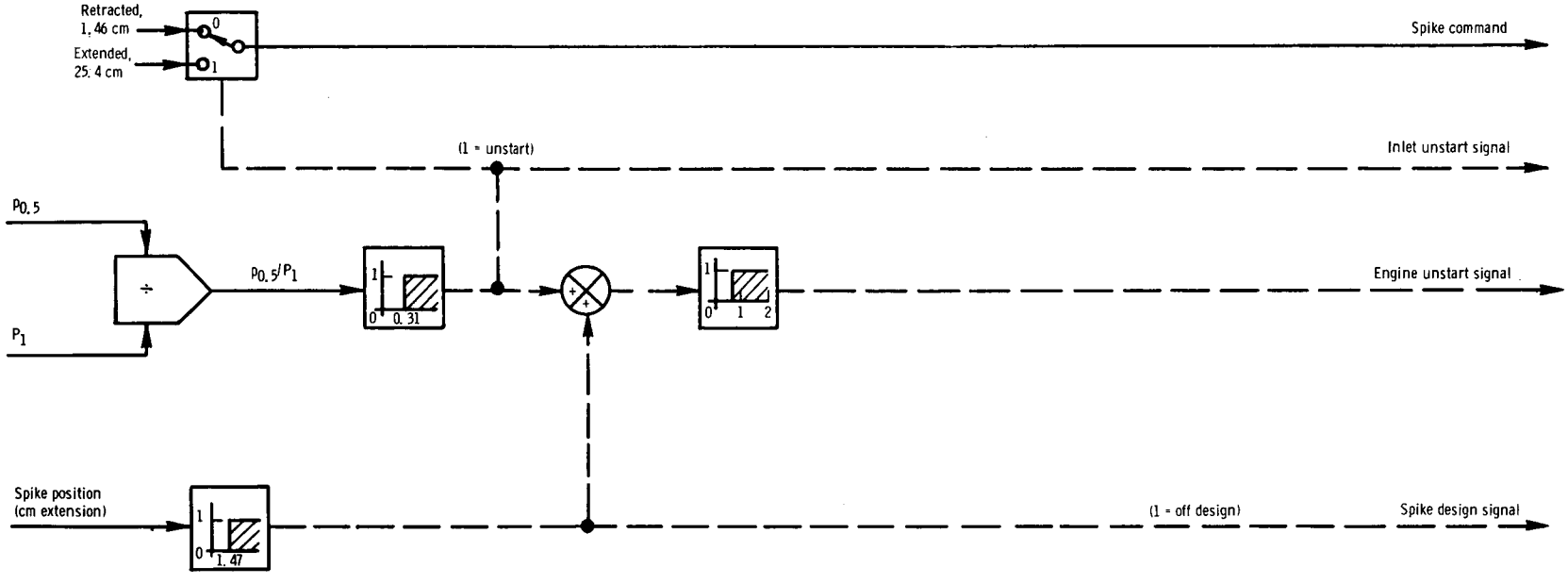

(b) Spike and restart control.

Figure 14. - Continued.

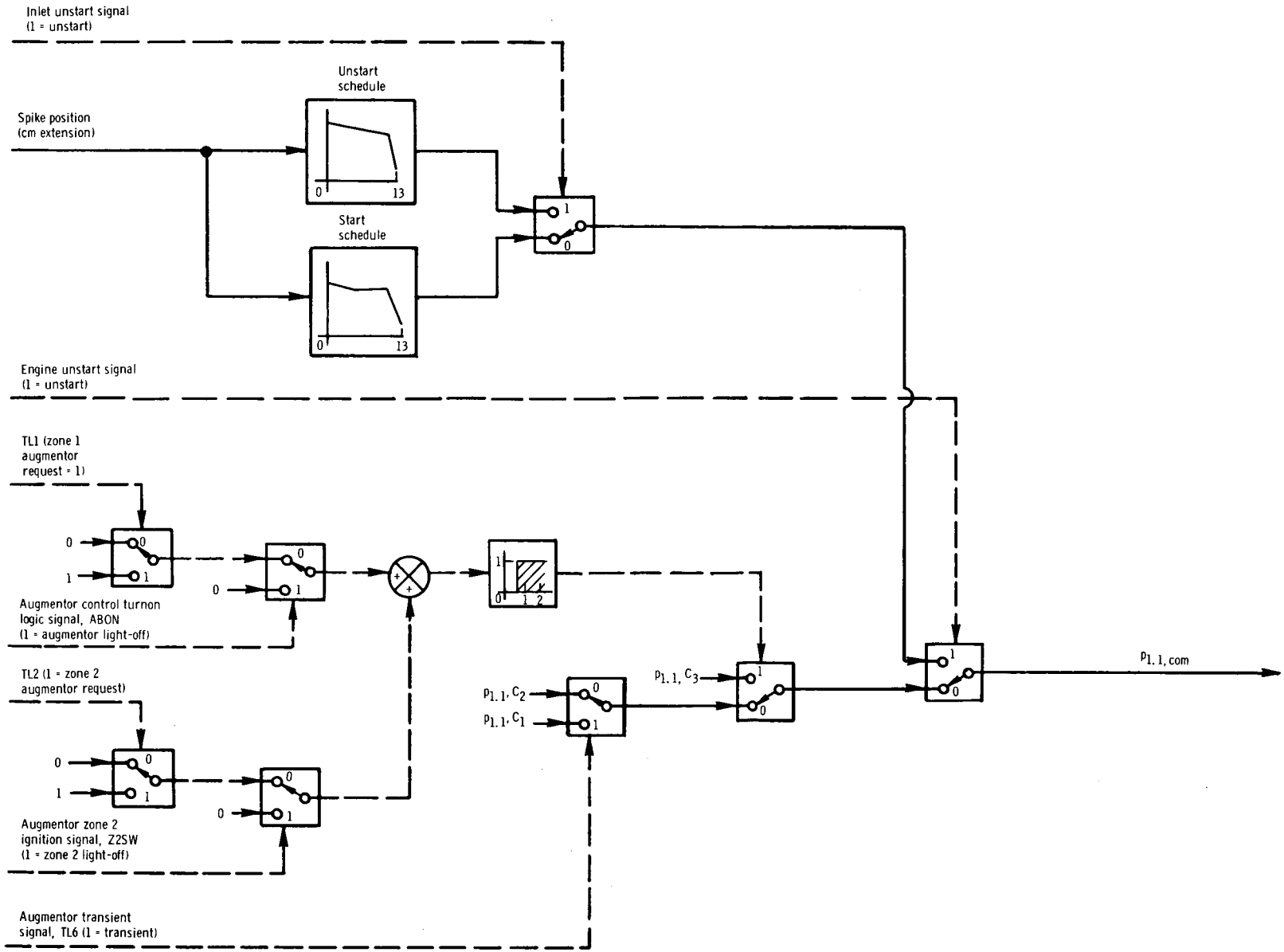

(c) Shock position command logic.

Figure 14. - Concluded.

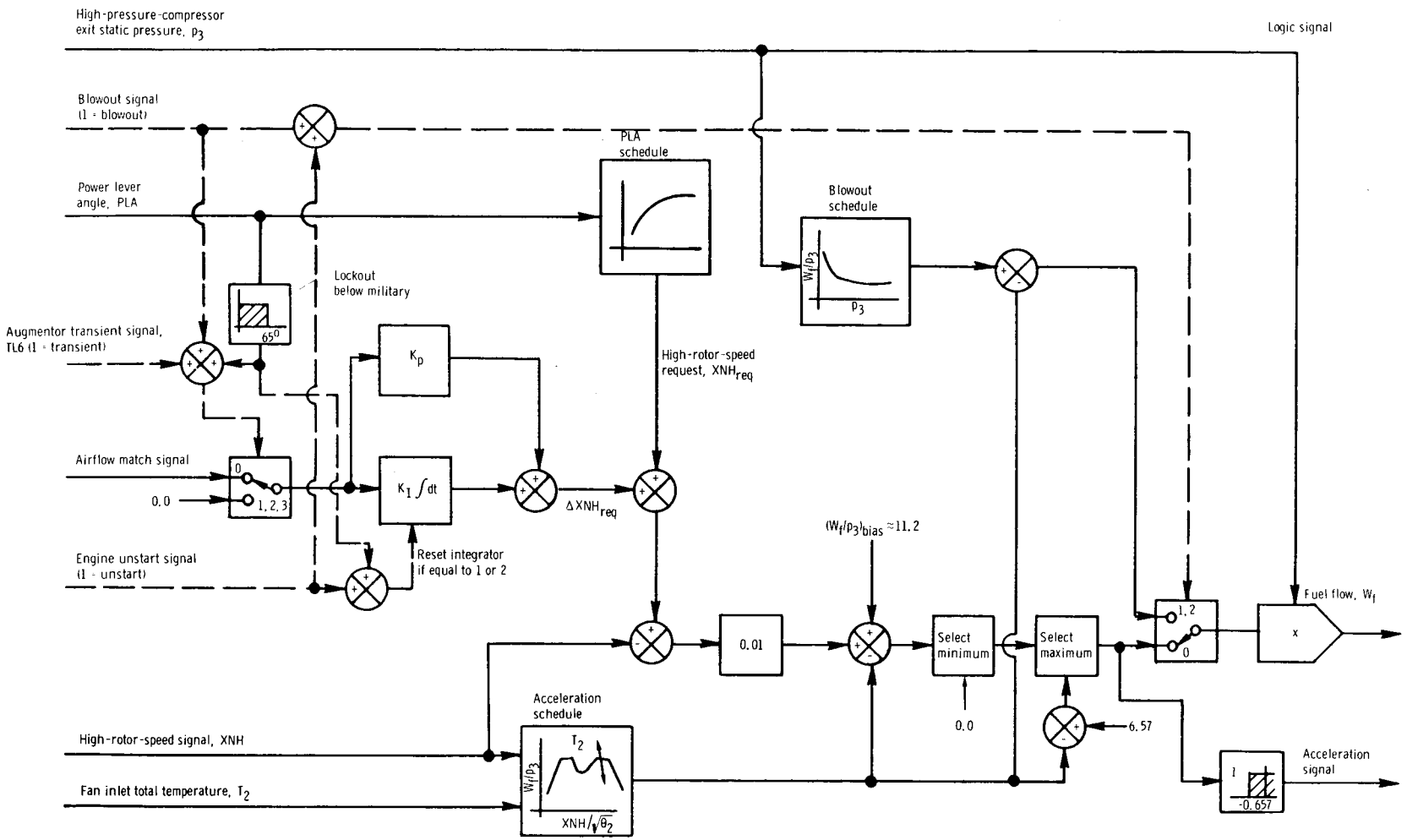

Figure 15. - Block diagram of digital integrated engine main fuel control. (See appendix A for symbol definition. PLA function shown for clarity, but not actually implemented. XNH_{req} was constant due to constant wind tunnel conditions.)

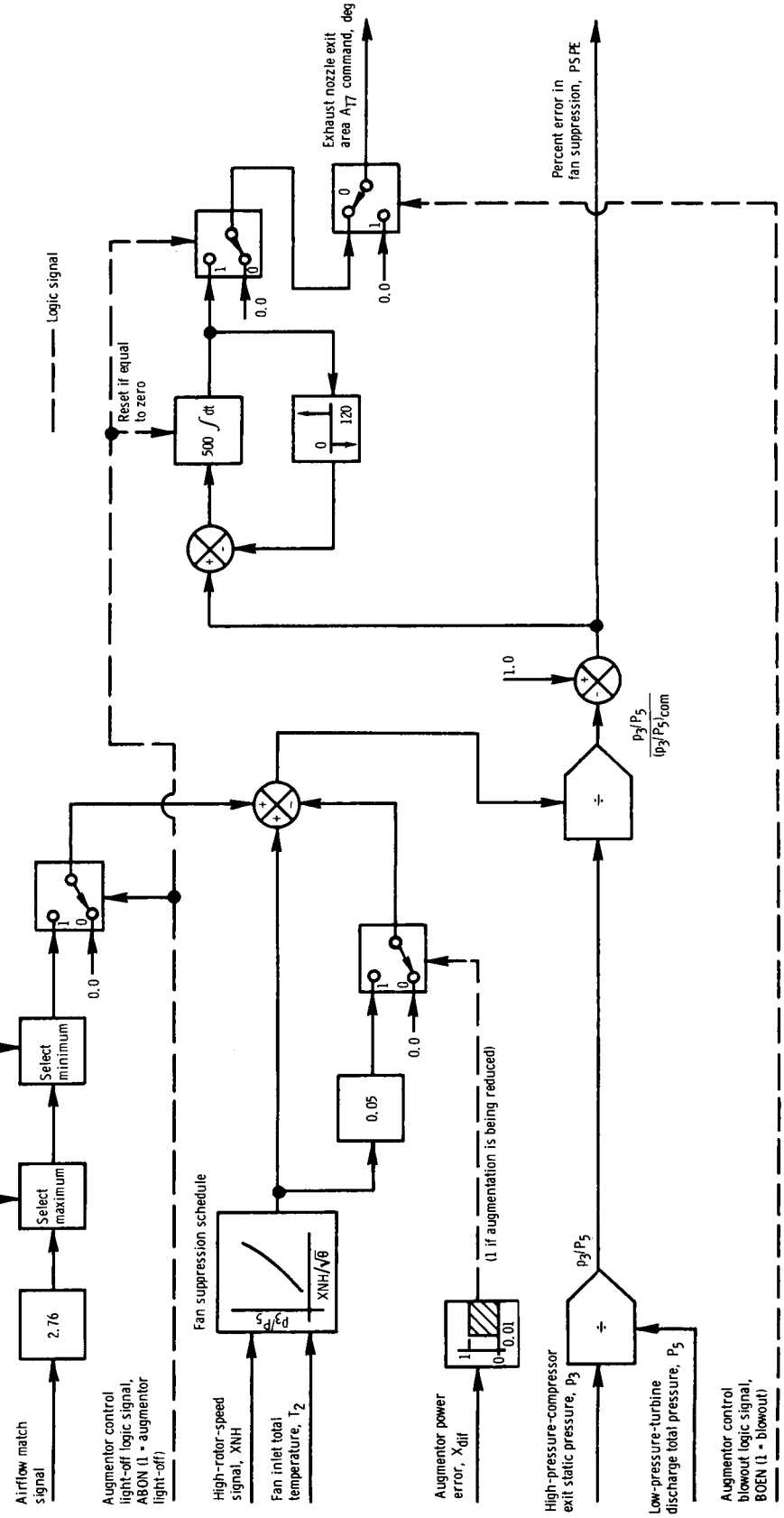

(a) Exhaust nozzle control.

Figure 16. - Block diagram of digital integrated augmentor and exhaust nozzle control. (See appendix A for symbol definition.)

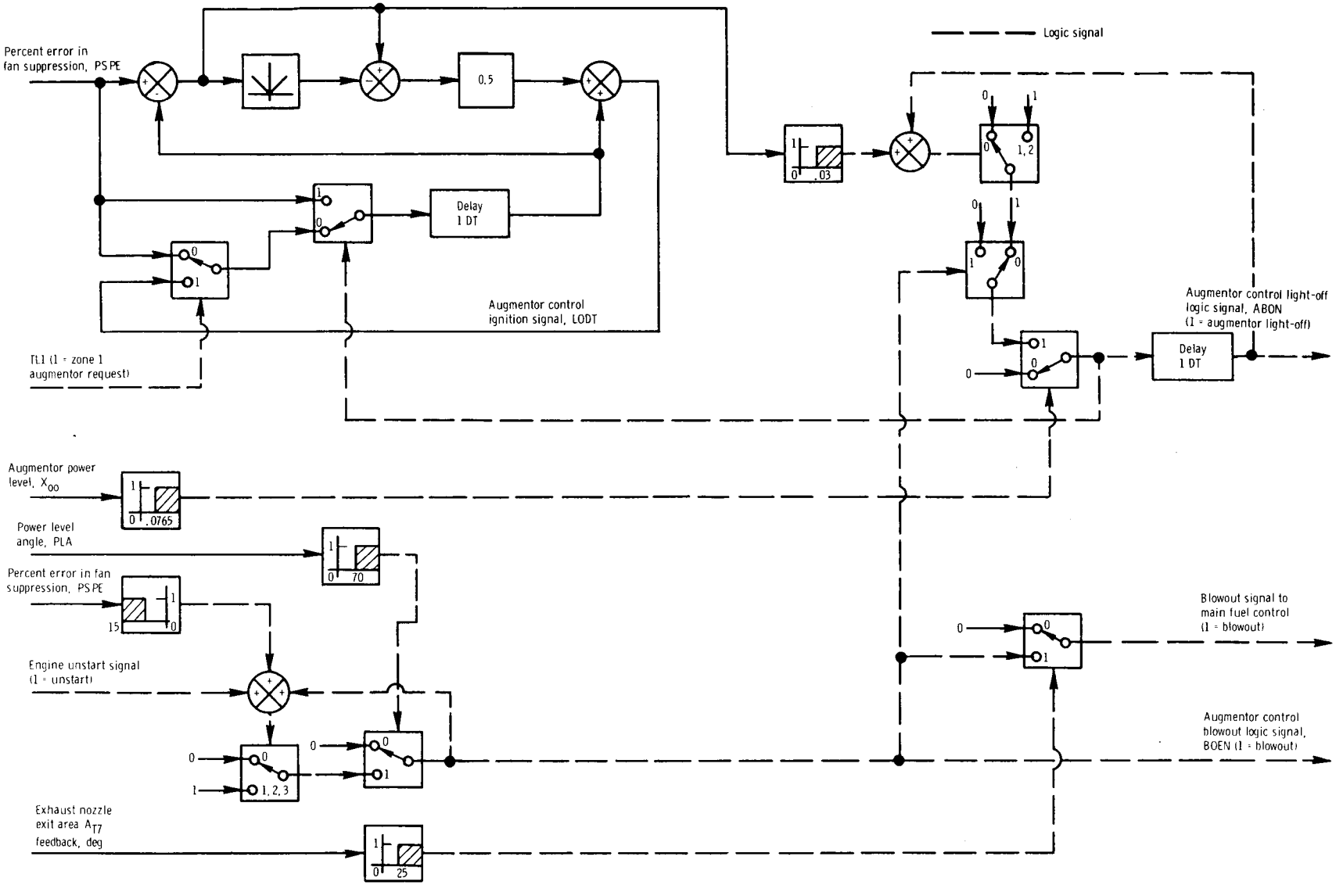

(b) Light-off and blowout detectors.

Figure 16. - Continued

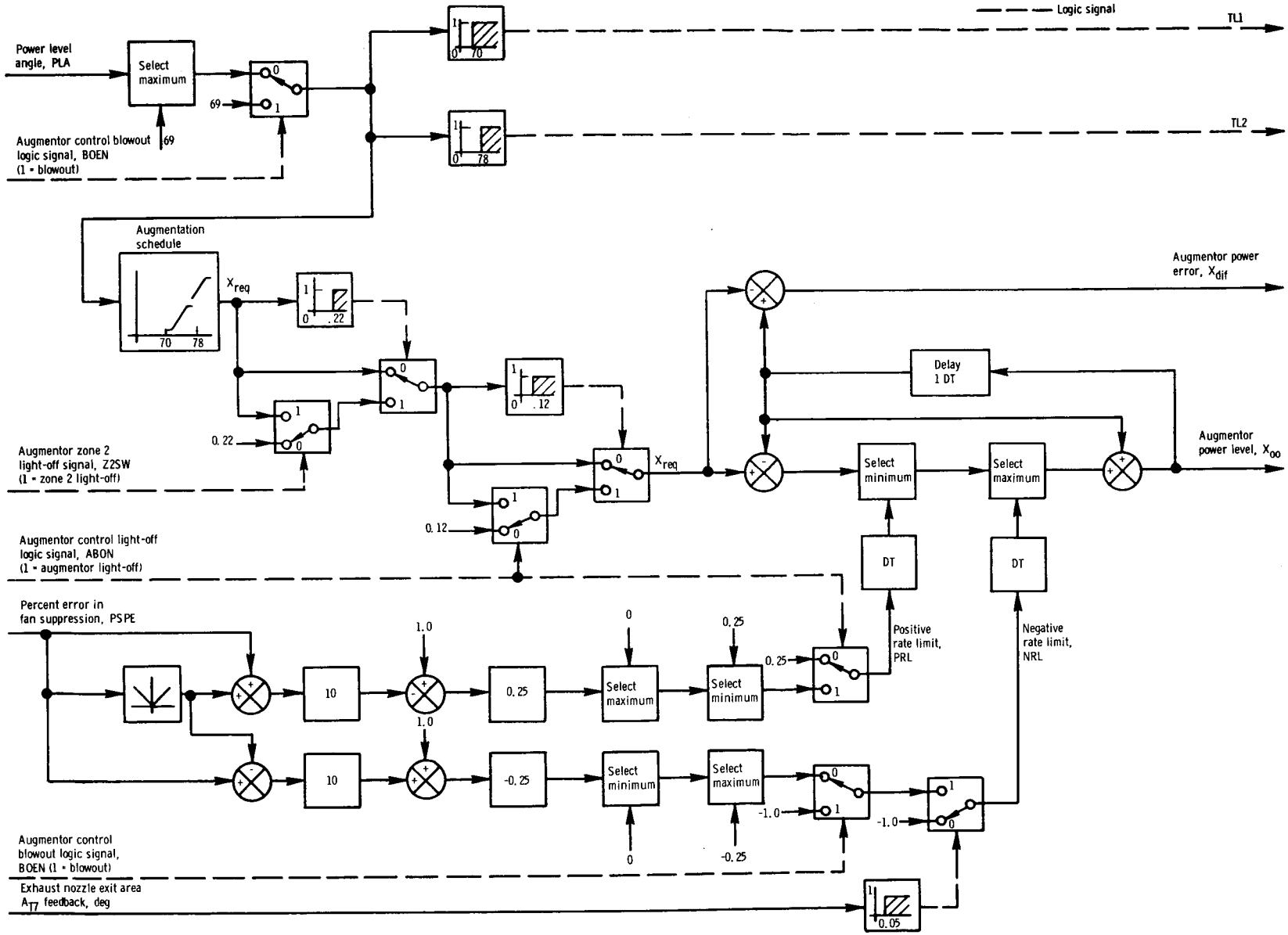

(c) Augmentor power level request logic.

Figure 16. - Continued

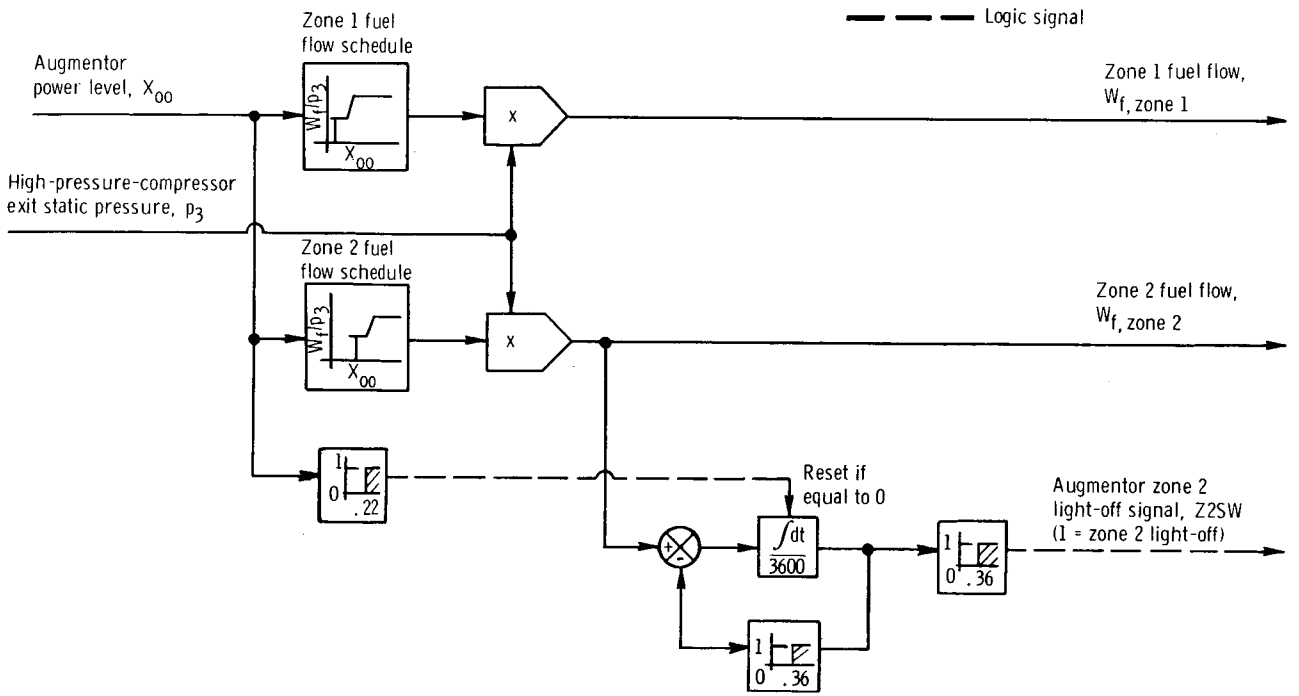

(d) Fuel flow schedules and zone 2 ignition detector.

Figure 16. - Continued.

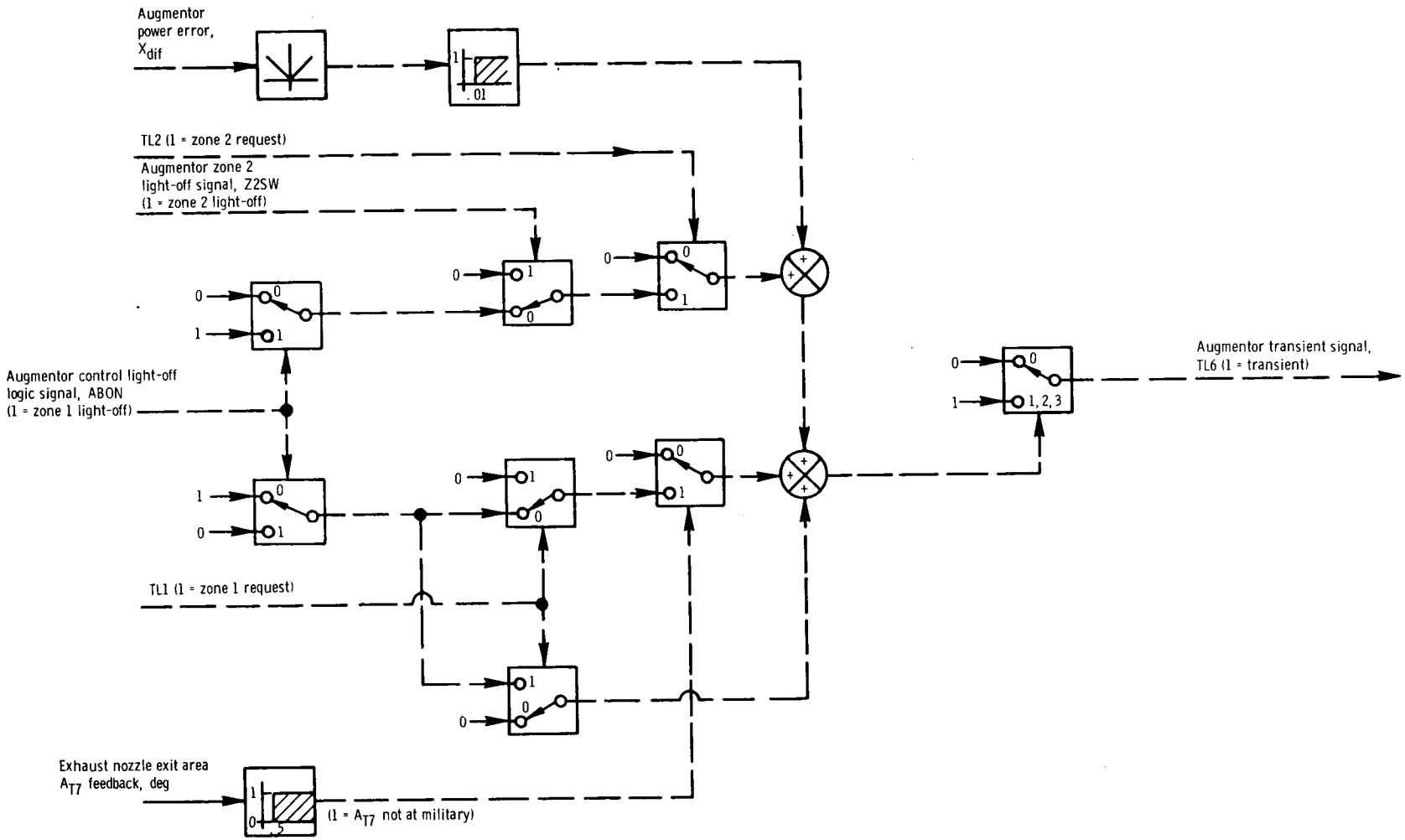

(e) Augmentor transient signal logic.

Figure 16. - Concluded.

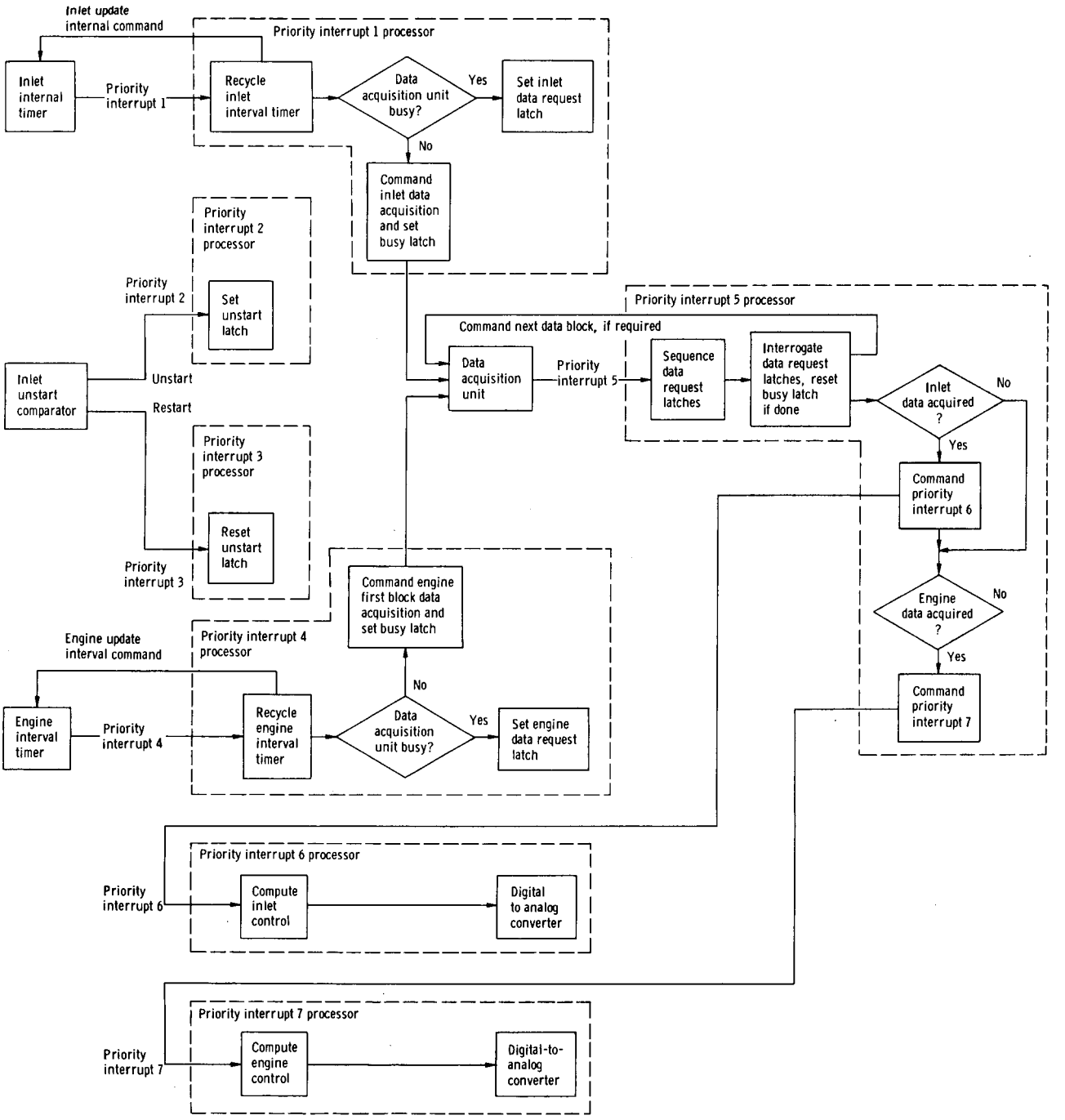

Figure 17. - Block diagram of digital computer programming showing priority interrupt structure for program sequencing.

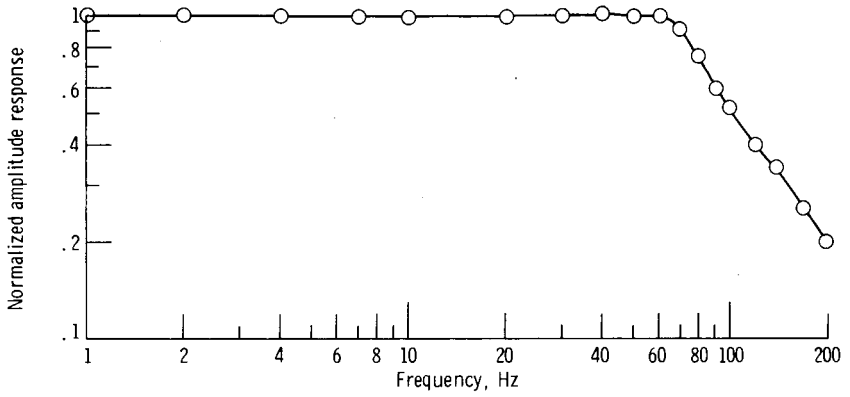

Figure 18. - Inlet overboard bypass door frequency response at 80-hertz-bandwidth setting, normalized to 37 percent peak-to-peak.

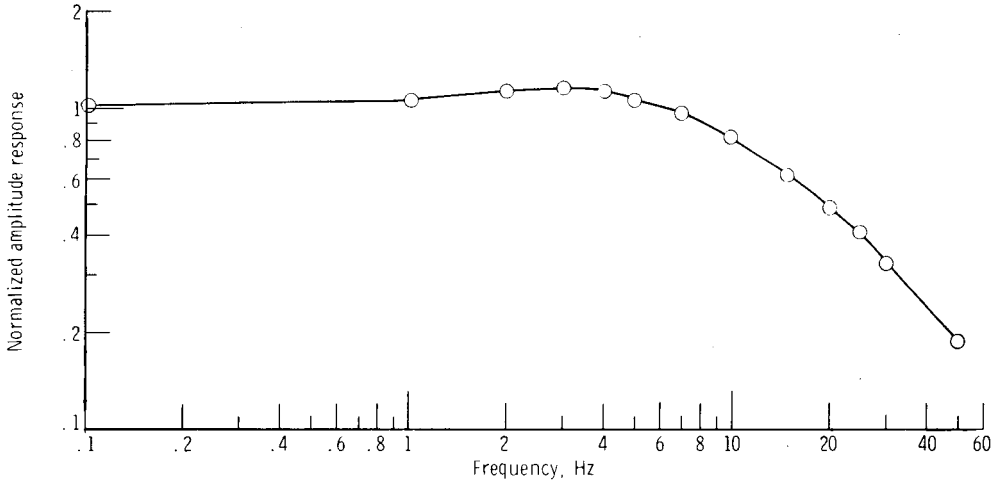

Figure 19. - Inlet overboard bypass door frequency response at 10-hertz-bandwidth setting, normalized to 20-percent peak-to-peak.

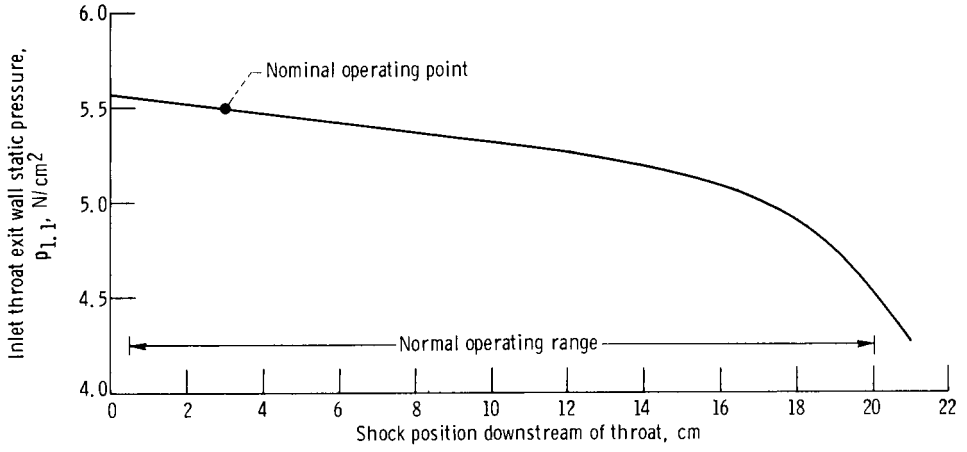

Figure 20. - Inlet throat exit wall static pressure recovery as function of inlet terminal shock location. Mach number, 2.5; free-stream total pressure, P_0, 9.3 N/cm^2.

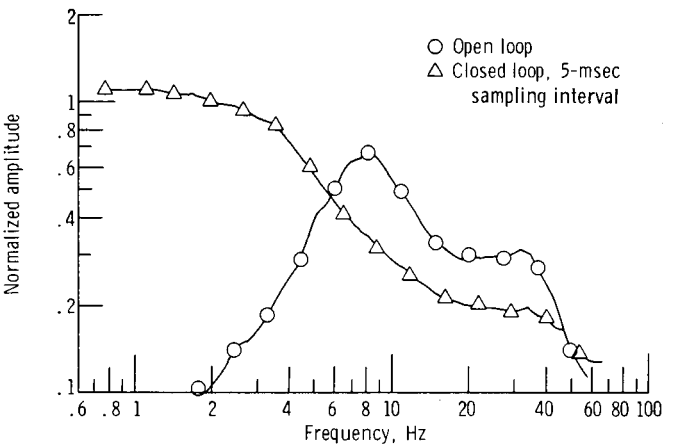

Figure 21. - Comparison of open- and closed-loop frequency responses of inlet throat exit wall static pressure $p_{1.1}$ error, normalized to open-loop value of 0.1 hertz.

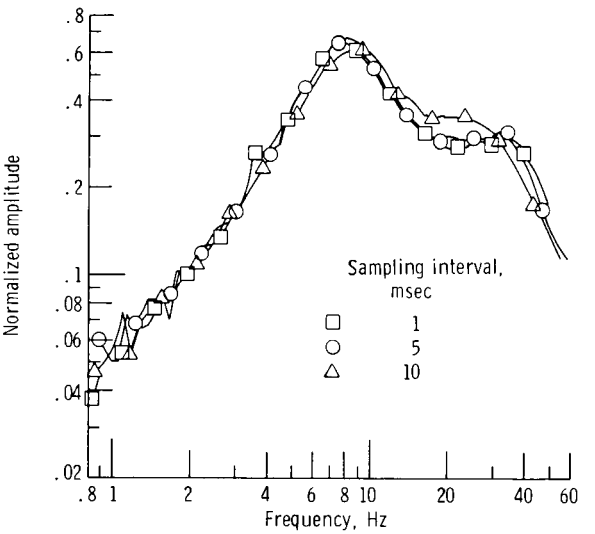

Figure 22. - Comparison of closed-loop frequency response of inlet throat exit wall static pressure $p_{1.1}$ error for three different sampling intervals, normalized to open-loop value of 0.1 hertz.

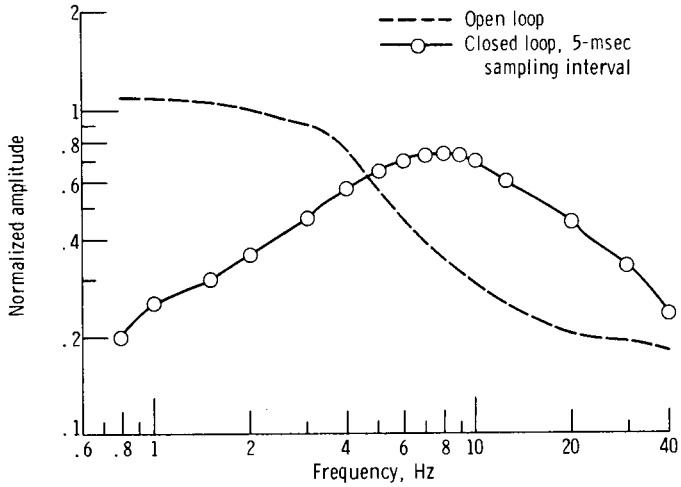

Figure 23. - Comparison of open- and closed-loop frequency responses of inlet throat exit wall static pressure $p_{1.1}$ error, normalized to open-loop value of 0.1 hertz - 10-hertz-bandwidth bypass door control.

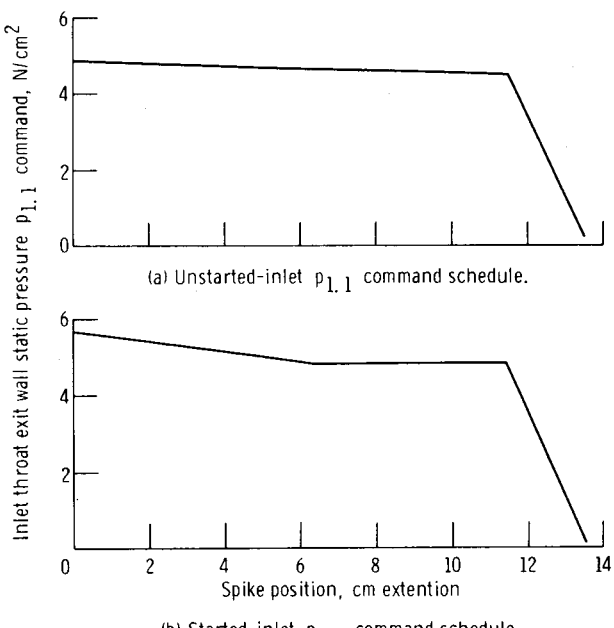

Figure 24. - Inlet throat exit wall static pressure $p_{1.1}$ command schedules as function of spike position during inlet restart sequence.

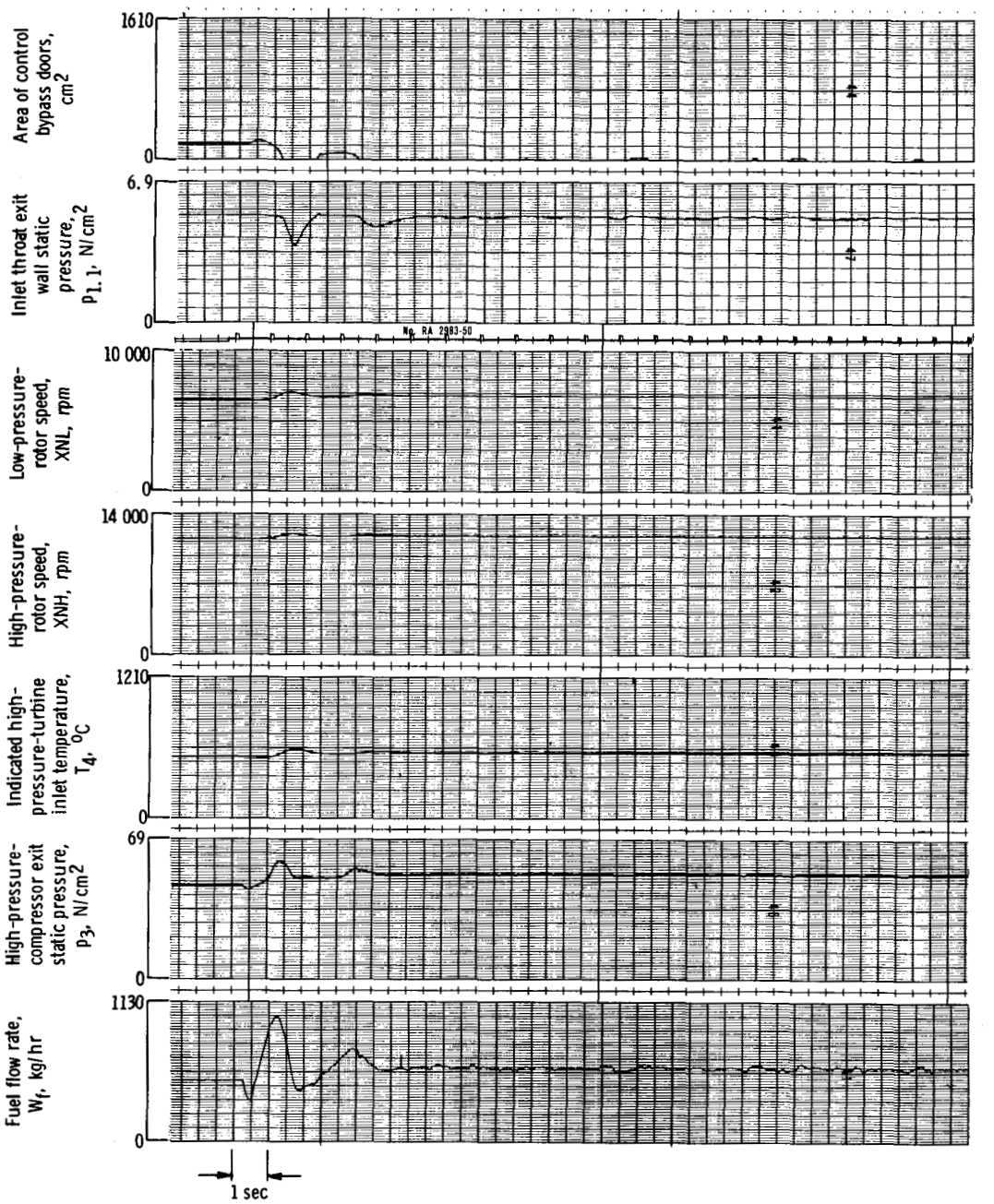

Figure 25. - Activation of digital integrated control - 80-hertz-bandwidth bypass doors.

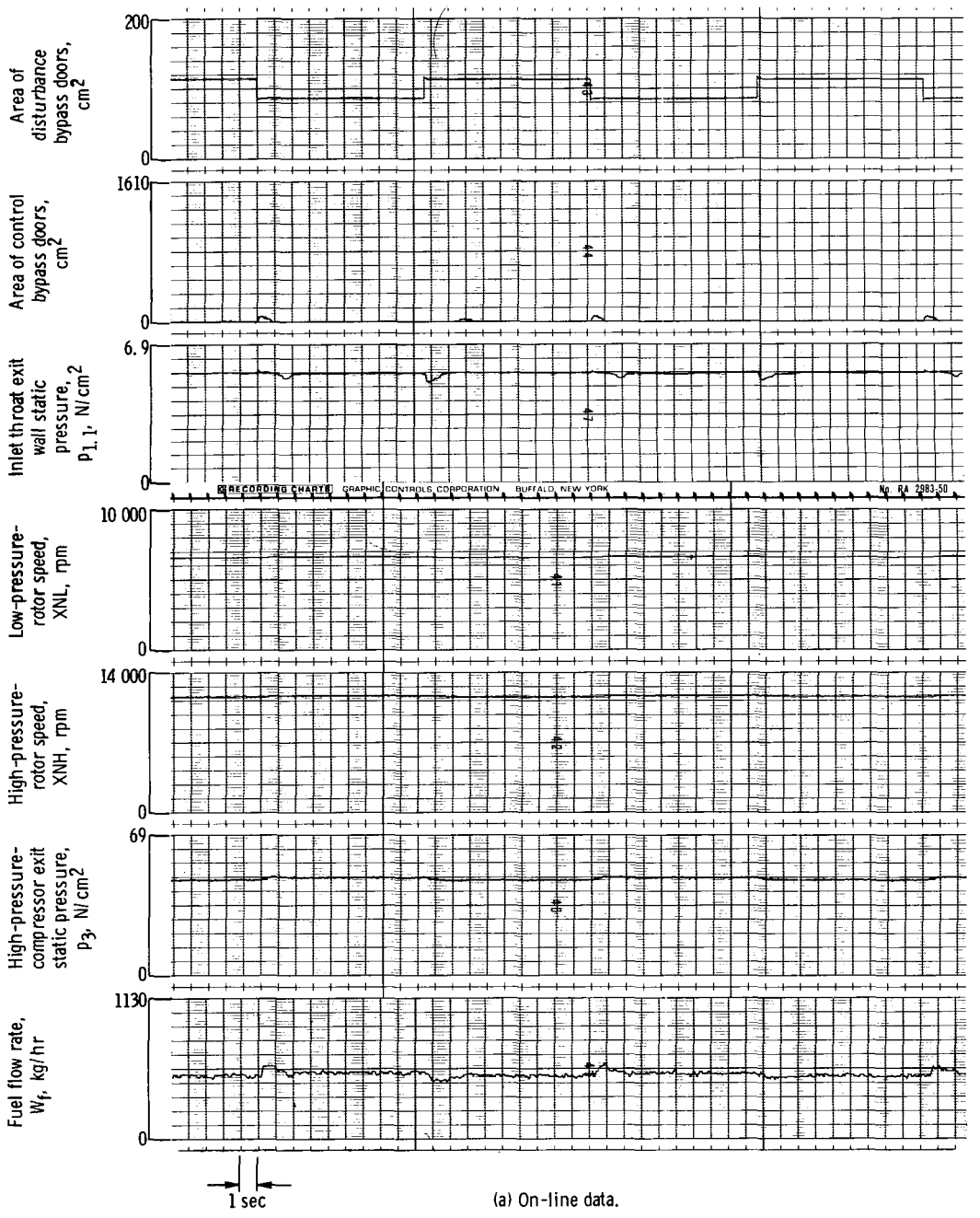

(a) On-line data.

Figure 26. - Square-wave airflow disturbance - digital integrated control with 80-hertz-bandwidth bypass doors.

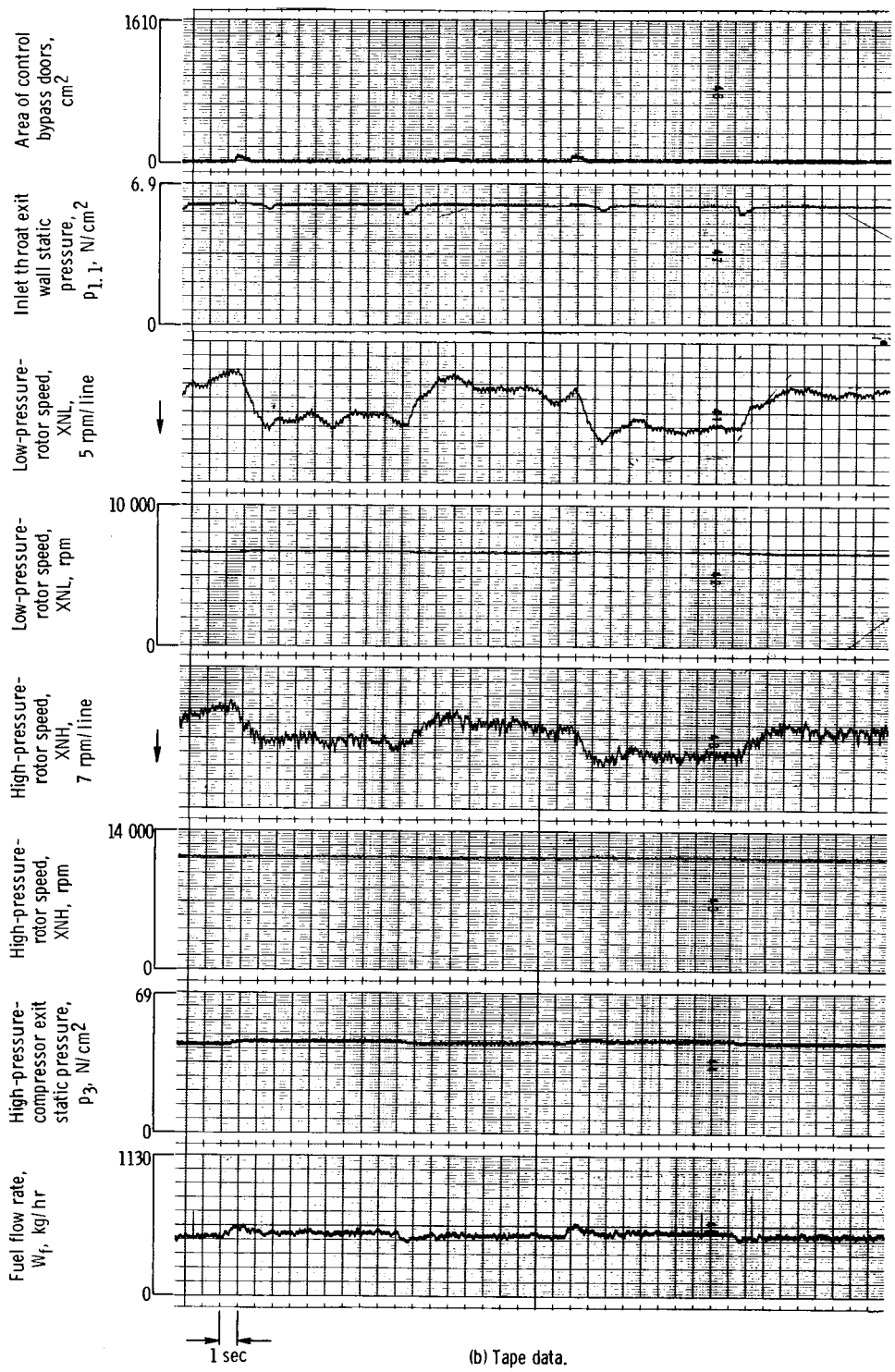

(b) Tape data.

Figure 26. - Concluded.

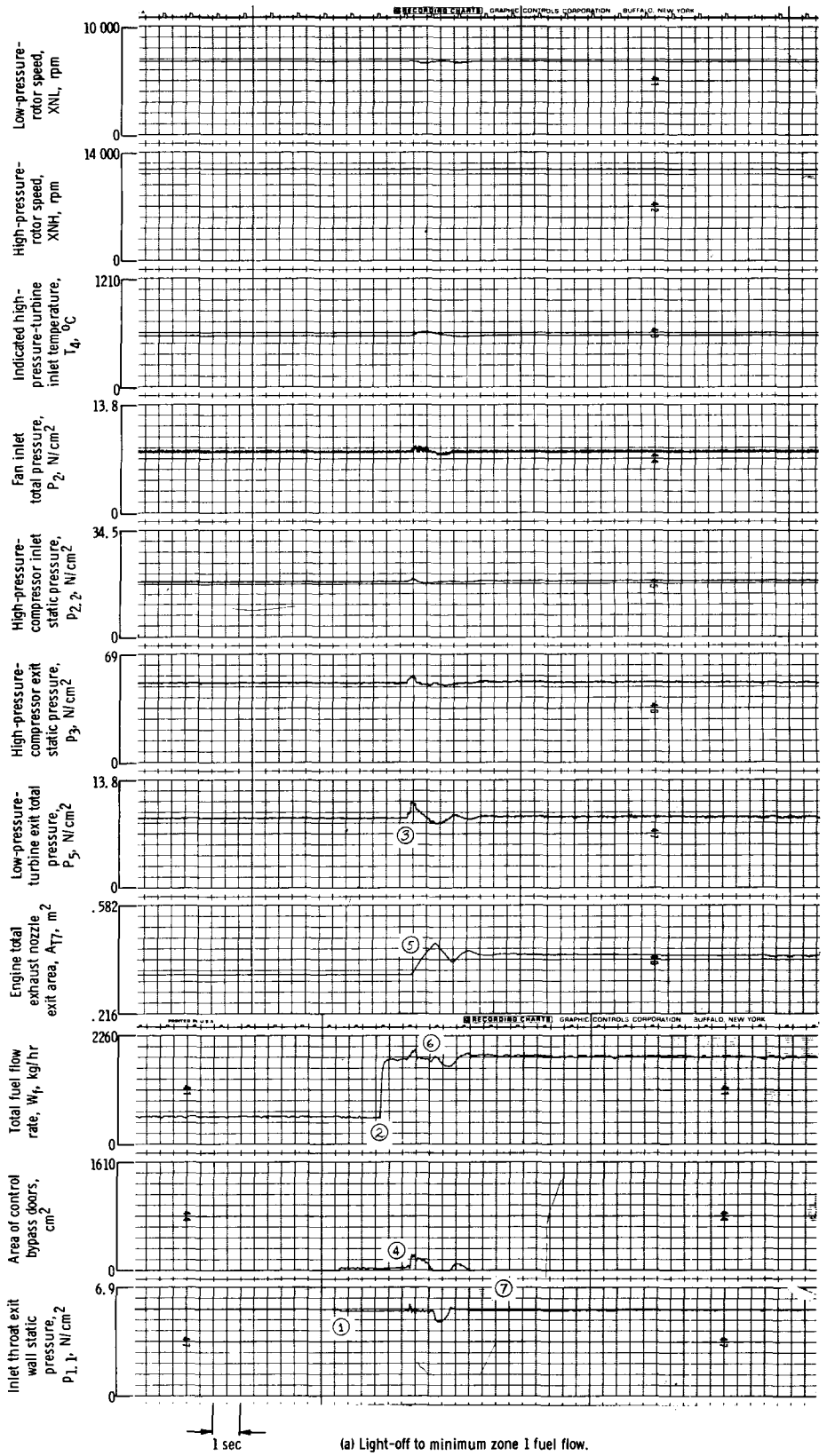

(a) Light-off to minimum zone 1 fuel flow.

Figure 27. - Augmentor light-off transients - digital integrated control with 80-hertz-bandwidth bypass doors.

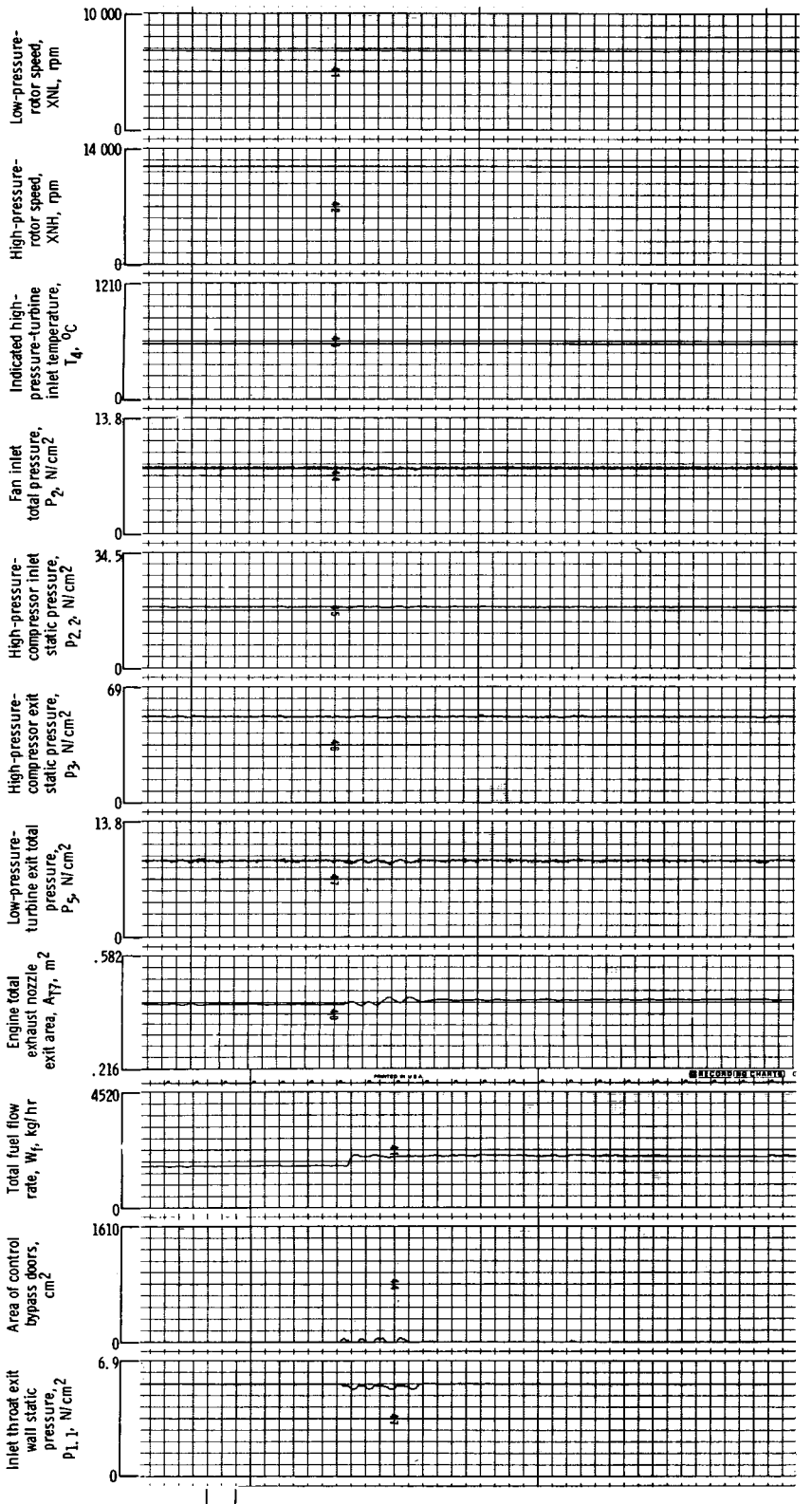

(b) Maximum zone 1 fuel flow to minimum zone 2 fuel flow.

Figure 27. - Continued.

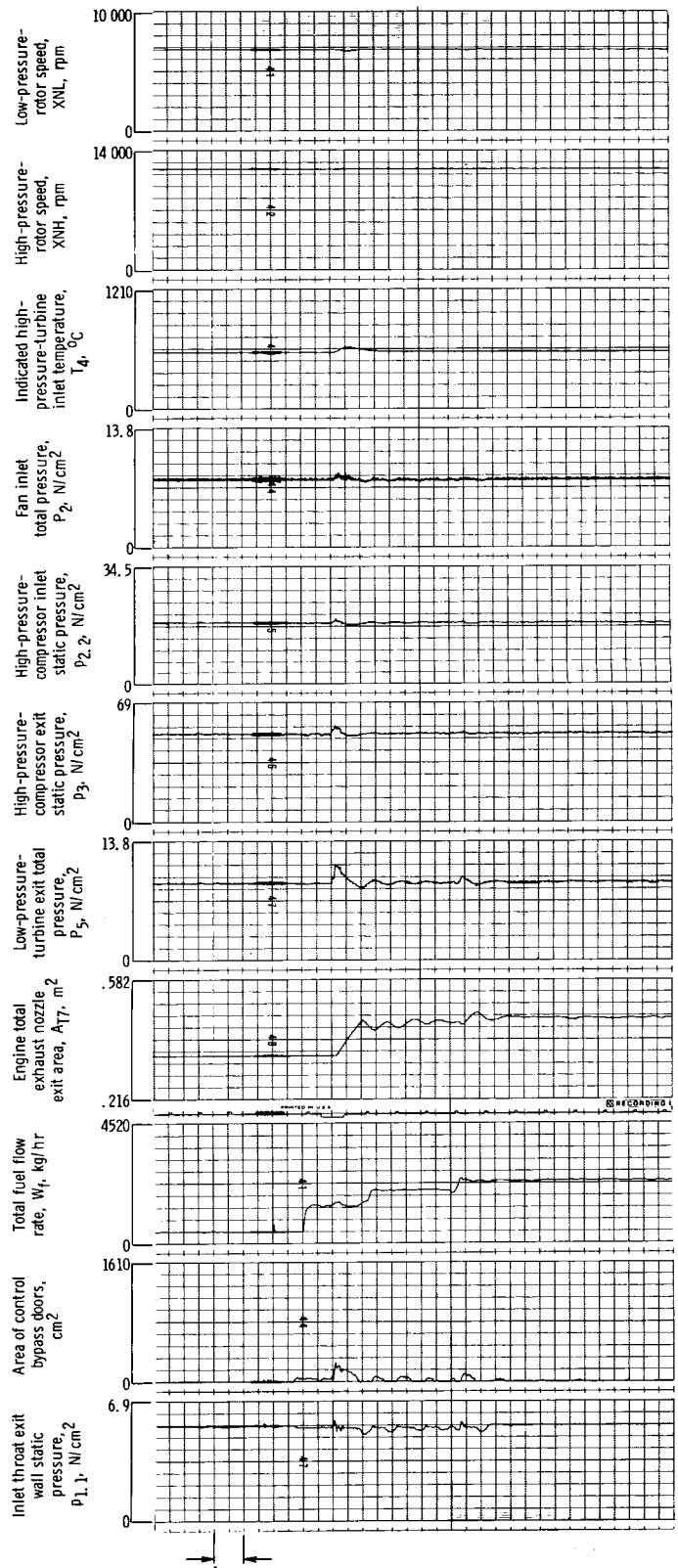

(c) Light-off to maximum zone 2 fuel flow.

Figure 27. - Concluded.

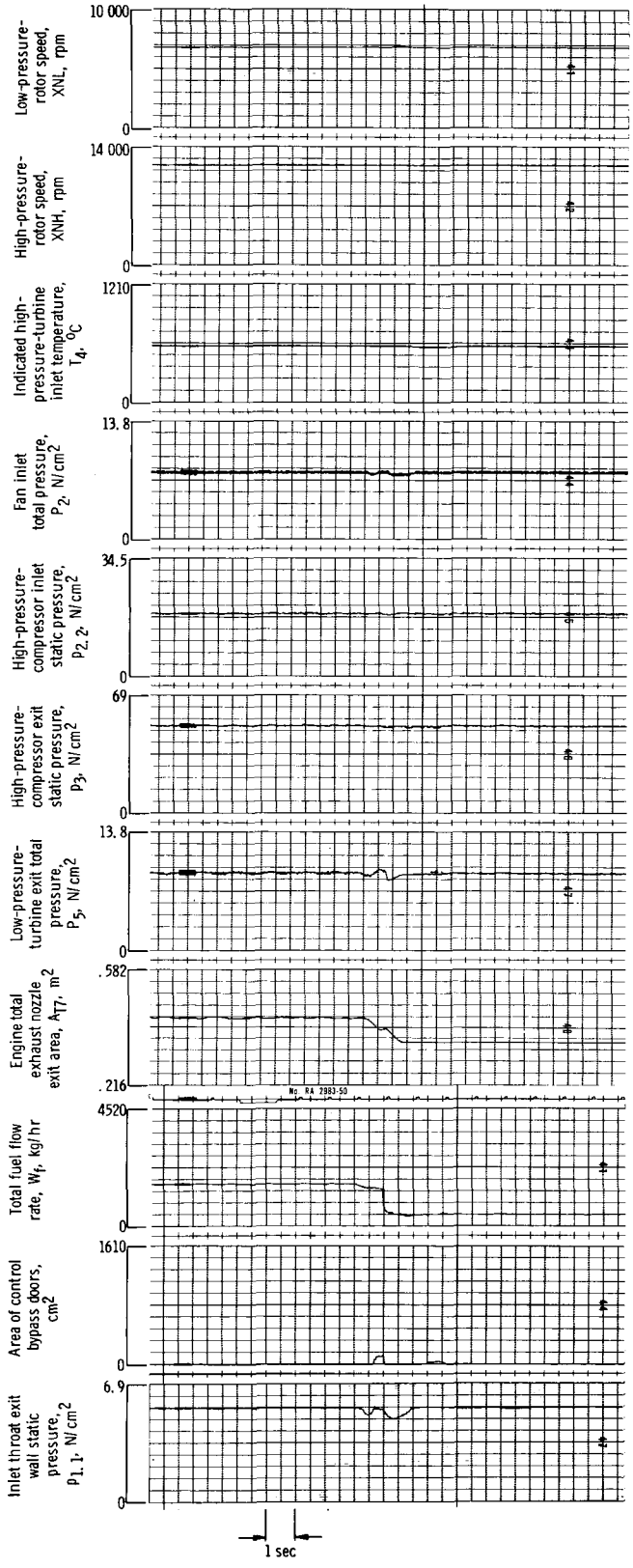

Figure 28. - Augmentor cutoff transient from maximum zone 1 fuel flow - digital integrated control with 80-hertz-bandwidth bypass doors.

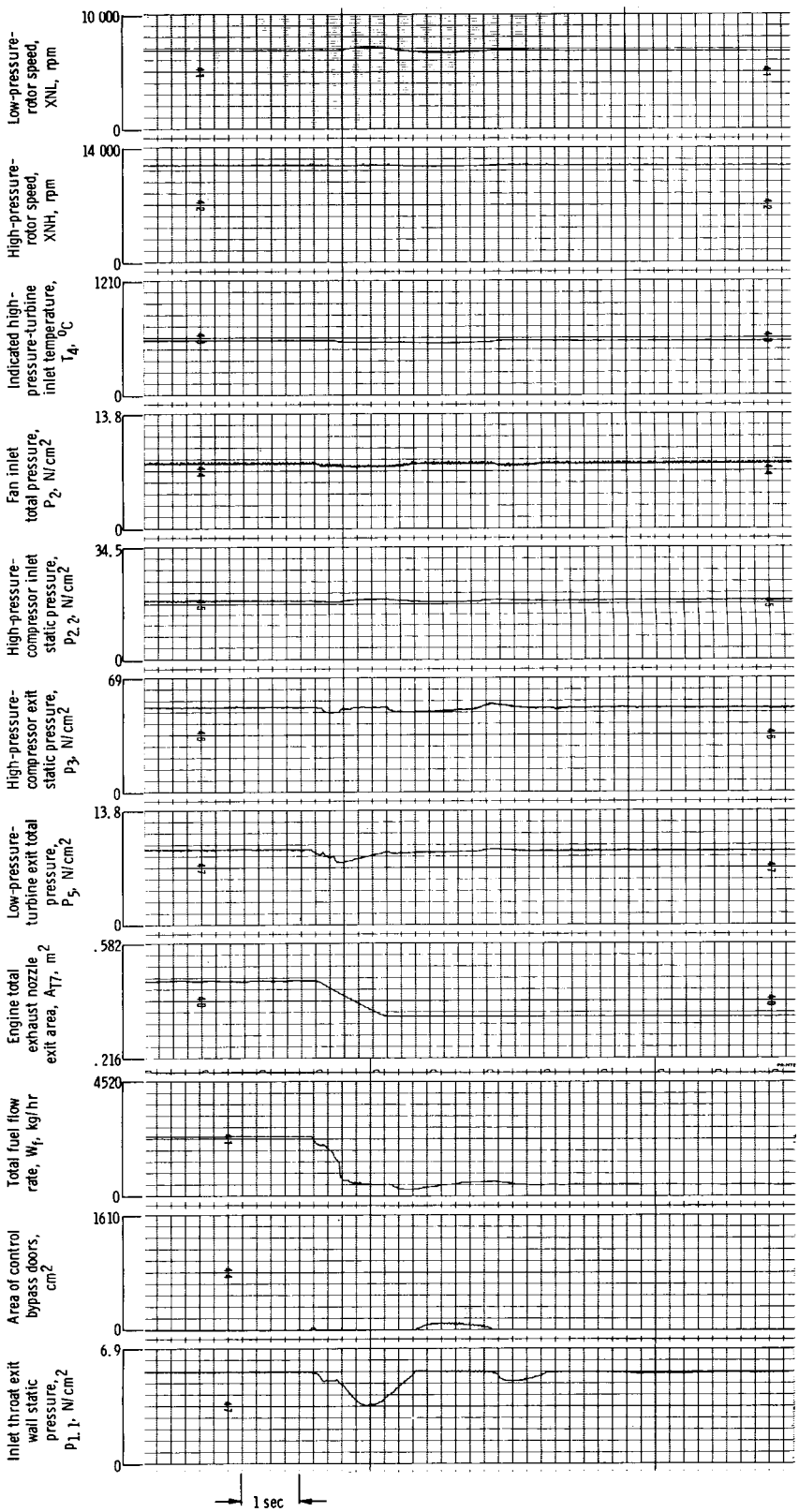

Figure 29. - Augmentor cutoff transient from maximum zone 2 fuel flow during which a blowout occurs - digital integrated control with 80-hertz-bandwidth bypass doors.

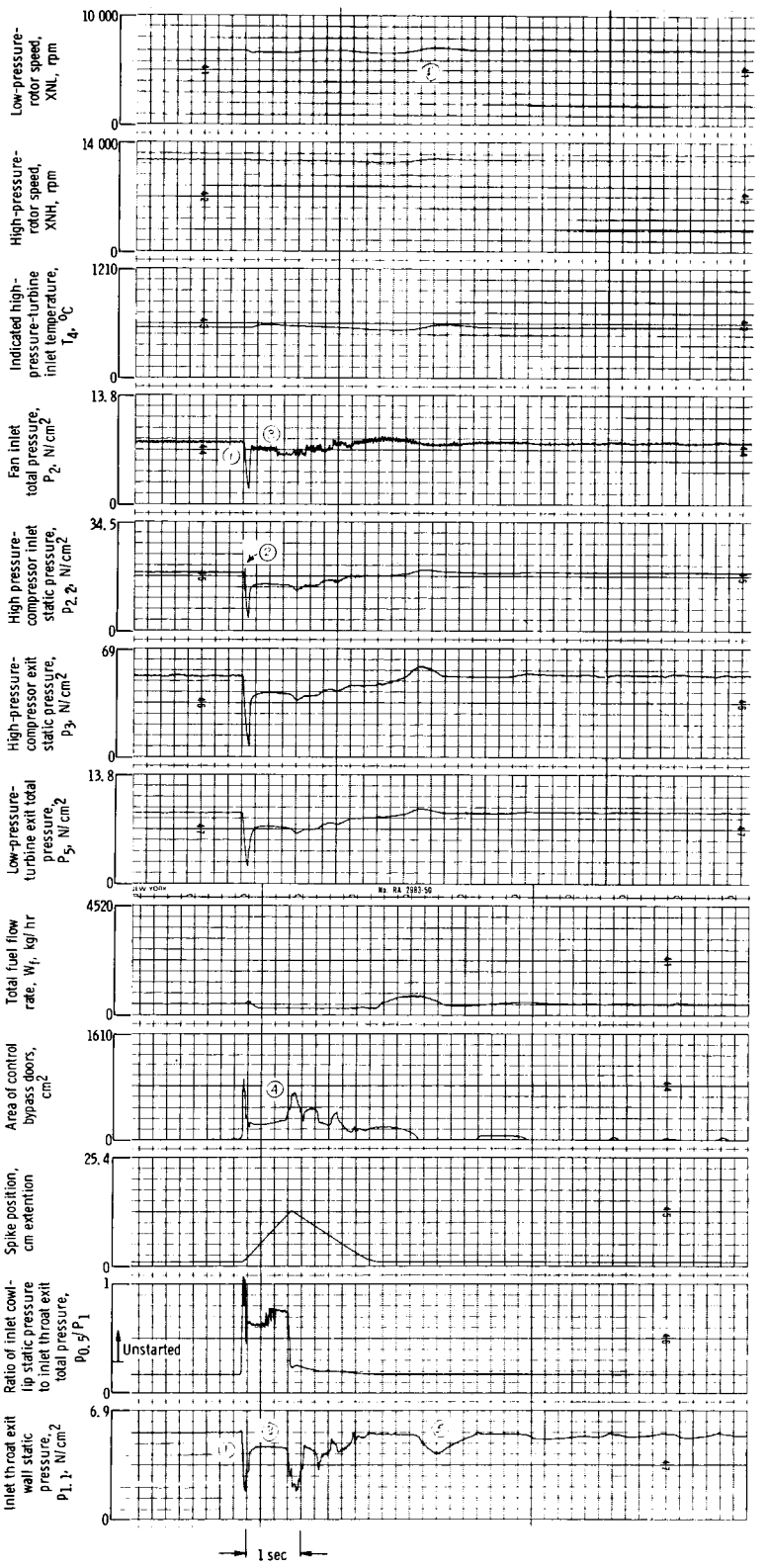

Figure 30. - Inlet unstart and automatic restart - early digital integrated control with 80-hertz-bandwidth bypass doors.

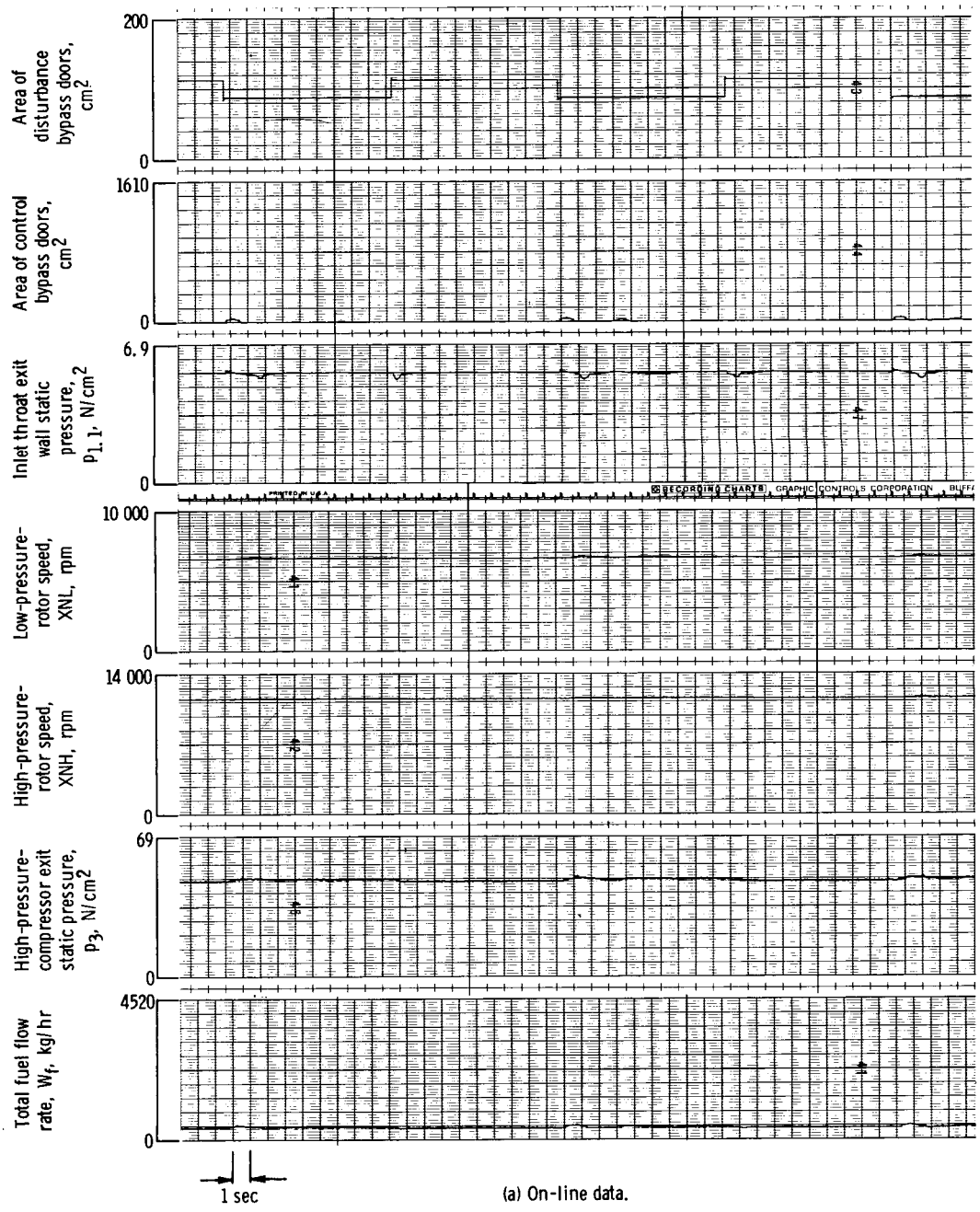

(a) On-line data.

Figure 31. - Square-wave airflow disturbance - digital integrated control with 10-hertz-bandwidth bypass doors.

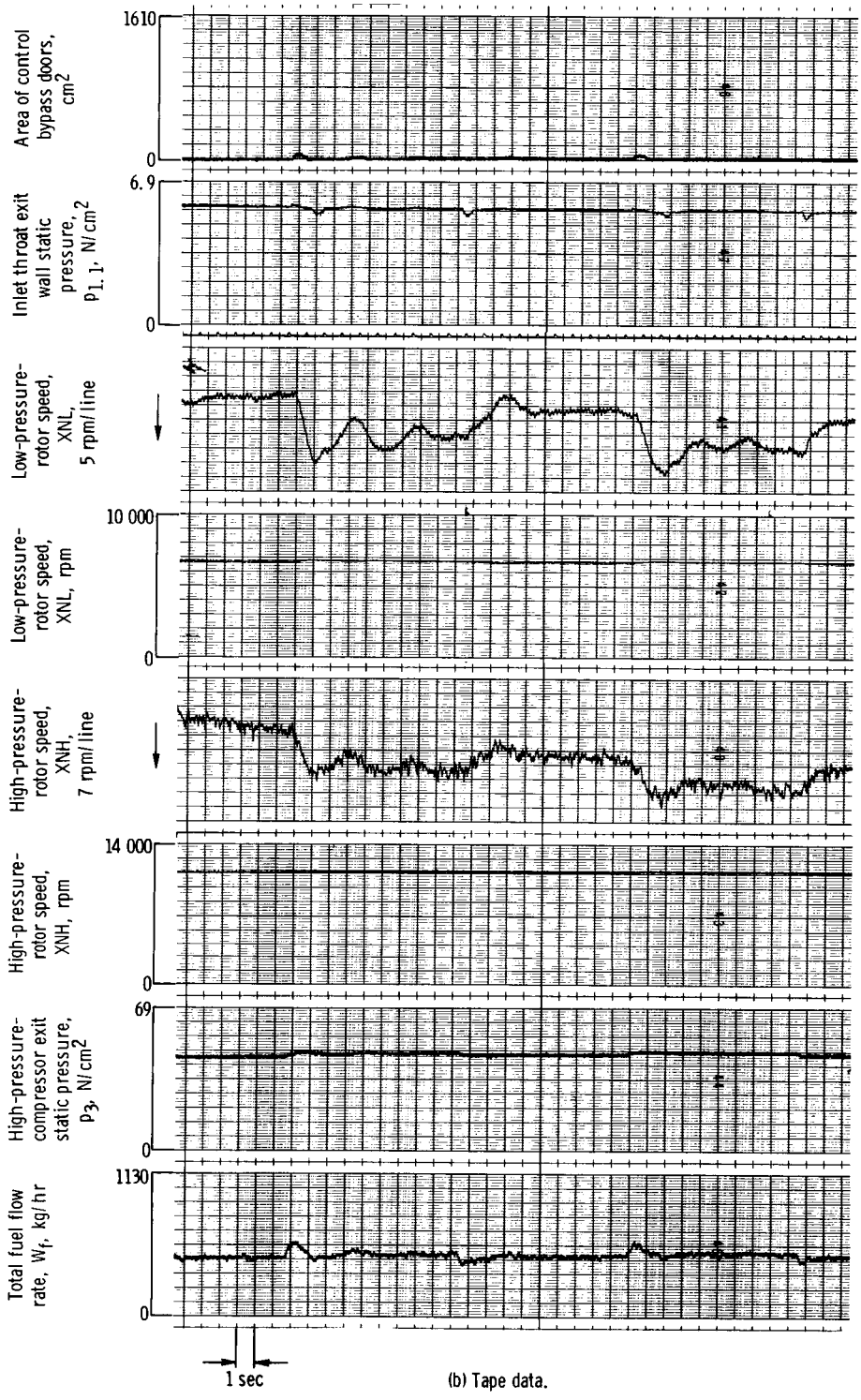

(b) Tape data.

Figure 31. - Concluded.

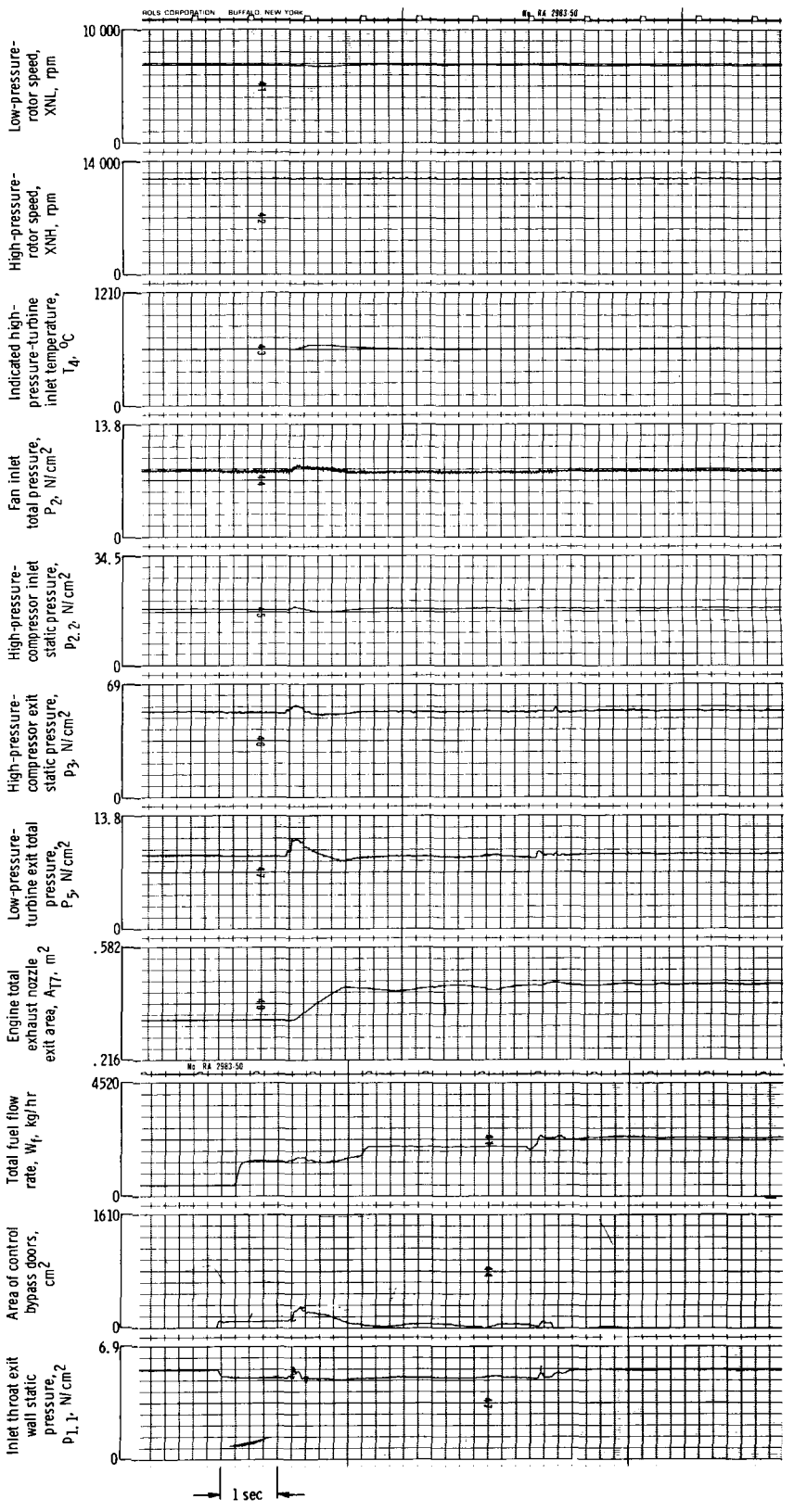

Figure 32. - Augmentor light-off to maximum zone 2 fuel flow - digital integrated control with 10-hertz-bandwidth bypass doors.

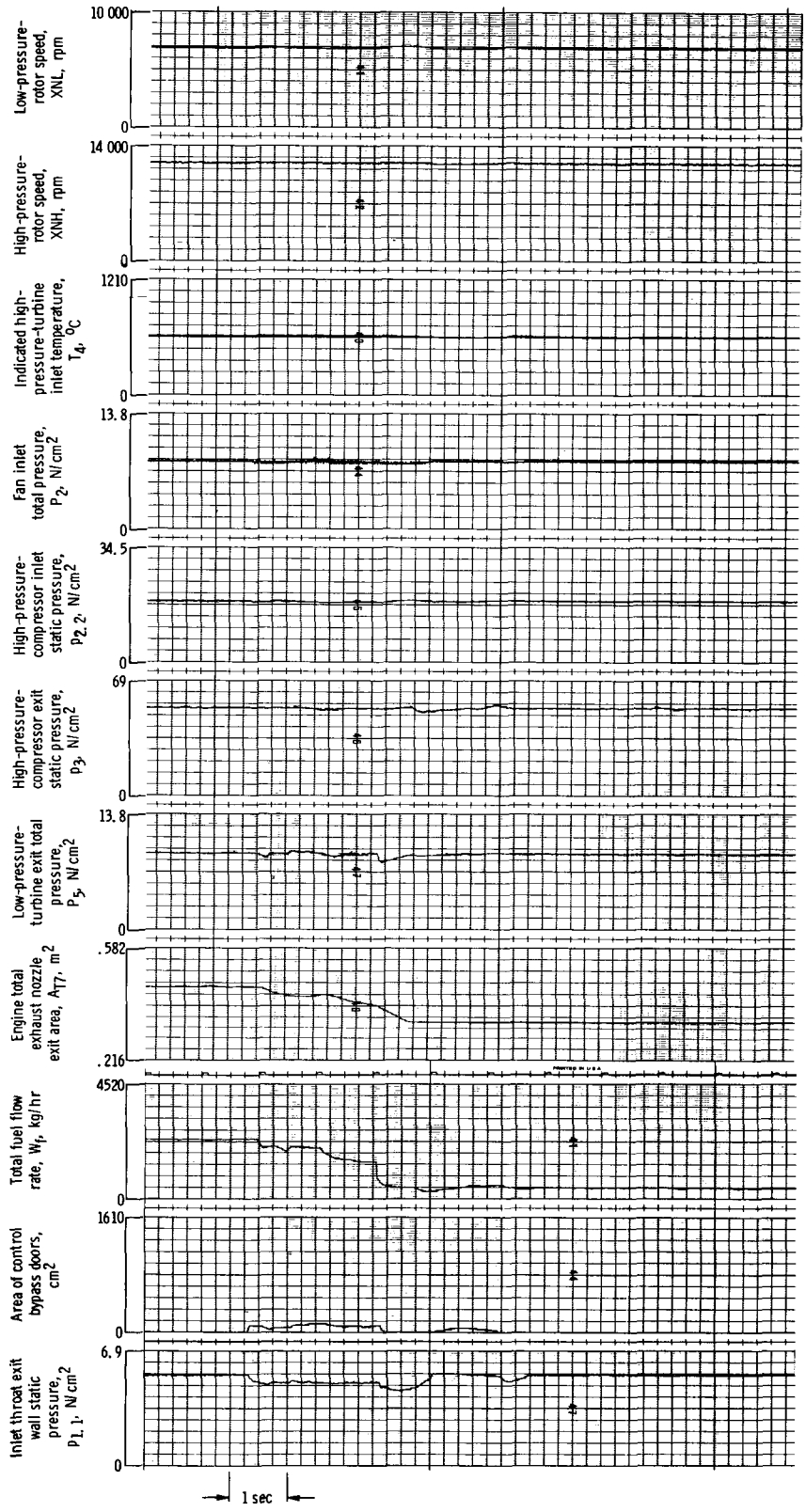

Figure 33. - Augmentor cutoff transient from maximum zone 2 fuel flow - digital integrated control with 10-hertz-bandwidth bypass doors.

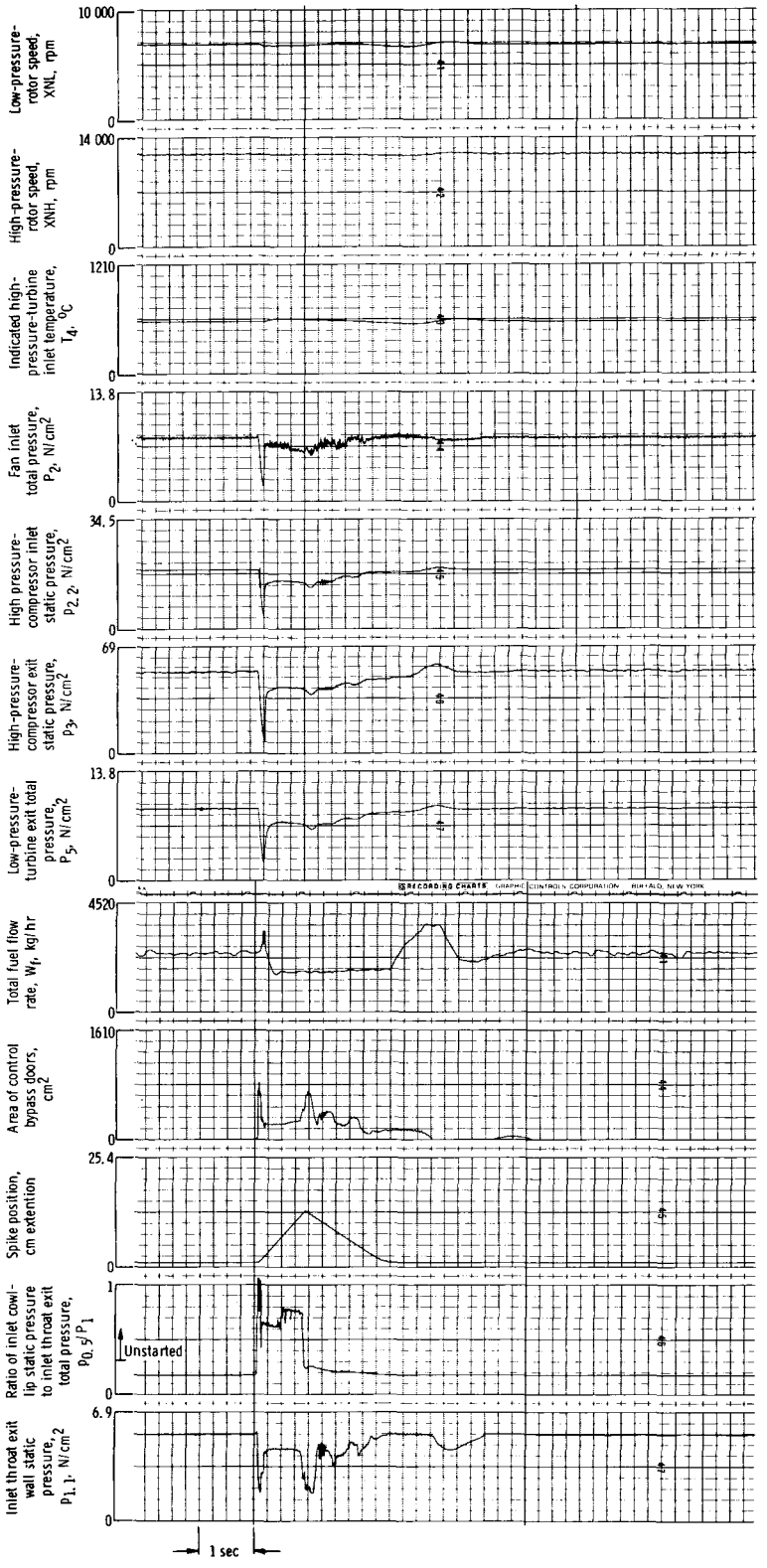

Figure 34. - Inlet unstart and restart - digital integrated control with 10-hertz-bandwidth bypass doors.

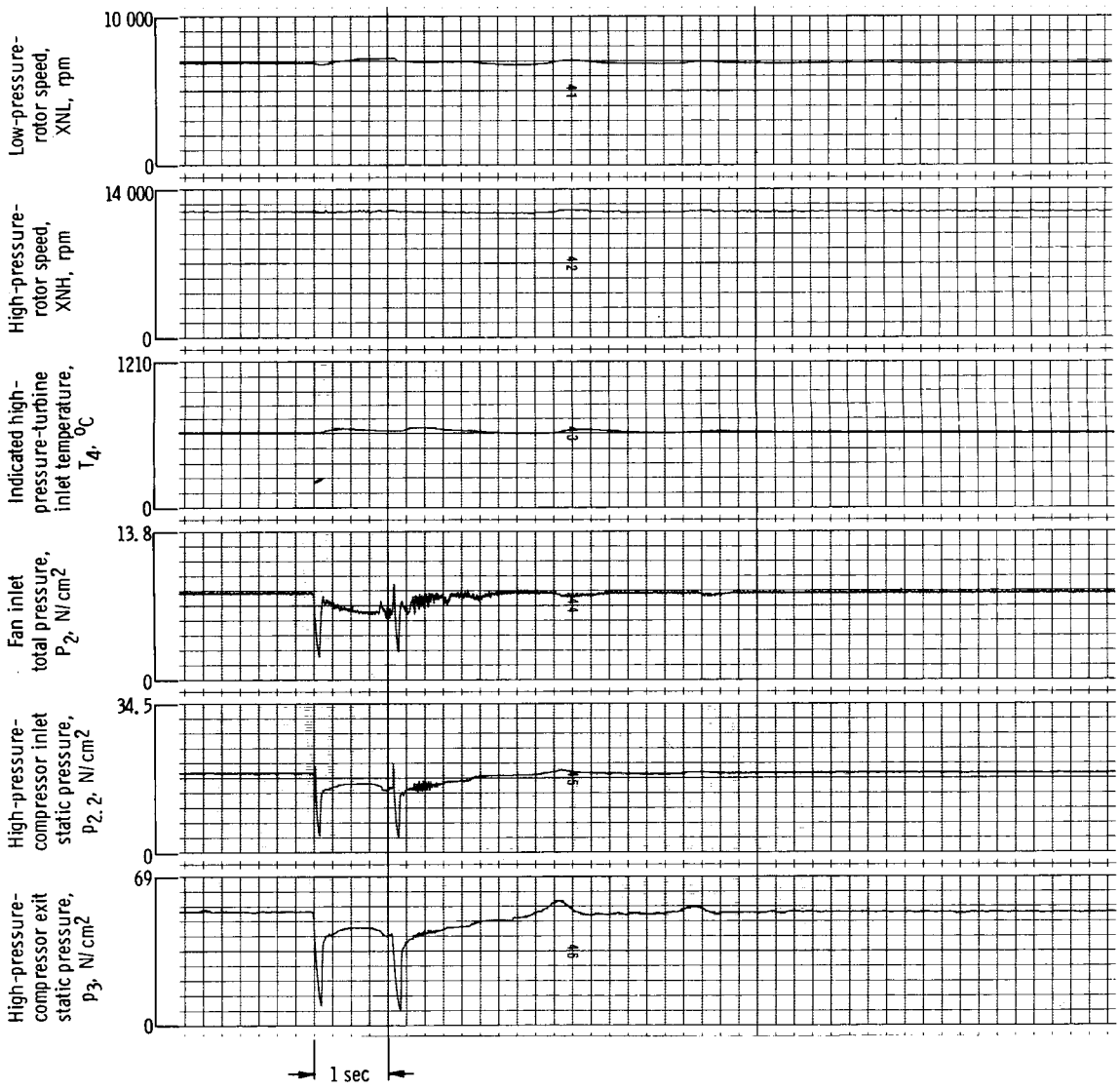

Figure 35. - Inlet unstart and restart (unstart from maximum zone 2 augmentation), showing second unstart due to an engine stall just after restart - digital integrated control with 10-hertz-bandwidth bypass doors.

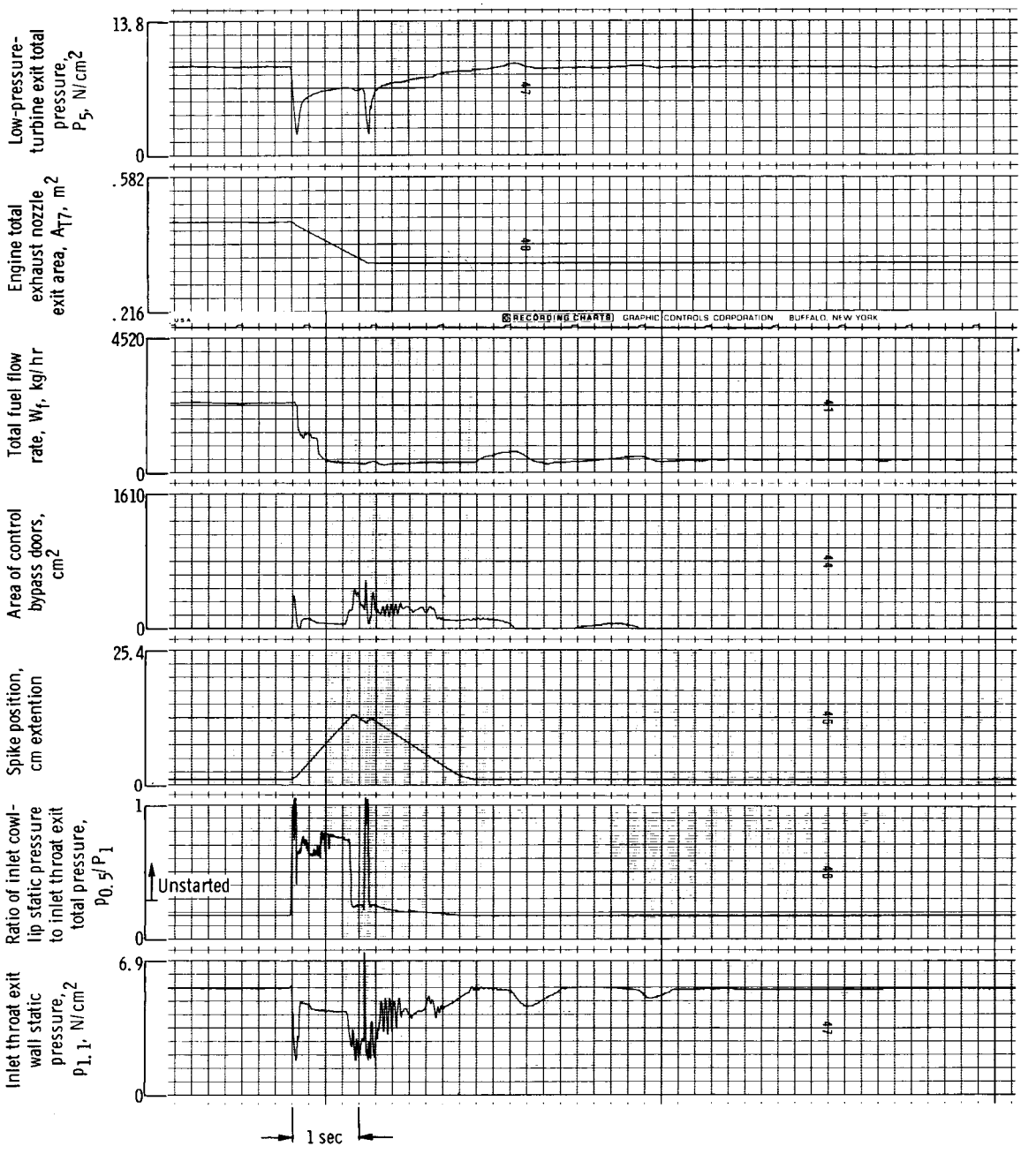

Figure 35. - Concluded.

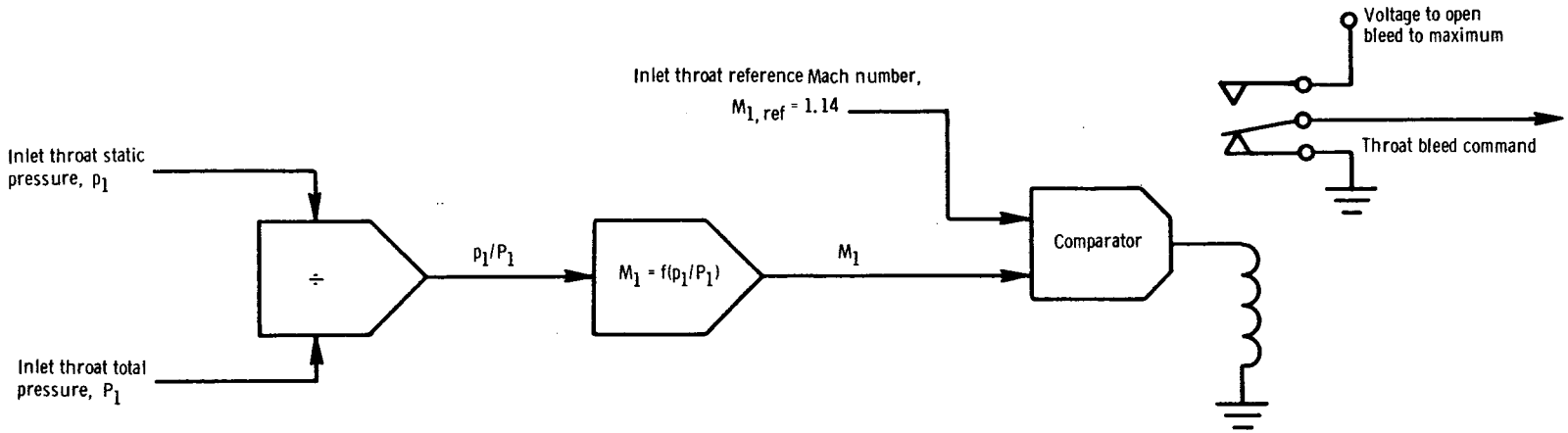

Figure 36. - Block diagram of variable inlet throat bleed control. ($M_1 = f(p_1/P_1) = -1.953\ p_1/P_1 + 2.03$.)

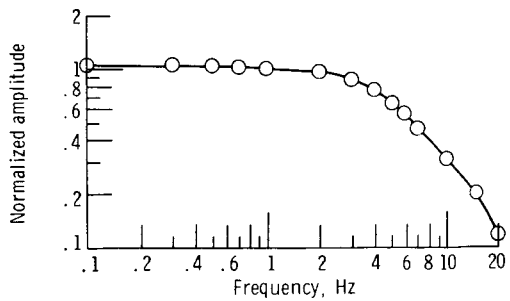

Figure 37. - Frequency response of throat bleed butterfly valves, normalized to 50 percent peak-to-peak.

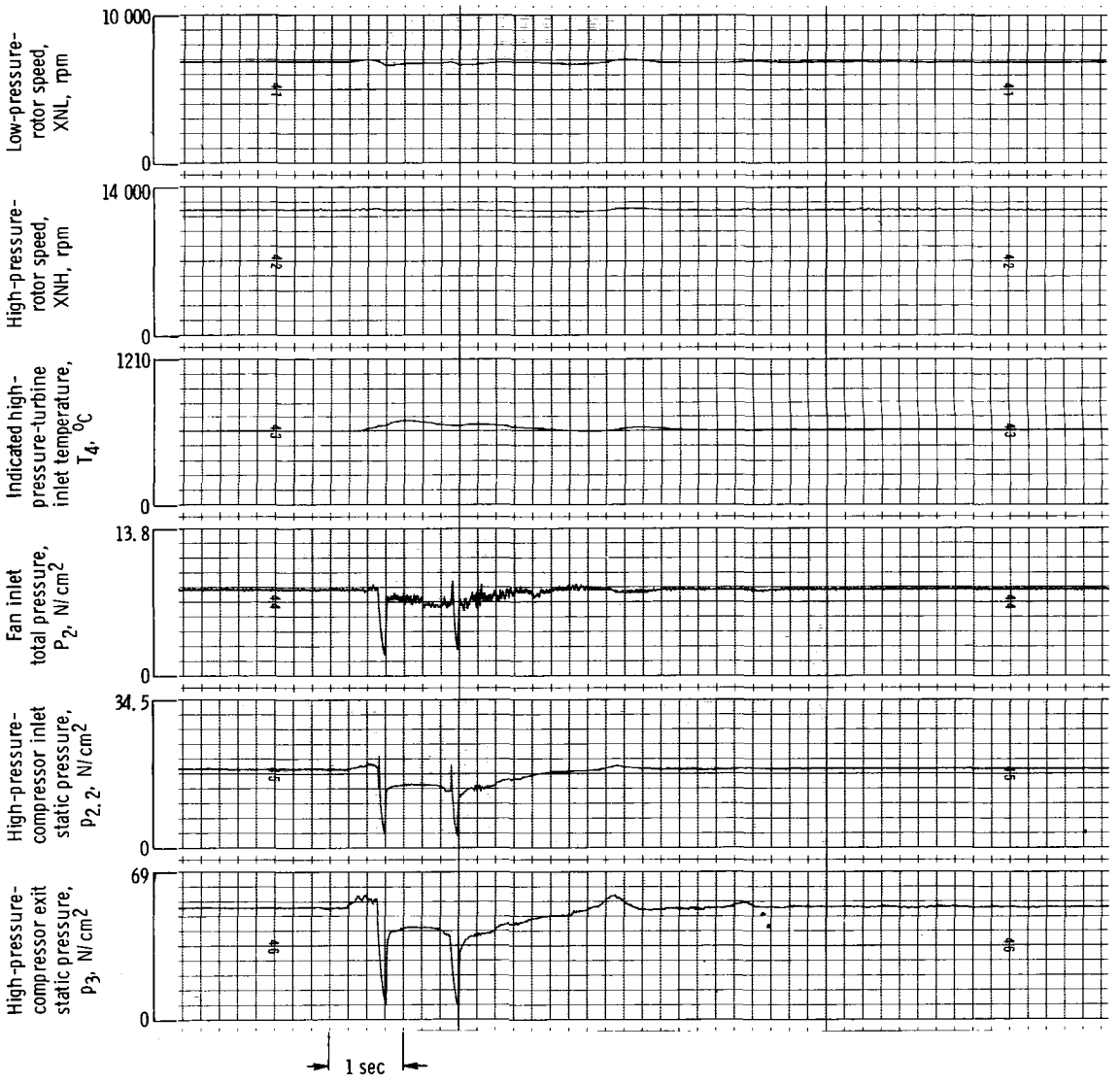

Figure 38. - Inlet unstart caused by an augmentor light-off attempt without pulling shock downstream far enough to avoid unstart - digital integrated control with 10-hertz-bandwidth bypass doors.

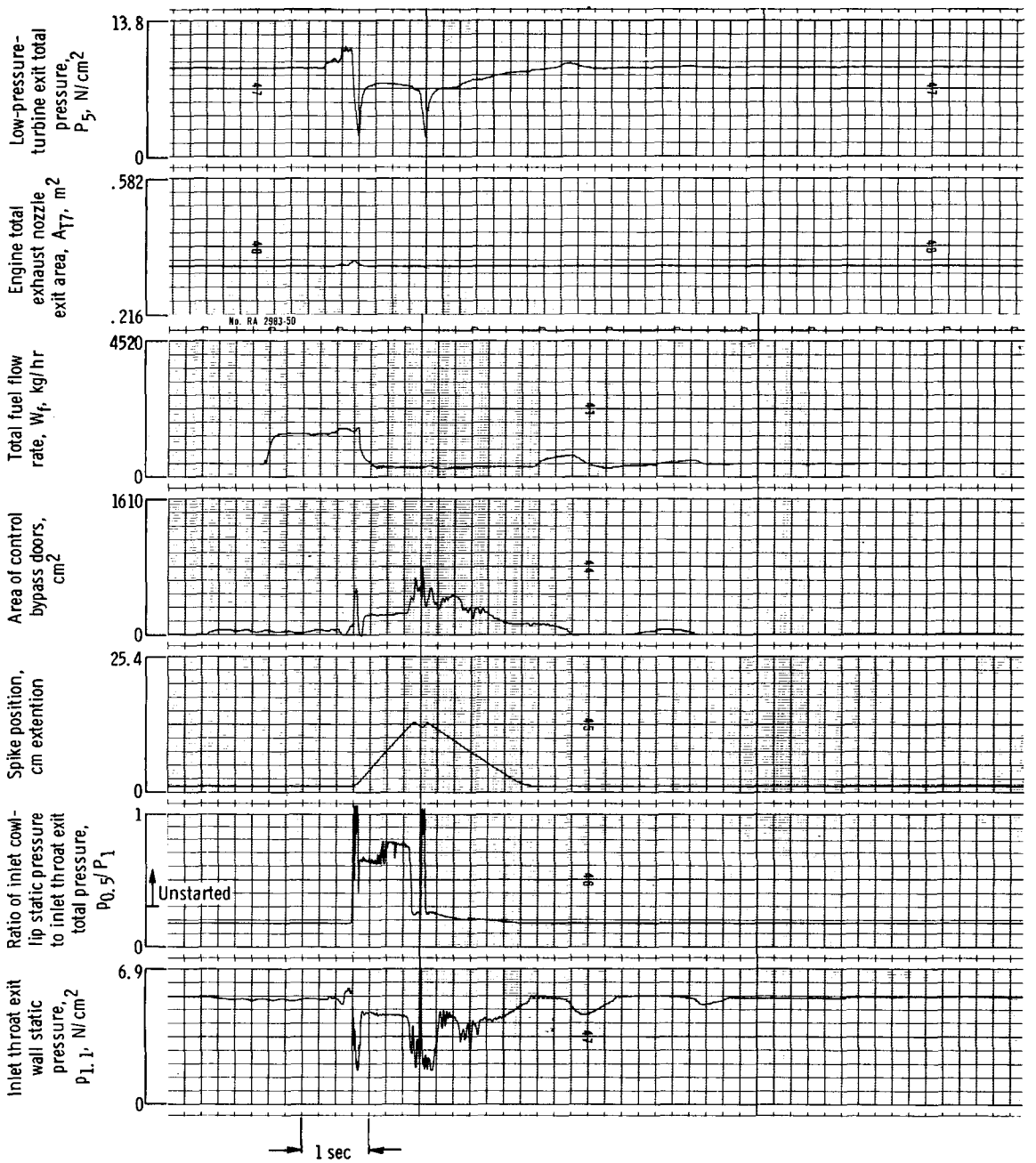

Figure 38. - Concluded.

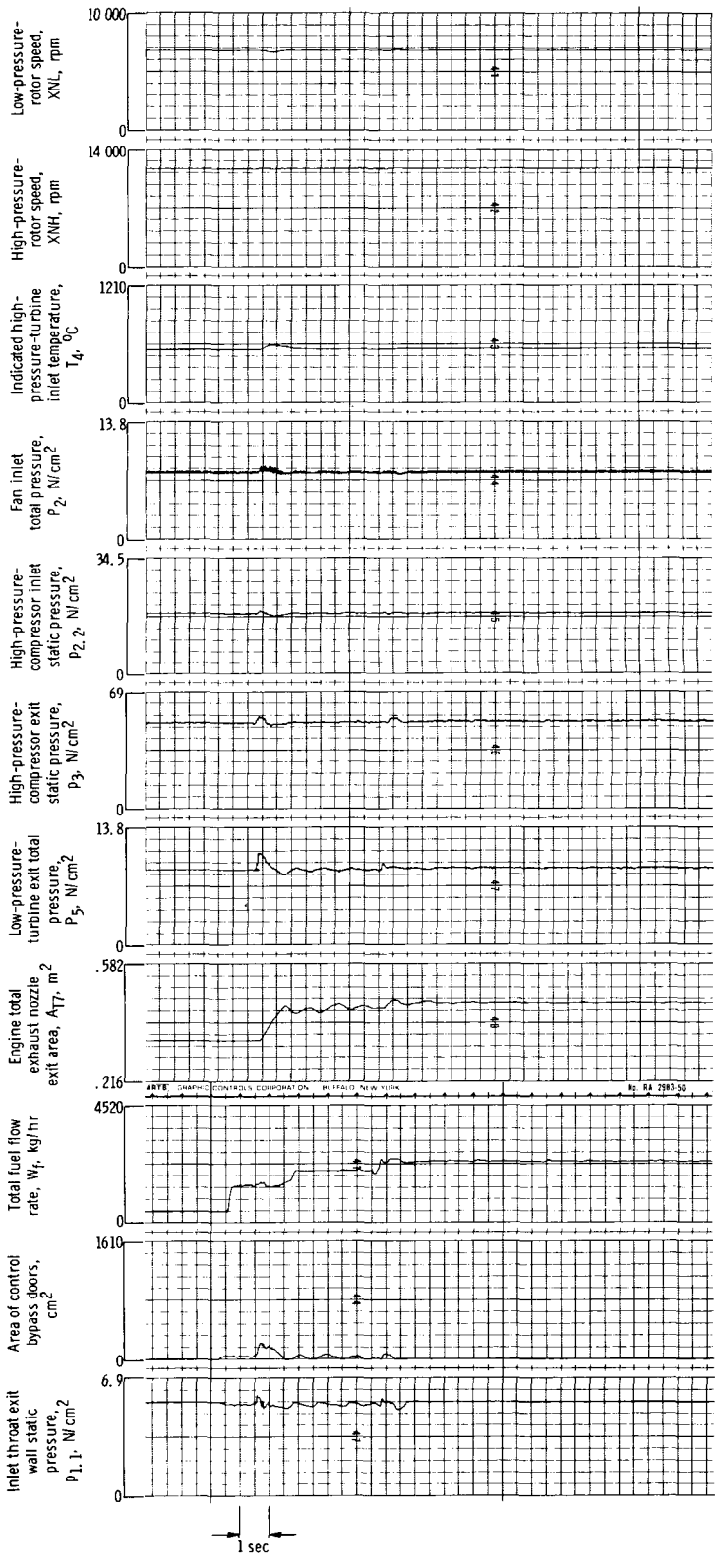

Figure 39. - Augmentor light-off transient with variable throat bleed control - digital integrated control with 10-hertz-bandwidth bypass doors.

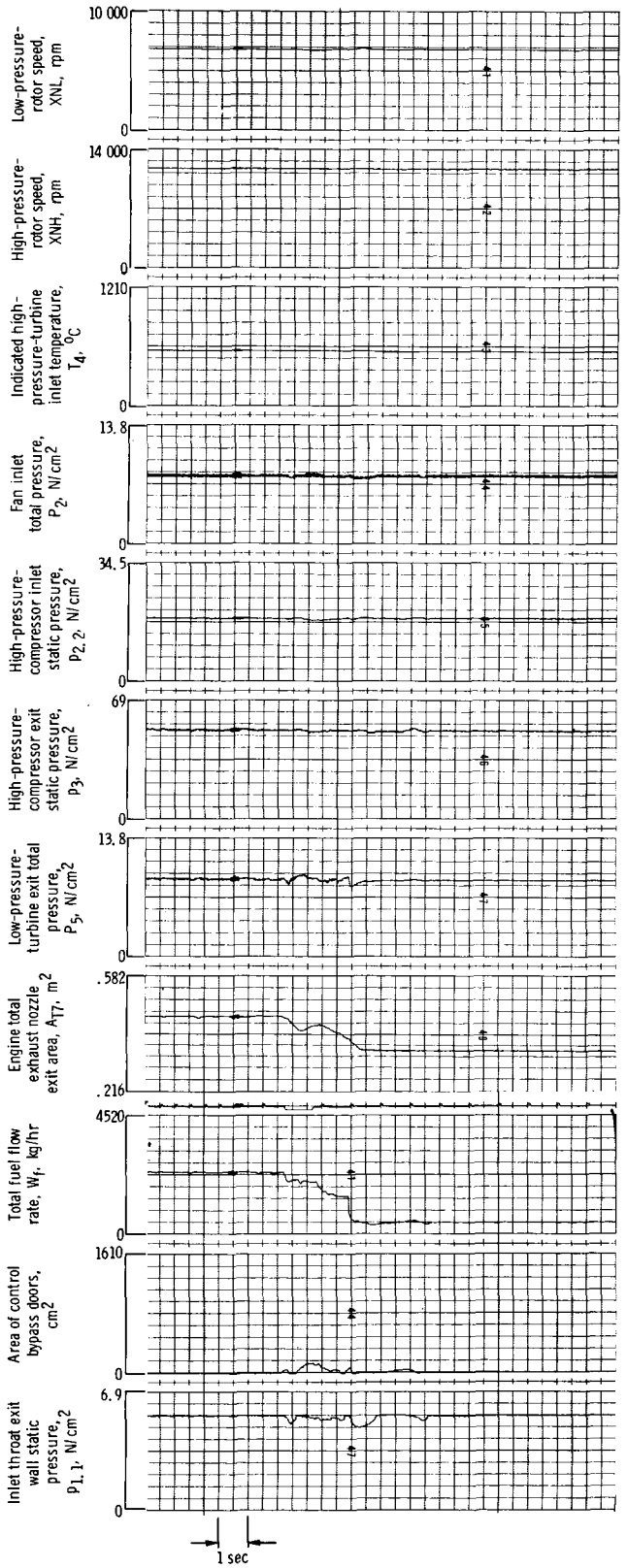

Figure 40. - Augmentor cutoff transient with variable throat bleed control - digital integrated control with 10-hertz-bandwidth bypass doors.

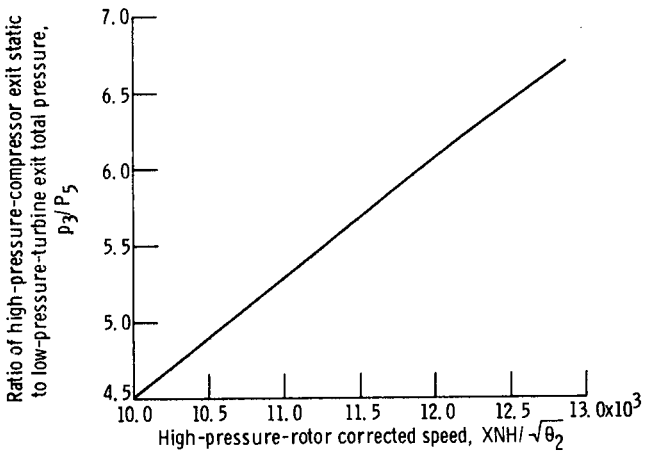

Figure 41. - Fan suppression schedule.

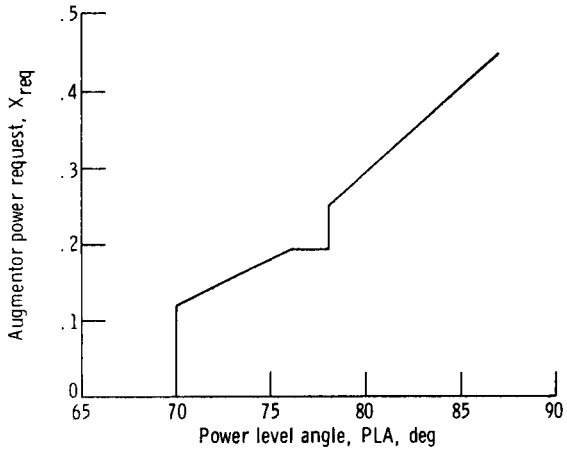

Figure 42. - Power lever response to augmentor power level request.

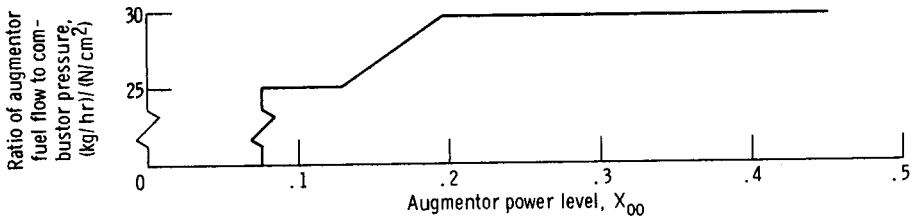

Figure 43. - Augmentor zone 1 ratio-of-fuel-flow-to-combustor-pressure schedule.

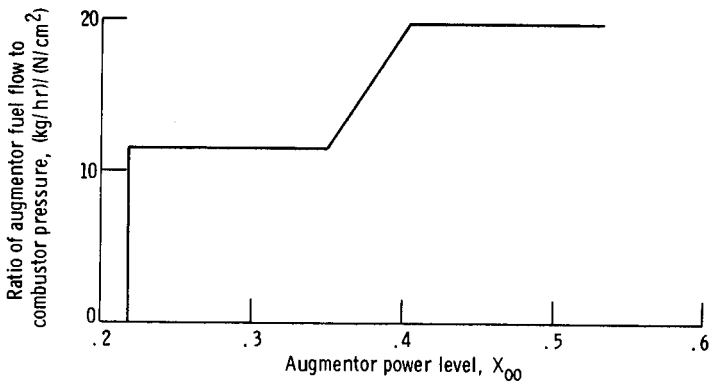

Figure 44. - Augmentor zone 2 ratio-of-fuel-flow-to-combustor-pressure schedule.